MECHANISMS OF SUPEROXIDE DISMUTASE 1 AGGREGATE FORMATION IN FAMILIAL AMYOTROPHIC LATERAL SCLEROSIS

By

CELESTE MARIE KARCH

A DISSERTATION PRESENTED TO THE GRADUATE SCHOOL
OF THE UNIVERSITY OF FLORIDA IN PARTIAL FULFILLMENT
OF THE REQUIREMENTS FOR THE DEGREE OF
DOCTOR OF PHILOSOPHY

UNIVERSITY OF FLORIDA

2009

To my family for their love and support

ACKNOWLEDGMENTS

I would like to thank my advisor, Dr. David R. Borchelt, for his support and guidance. I will always be grateful for the many opportunities that Dr. Borchelt provided. I also thank Dr. Borchelt for challenging me and for teaching me how to think like a scientist. I express my gratitude to my committee members: Dr. Lucia Notterpek, Dr. Wolfgang Streit, and Dr. William Dunn. I would like to thank Dr. Susan Semple-Rowland for her contributions to my growth as a scientist. I would also like to thank our collaborators for their advice, support, and assistance: Dr. Joan Valentine and the members of her laboratory in the Department of Chemistry at the University of California at Los Angeles, Dr. Julian Whitelegge and the members of his laboratory in the Pasarow Mass Spectrometry Laboratory at the University of California at Los Angeles, and Dr. P. John Hart and the members of his laboratory at the University of Texas at San Antonio. Finally, I would like to thank past and present members of the Borchelt laboratory for their advice, guidance, and friendship. In particular, I would like to thank Mercedes Prudencio for her support.

TABLE OF CONTENTS

page

LIST OF TABLES

LIST OF FIGURES

Abstract of Dissertation Presented to the Graduate School
of the University of Florida in Partial Fulfillment of the
Requirements for the Degree of Doctor of Philosophy

MECHANISMS OF SUPEROXIDE DISMUTASE 1 AGGREGATE FORMATION IN FAMILIAL AMYOTROPHIC LATERAL SCLEROSIS

By

Celeste Marie Karch

May 2009

Chair: David R. Borchelt
Major: Medical Sciences – Neuroscience

Familial amyotrophic lateral sclerosis (FALS) is a late onset neurodegenerative disease that is characterized by selective death of neurons in the upper and lower motor neuron pathways, resulting in progressive paralysis. A subset of FALS cases are linked to dominantly inherited missense mutations in Cu,Zn superoxide dismutase 1 (SOD1). More than 100 mutations in SOD1 are known to cause FALS by a proposed gain of toxic property. One possible mechanism for this toxicity is the formation of aggregates. In the spinal cords of mouse models of ALS overexpressing mutant SOD1, detergent-insoluble, high-molecular-weight, SOD1 aggregates accumulate as mice develop paralysis. The mechanism underlying the formation and function of these aggregates is poorly understood. In this study, we examined the intrinsic factors that mediate the aggregation of SOD1 using a mutagenesis approach and cell culture assay for aggregation. In cell culture, our data suggest that in SOD1 aggregates, cysteines 6 and 111 of SOD1 may play important roles in the early stages of aggregate formation with other structural features of the aggregate providing additional stability. Furthermore, we found that amino acids in β-strands 6 and 7 in human SOD1 are important for aggregation and that species-specific interactions between these two regions are important for enhancing aggregation. In our animal model of ALS, our findings demonstrate that the accumulation of

disulfide cross-linked mutant protein is co-incident with the accumulation of detergent-insoluble aggregates of mutant protein, with both of these events occurring well after the appearance of multiple pathologic abnormalities but concurrent with the onset of symptoms. Together, these studies demonstrate that aggregates are composed of globally misfolded, immature SOD1 protein that contribute to the conversion of disease phenotype. We suggest that alternative forms of misfolded SOD1 proteins impart toxicity early in the disease course.

CHAPTER 1
INTRODUCTION

Amyotrophic Lateral Sclerosis

Amyotrophic lateral sclerosis (ALS) is a progressive neurodegenerative disease that selectively targets motor neurons (1). Motor neuron death occurs in the motor cortex, brainstem, and spinal cord, primarily affecting the corticobulbar and corticospinal tracts. Atrophy in these motor tracts results in the development of muscle weakness, fasiculations, atrophy, dysarthria, dysphagia, and respiratory failure (2). Respiratory failure and death occurs three to five years after onset of ALS symptoms (1). The current therapy for all forms of ALS is riluzole (3), which blocks glutamate receptors. However, riluzole does little to extend the survival of ALS patients. The majority of the cases of ALS have no apparent cause, termed sporadic ALS, while 10% of the cases are genetically linked, termed familial ALS (FALS).

Genetics of FALS

Eight FALS loci and six ALS-related genes have been identified and linked to ALS. Four forms of the disease are inherited by autosomal dominance and have clinical features indistinguishable from sporadic ALS: ALS1, ALS3, ALS6, and ALS7. In ALS1, mutations were identified at chromosome 21q22.21 in the gene encoding superoxide dismutase 1 (SOD1) protein, which is a superoxide scavenging enzyme (4). ALS3 involves mutations occurring in chromosome 18q21 at an unknown gene (5). ALS6 is associated with mutations in the fused in sarcoma (FUS) gene located at chromosome 16q12, which is involved in the regulation of transcription and RNA splicing (6). ALS7, located at chromosome 20ptelp13, has an unidentified gene associated with the illness (7, 8). Recently, mutations have been identified in TAR DNA binding protein (TARDBP) at chromosome 1p36; however, to date, only a single family has been described (9). Four forms of FALS are inherited by autosomal dominance and

have clinical features that differ from sporadic ALS: ALS-FTD, ALS with Parkinsonism and dementia, Progressive lower motor neuron disease, and ALS8. ALS-FTD (frontotemporal dementia) results from mutations that occur in chromosome 9q21-q22 (10). ALS with Parkinsonism and dementia is associated with mutations at chromosome 17q21.1 (11) in a gene that encodes for microtubule associated protein tau (MAPT), which functions to stabilize microtubules and promote their assembly (12). Progressive lower motor neuron (LMN) disease is associated with chromosome 2q13 in the p150 subunit of the dynactin 1 (DCTN1) gene (13), which binds to microtubules and cytoplasmic dynein during vesicle transport (14). ALS8 results from mutations at chromosome 20q13.3 (15, 16) in the vesicle associated membrane protein B (VAPB) gene, which is a membrane protein that associates with microtubules (17). The clinical features of this form of ALS are marked by lower motor neuron symptoms, postural tremor, cramps, and fasiculations. ALS4 is a juvenile onset, autosomal dominant form of ALS that is associated with mutations at chromosome 9q34 in the SETX gene (18, 19). SETX is homologous to genes that function in RNA processing. Two forms of the disease are juvenile onset and autosomal recessive: ALS2 and ALS5. ALS2 results from mutations in the ALS2 gene at chromosome 2q33, which encodes for the Alsin protein and functions as a guanine exchange factor for Ran, Rho, and Rab GTPases (20, 21). ALS2 has a slow disease progression and includes primary lateral sclerosis. ALS5 is associated with mutations at chromosome 15q15.1-q21.1 (22) and has no pseudobulbar signs with slow disease progression. Together, the variability in gene loci and resulting disease phenotypes have lead some in the field to propose that ALS is a spectrum disease.

SOD1-Linked FALS

Genetics of SOD1-Linked FALS

Approximately 20% of the FALS cases are caused by dominantly inherited mutations in Cu-Zn superoxide dismutase (SOD1) (Table 1-1) (4). SOD1-linked FALS is characterized as an autosomal dominant disorder, meaning that a single copy of the mutant SOD1 gene is sufficient to cause the ALS phenotype, and one copy of the wild-type gene is present in every cell. However, as more SOD1-linked FALS families are identified, it appears that mutations in SOD1 can be grouped into three types: autosomal dominant with complete penetrance, autosomal dominant with incomplete penetrance, and recessive. SOD1 mutations that produce complete penetrance are those in which all mutant gene carriers develop disease in an age dependent manner: A4V, G37R, L38V, G41S, H43R, D76V, L84F, L84V, N86K, E100G, D101H, I104F, G108V, C111Y, I112M, G114A, L126X, G127X, G141E, L144F, V148G, V148I (Table 1-1). SOD1 mutations that produce incomplete penetrance are those in which not every carrier of the mutant gene develops the disease: A4T, L8Q, V14G, G16S, N19S, E21G, N65S, G72S, D76Y, N86S, A89V, D90A, G93S, A95T, D101N, S105T, I113T, V118L, V118KTGPX, L126S, N139H (Table 1-1). A small subset of mutations are recessively inherited and require two copies of the mutant gene for disease to manifest: D90A and D96N (Table 1-1) (P. Andersen, personal communication).

Disease pathology and progression of SOD1-linked FALS is similar to sporadic ALS. Mutations in SOD1 produce a spectrum of disease variants in ALS, ranging in the age of disease onset, the location of first symptoms, the rate of progression, and the length of disease duration. A subset of mutations result in a more aggressive form of the disease, in which patients die within 3 years of onset: A4T, A4V, C6F, C6G, V7E, L8Q, G10V, G41S, H43R, H48Q, D90V, G93A, D101G, D101H, D101Y, L106V, I112T, R115G, D125H, S134N, V148I, V148G (Table

1-1). A second set of mutations result in longer than average survival after disease onset: K12R, E21G, G41D, H46R, N65S, D76V, A89V, D90A, G93C, G93D, G93S, G93V, E100K, I104F, I113F, L126S, L144F, I149T (Table 1-1). Nevertheless, there are many mutations that produce variable survival times in patients: E21G, G37R, L38V, D76Y, L84F, L84V, N86S, D90A, G93R, I113T, L144S (Table 1-1) (P. Andersen, personal communication).

More than 100 mutations in SOD1 have been identified in FALS cases (Table 1-1). The vast majority are point mutations located within β-strands, a prominent structural element of the protein (23). An additional subset of SOD1 mutations includes frameshift mutations and truncation mutations that occur near the carboxyl terminus of the protein and cause early termination of the protein. The effects of the mutations on normal enzyme activity, protein turnover, and folding vary considerably (24-26). In cell culture and *in vitro* models, enzyme activity ranges from undetectable to near normal (24, 27-30); most mutations accelerate the rate of protein turnover (24, 29); and many mutations increase the susceptibility of SOD1 to disulfide reduction (31). Because some SOD1 mutants retain high activity (29) and because the targeted deletion of SOD1 in mice does not induce ALS-like symptoms (32), mutant SOD1 is proposed to cause disease by the acquisition of toxic properties.

This work focuses on SOD1-linked FALS as this genetically linked form of the disease most closely mimics disease progression and symptoms of classic, sporadic ALS. Thus, insights into disease progression and disease mechanisms may be translatable to the sporadic form of the disease.

SOD1 Protein

SOD1 is a metalloenzyme responsible for metabolizing oxygen radicals that are produced during normal cellular respiration (33). SOD1 converts oxygen radicals into hydrogen peroxide

and oxygen. SOD1 is ubiquitously expressed in all cell types. Within the cell, SOD1 is primarily located in the cytosol but has been found at lower levels in nuclei, peroxisomes, and mitochondria (34-36). The active enzyme is a homodimer of two 153 amino acid subunits. Each subunit binds one atom of copper in the active site (H46, H48, H63, and H120) and one atom of zinc in the zinc loop (H63, H71, H80, and D83), which provides structural stability (37). Each normally folded SOD1 subunit is characterized by a β-barrel containing eight anti-parallel β-strands, an electrostatic loop that directs the substrate into the active site, and an intramolecular disulfide bond between cysteine 57 and cysteine 146 (38). Together, these structural features produce an extremely stable protein, retaining its structure in 1% SDS and 8M urea (39).

Table 1-1. SOD1-linked familial ALS mutations

SOD1 mutant	Penetrance*	Disease course*	Activity	Aggregation	Reference
A4S	N/A	N/A	N/A	N/A	(40)
A4T	Incomplete	Aggressive	N/A	++++	(41) #
A4V	Complete	Aggressive	Normal	+++	(42-44)
V5L	N/A	N/A	N/A	N/A	•
C6F	N/A	Aggressive	N/A	+++	(45, 46)
C6G	N/A	Aggressive	N/A	+++	(46, 47)
V7E	N/A	Aggressive	Normal	N/A	(48, 49)
L8Q	Incomplete	Aggressive	Normal	N/A	(49, 50)
L8V	N/A	N/A	N/A	N/A	(51)
G10V	N/A	Aggressive	N/A	N/A	(52)
G12R	N/A	Slow	N/A	N/A	(53)
V14G	Incomplete	N/A	N/A	+++	(54) #
V14M	N/A	N/A	N/A	N/A	(55)
G16A	N/A	N/A	N/A	N/A	(51)
G16S	Incomplete	N/A	N/A	N/A	(56)
N19S	Incomplete	N/A	N/A	N/A	(51)
F20C	N/A	N/A	N/A	N/A	(51)
E21G	Incomplete	Variable	N/A	++	(50) #
E21K	N/A	N/A	N/A	++	(57)
Q22L	N/A	N/A	N/A	N/A	(51)
V29A	N/A	N/A	N/A	N/A	•
V29insA	N/A	N/A	N/A	N/A	(58)
G37R	Complete	Variable	Normal	++	(4, 43, 49)
L38R	N/A	N/A	N/A	N/A	(59)
L38V	Complete	Variable	Normal	N/A	(4, 44, 49)
G41D	N/A	Slow	Normal	++	(4, 43, 49)
G41S	Complete	Aggressive	Normal	+++	(4, 44) #
H43R	Complete	Aggressive	Normal	+++	(4, 44) #
F45C	N/A	N/A	N/A	N/A	(60)
H46R	Complete	Slow	Reduced	++	(43, 44, 61)
V47A	N/A	N/A	N/A	N/A	(51)
V47F	N/A	N/A	N/A	N/A	(51)
H48Q	N/A	Aggressive	Reduced	++	(43, 49, 62)
H48R	N/A	N/A	N/A	N/A	(51)
E49K	N/A	N/A	N/A	N/A	(59)
T54R	N/A	N/A	N/A	N/A	(51)
S59I	N/A	N/A	N/A	N/A	(51)
N65S	Incomplete	Slow	N/A	N/A	(63)
P66A	N/A	N/A	N/A	N/A	•
L67R	N/A	N/A	N/A	N/A	(59)
G72S	Incomplete	N/A	Normal	N/A	(44, 64)
G72C	N/A	N/A	N/A	N/A	(65)

Table 1-1. Continued

SOD1 mutant	Penetrance*	Disease course*	Activity	Aggregation	Reference
D76V	Complete	Slow	N/A	N/A	(66)
D76Y	Incomplete	Variable	Normal	N/A	(44, 54)
H80R	N/A	N/A	N/A	+	(67)
L84F	Complete	Variable	N/A	N/A	(64)
L84V	Complete	Variable	Normal	+++	(49, 55) #
G85R	N/A	Variable	Reduced	+++	(4, 44)
N86I	N/A	N/A	N/A	N/A	•
N86D	N/A	N/A	N/A	N/A	(68)
N86K	Complete	N/A	N/A	N/A	(69)
N86S	Incomplete	N/A	Normal	N/A	(49, 70)
V87A	N/A	N/A	N/A	N/A	(51)
V87del	N/A	N/A	N/A	N/A	(51)
T88delACTGCTGAC	N/A	N/A	N/A	N/A	(51)
A89V	Incomplete	Slow	N/A	N/A	(71)
A89T	N/A	N/A	N/A	N/A	(51)
D90A	Incomplete	Variable	Normal	+++	(44, 72) #
D90A	Recessive	Slow	Normal	+++	(44, 72) #
D90V	N/A	Aggressive	N/A	N/A	(73)
G93A	N/A	Aggressive	Normal	+++	(4, 44) #
G93C	N/A	Slow	Normal	+++	(4, 43, 49)
G93D	N/A	Slow	N/A	++	(74)(49) #
G93R	N/A	Variable	Normal	++++	(75)(49) #
G93S	Incomplete	Slow	N/A	+++	• #
G93V	N/A	Slow	Normal	+++	(76) #
A95T	Incomplete	N/A	N/A	N/A	(60)
A95V	N/A	N/A	N/A	N/A	(51)
D96N	Recessive	N/A	N/A	N/A	(77)
D96V	N/A	N/A	N/A	N/A	•
V97M	N/A	N/A	N/A	N/A	(51)
I99V	N/A	N/A	N/A	N/A	•
E100G	Complete	Variable	Normal	+++	(4, 49) #
E100K	N/A	Slow	Normal	++++	(44) • #
D101G	N/A	Aggressive	Normal	++++	(78) (49) #
D101H	Complete	Aggressive	N/A	N/A	(79)
D101N	Incomplete	Aggressive	Normal	+	(44, 80) #
D101Y	N/A	Aggressive	N/A	N/A	(81)
I104F	Complete	Slow	N/A	N/A	(82)
I104del	N/A	N/A	N/A	N/A	(51)
S105L	N/A	N/A	N/A	N/A	(51)
S105delTCACTC	Incomplete	N/A	N/A	N/A	(51)
L106V	N/A	Aggressive	N/A	N/A	(42)
G108V	Complete	N/A	N/A	N/A	(83)
C111Y	Complete	N/A	N/A	++	(46, 84)

Table 1-1. Continued

SOD1 mutant	Penetrance*	Disease course*	Activity	Aggregation	Reference
I112M	Complete	N/A	N/A	N/A	(63)
I112T	N/A	Aggressive	N/A	N/A	(74)
I113F	N/A	Slow	N/A	N/A	(51)
I113T	Incomplete	Variable	Normal	++	(4, 43, 49)
G114A	Complete	N/A	N/A	N/A	(51)
R115G	N/A	Aggressive	Normal	N/A	(49, 85)
V118L	Incomplete	N/A	N/A	N/A	(51)
V118insAAAAC	N/A	N/A	N/A	N/A	(86)
V118KTGPX	Incomplete	N/A	N/A	N/A	•
D124G	N/A	N/A	N/A	N/A	(51)
D124V	N/A	N/A	Reduced	+++	(76)
D125H	N/A	Aggressive	Reduced	+	(44, 62) #
D125delTT	N/A	N/A	N/A	N/A	(87)
L126S	Incomplete	Slow	Reduced		(88)
L126stop	N/A	N/A	N/A	+++	(50)
L126insTT	Complete	N/A	Reduced	++++	(89)
G127insTGGG	N/A	N/A	N/A	N/A	(54)
Q132insTT	N/A	N/A	N/A	N/A	(83)
Q132del	N/A	N/A	N/A	N/A	(76)
E133V	N/A	N/A	N/A	N/A	•
E133del	N/A	N/A	N/A	+	(76)
E133insTT	N/A	N/A	N/A	N/A	(83)
S134N	N/A	Aggressive	Reduced	+	(44, 90) #
N139H	Incomplete	N/A	N/A	N/A	(91)
N139K	N/A	N/A	Reduced	+++	(89)
A140G	N/A	N/A	N/A	N/A	(92)
G141E	Complete	N/A	N/A	N/A	(79)
G141stop	N/A	N/A	N/A	N/A	(51)
L144F	Complete	Slow	Normal	++	(49, 93) #
L144S	N/A	Variable	N/A	++	(94) #
A145G	N/A	N/A	N/A	N/A	•
A145T	N/A	N/A	N/A	N/A	(94)
C146R	N/A	N/A	N/A	N/A	(46, 50)
G147R	N/A	N/A	N/A	N/A	(51)
V148G	Complete	Aggressive	Normal	+++	(49, 93) #
V148I	Complete	Aggressive	N/A	+	(82)
I149T	N/A	Slow	Normal	N/A	(49, 89)
I151S	N/A	N/A	N/A	N/A	(51)
I151T	N/A	N/A	N/A	N/A	(95)

+ - low (no aggregation in 24 hours), ++ - moderate (<0.5), +++ - high (0.7-1.7), ++++ - extreme (>1.8)

- Prudencio M, Hart PJ, Borchelt DR, Andersen PM. Submitted.

* - PM Andersen, personal communication

• - http://alsod.iop.kcl.ac.uk/Als/index.aspx

Toxic Property of Mutant SOD1

Two hypotheses have been proposed to explain the toxic property that mutant SOD1 acquires: the oxidative damage hypothesis and the oligomerization hypothesis. The oxidative damage hypothesis suggests that mutant SOD1 aberrantly produces hydrogen peroxide and peroxynitrite, resulting in damage to the cell (96). Under normal conditions, wild-type SOD1 has a very low propensity to produce these toxic side products: wild-type SOD1 may undergo peroxidation through interaction with hydrogen peroxide, producing toxic hydroxyl radicals (30, 97, 98), or wild-type SOD1 may react with peroxynitrates, which result in nitronium ions that can covalently modify tyrosines (99-101). Under the oxidative stress hypothesis, mutations in SOD1 may increase the propensity to form these toxic side products. The caveat to the oxidative damage hypothesis is that it requires mutant SOD1 to bind copper, an essential element for SOD1 activity. A subset of FALS-linked SOD1 mutants are classified as metal binding mutants due to defects at or near metal binding sites (26, 27, 102, 103). Metal binding mutants have no SOD1 activity and do not produce hydrogen peroxide or peroxynitrite (26). In transgenic mice modeling FALS, mice overexpressing SOD1 with two (H46R/H48Q) or four (H46R/H48Q/H H63G/H120G) of the copper binding sites mutated to FALS residues develop paralysis (43, 104). Thus, mouse studies have demonstrated that SOD1 activity and the correct binding of copper is not required for FALS phenotype.

Alternatively, the oligomerization hypothesis proposes that misfolded SOD1 proteins interact to form increasingly high-molecular-weight oligomers (105). Mutations in SOD1 destabilize the native state protein and possibly promote aggregation by diminishing metal binding and altering the secondary, tertiary, or quaternary structures (106-111). Tissues from FALS patients (112) and from SOD1 transgenic mice (113) contain SOD1 positive inclusions in the brainstem and spinal cord. Aggregated forms of mutant SOD1 can also be detected by

detergent-insolubility or size exclusion filtration (23, 43, 114, 115). Some suggest that SOD1 aggregate-mediated toxicity occurs by sequestering cellular proteins and heat shock proteins (116); the clogging of proteasomes by indigestible protein fragments (117); or the localization of SOD1 aggregates to vital organelles (118).

Because SOD1 mutants have a diverse range of biophysical characteristics and produce a similar ALS phenotype, we are searching for a common mechanism of toxicity. We propose that mutations in SOD1 predispose the protein to self-oligomerize and that SOD1 aggregates play a significant role in toxicity and disease course.

Models of FALS

Mouse Models of FALS

Mouse models of FALS provide insight into the role of mutant SOD1 in motor neuron death, the progression of the disease, and the effectiveness of possible drug targets. All mouse models of FALS that overexpress mutant human SOD1 share a similar phenotype of motor neuron loss, muscle wasting, and hindlimb paralysis. Mouse models of FALS differ from the human ALS phenotype in that there is no upper motor neuron pathology. In these mouse models, human genomic SOD1 is expressed under the control of the human SOD1 promoter, which produces ubiquitous expression of the human protein. FALS-linked SOD1 mutants that have been expressed in mice include: G93A (119), G37R (120), G85R (113), L126Z (115), G86R (121), D90A (122), and Gins127TGGG (123). Mouse models have also been developed to express forms of mutant SOD1 that combine disease-linked mutations and include experimental mutations to study the mechanism of SOD1 toxicity: H46R/H48Q (104) and H46R/H48Q/H63G/H120G (43). There is some variability in survival of different mutant mice, which may be due to expression levels of the transgene.

FALS-linked SOD1 mutant mice are predominantly characterized by loss of motor neurons, inclusions, and neuropils in the brainstem and spinal cord (119, 124, 125). Prominent neuronal loss occurs in the ventral horn of the spinal cord (125). Surviving, atrophic motor neurons exhibit hyaline filamentous, neurofilament-rich, spheroidal inclusions (125). Within the ventral horn, SOD1 positive inclusions are predominantly detected in neurons (125). Protein inclusions are primarily positive for SOD1 and ubiquitin (125-127). However, some inclusions have varied reactivity with Hsp40, Hsp60, Hsp70, Hsp90 (125), and small heat shock proteins (Hsp25 and αB crystallin) (43, 115). Filamentous structures bound to SOD1 have morphology similar to amyloid fibrils (128-130). These structures also bind Congo red and Thioflavin T and S (43, 104, 108), markers for extensive β-sheet stacking. Wild-type SOD1 transgenic mice do not develop neuronal loss or inclusions (113, 119).

In all SOD1 transgenic mice, the appearance of symptoms is associated with an accumulation of sedimentable structures that are detergent-insoluble, which is diagnostic for protein aggregation (43, 104, 114, 115, 117, 123, 131, 132). Detergent-insoluble SOD1 protein is exclusively located in the affected tissues (brainstem and spinal cord) (114). Because inclusion bodies differ in abundance and cause difficulty for correlation to disease in mouse models, we prefer to measure aggregation by detergent-insolubility of SOD1 protein.

Alternative mouse models of SOD1-linked FALS

Several groups of created alternative mouse models of FALS that produce varying in expression patterns in order to address key questions that remain in the field. Recently, mice were generated that express mutant SOD1 (G93A) under the control of the Thy1.2 promoter, which produces mutant SOD1 expression specifically in neuronal cells (133). Heterozygous Thy1.2-G93A mice do not develop the ALS phenotype; however, when these mice are bred for

homozygousity or crossed to SOD1-wild-type mice, mice develop disease by 20 months with detectable aggregates of the mutant protein in affected tissue (133). Other groups have also demonstrated that breeding mutant SOD1 transgenic mice (ubiquitously expressing, traditional models) to wild-type SOD1 transgenic mice produces accelerated disease with more robust levels of SOD1 aggregates accumulating in affected tissues (134).

SOD1 toxicity is non-cell autonomous

Several groups have generated evidence to suggest that mutant SOD1 toxicity affects multiple types of cells in the nervous system. Recent studies have examined the role of mutant SOD1 toxicity in motor neurons (135), microglia (135), muscle (136), astrocytes (137), and Schwann cells (137) in SOD1 transgenic mice. Results from these studies demonstrate that the expression of mutant SOD1 in motor neurons is a primary determinant of disease onset and progression. However, the aberrant function of mutant SOD1 in other cells may also influence the progression of the disease. Chimeric mice that selectively express mutant SOD1 in motor neurons develop ALS; however, chimeric mice that have a majority of non-mutant cells survive and mutant expressing cells do not appear sick (aggregates, inclusions, or vacuoles) (138). Lowering levels of mutant SOD1 in microglia (135) or astrocytes (137) slows the later stages of disease progression, while the onset remains unchanged. Lowering mutant SOD1 in muscle, however, has no effect on disease onset, progression, or survival (136). Furthermore, mice selectively expressing mutant SOD1 (G93A) in muscle tissue develop muscle abnormalities without developing ALS symptoms (139). Together, these studies suggest that damage to cells other than motor neurons, mediated by mutant SOD1, may be an important feature of FALS disease progression. This feature of the disease provides an interesting avenue for the future studies of aggregates and the factors effecting their formation in specific tissues.

Cell Culture Model of Mutant SOD1 Aggregation

Cell culture models provide a valuable tool for screening for SOD1 aggregation, a hallmark feature of FALS in human and mouse models. In cell aggregation assays, mutant human SOD1 cDNA is expressed in human immortalized cell lines (HEK293-FT), and protein fractions are isolated by high-speed centrifugation and non-ionic detergent extraction to isolate the detergent-insoluble SOD1, representing aggregating SOD1 protein (43, 104, 114, 115). This cell aggregation assay accurately models aggregation in mutant SOD1 transgenic mice. All of the FALS mutants expressed in cell culture result in a heightened potential to form sedimentable structures that are detergent-insoluble (43, 104, 114, 115, 117, 123, 131, 132). As we continue to study more SOD1 mutants in cell culture, it is evident that all natural FALS mutants have some propensity to aggregate; however, the rate of aggregation can differ greatly (140). Furthermore, our group has shown that the rate of aggregation of individual mutants in cell culture inversely correlates with disease duration of that mutant in FALS patients (Prudencio M, Hart PJ, Borchelt DR, Andersen P, submitted).

Because we are searching for a common mechanism for toxicity, and all mutants possess some propensity to form detergent-insoluble, sedimentable species, we will focus on studying SOD1 aggregation in this cell culture model. The application of compounds to mutant SOD1-expressing cells can provide a means for identifying inhibitors of aggregation and for studying the factors effecting SOD1 aggregate formation.

CHAPTER 2

A LIMITED ROLE FOR DISULFIDE CROSS-LINKING IN THE AGGREGATION OF MUTANT SOD1 LINKED TO FAMILIAL AMYOTROPHIC LATERAL SCLEROSIS•

Introduction

One proposed toxic property of mutant SOD1 is aggregation of SOD1 protein. Our group and others have found that eight FALS mutants (in transgenic mouse models) and thirteen FALS mutants (in cell culture models) exhibit a heightened potential to form aggregates (43, 104, 114, 115, 117, 123, 131, 132). These detergent-insoluble (aggregated) forms of SOD1 proteins contain molecules that are cross-linked by intermolecular disulfide bonds (23, 141, 142). Each SOD1 subunit possesses four cysteine residues at amino acids 6, 57, 111, and 146, and an intramolecular disulfide bond, between cysteine residues at 57 and 146, is found in the natively folded holo-enzyme (38). In symptomatic SOD1 transgenic mice, high-molecular-weight forms of SOD1 are visible by SDS-PAGE when detergent-insoluble protein is electrophoresed in the absence of reducing agents (23, 141). These high-molecular-weight, disulfide-linked, forms of SOD1 become more abundant as ALS-like symptoms progress (23, 141, 142).

There has been considerable attention focused recently on the role of disulfide cross-linking in the aggregation of SOD1 (both FALS-mutant and wild-type protein) (23, 141-145). Initial studies of purified SOD1 *in vitro* suggest that all four cysteine residues of SOD1 are capable of forming intermolecular disulfide bonds, with cysteines at 57 and 146 perhaps playing more important roles (141). However, in the past year, there have been several studies that used cell culture models or *in vitro* aggregation studies to examine the role of individual cysteine residues in mutant SOD1 aggregation (143-145). Collectively, these studies have focused

• This work is adapted from a manuscript published in *The Journal of Biological Chemistry* 283(20):13528-37 (2008).

attention on cysteines 6 and 111 of SOD1 as playing important roles in modulating mutant SOD1 aggregation with the putative mechanism involving formation of aberrant intermolecular disulfide bonds.

In the present study, we have systematically examined the role of the four cysteine residues in SOD1 in the formation of aberrant disulfide bonds and protein aggregates. Our data suggest that although cysteines 6 and 111 may play critical roles in the formation of SOD1 aggregates, the mechanism of mutant protein aggregation does not appear to require extensive intermolecular disulfide linkages. Analysis of a series of experimental mutants led us to conclude that cysteines 6 and 111 may modulate structural features of the protein, apart from disulfide linkages, that influence aggregate formation.

Methods

Construction of SOD1 Expression Vectors

FALS and experimental mutations were created in the cDNA of human SOD1 or mouse SOD1 using standard PCR strategies with oligonucleotides that introduce specific point mutations (Table 2-1). All mutant cDNAs created in this manner were sequenced in their entirety to verify the presence of the desired mutations and the absence of undesired mutations. SOD1 mutants were expressed in the pEF-BOS vector (146).

Tissue Culture Transfection and Transgenic Mice

Human embryonic kidney 293 cells with a T antigen (HEK 293-FT) were cultured in 60-mm poly-D lysine coated dishes. Upon reaching 95% confluency, cells were transfected with Lipofectamine 2000 (Invitrogen, Carlsbad, CA, USA) and then harvested after 24 hours.

The SOD1 transgenic mice have been previously characterized: the G93A variant [B6SJL-TgN (SOD1-G93A)1Gur; Jackson Laboratory, Bar Harbor, ME, USA] (119), the G86R variant

[FVB-Tg(Sod1-G86R)M1Jwg/J; Jackson Laboratory, Bar Harbor, ME, USA] (121), and the wild type (WT) protein (line 76) (147).

Table 2-1. Aggregation propensity of SOD1 mutants at cysteine residues

SOD1 mutants	Average aggregation propensity	Production of aggregates°
WT	0.10	-
G85R	0.99	+++
C6G	0.92	+++
C6F	1.08	+++
C111Y	0.51	+++
C111S	0.07	-
C146R	1.3	+++
C6G/C111S	0.07	-
C6G/C111Y	0.06	-
C6F/C111S	0.45	++
G85R/C111S	0.12	-
CSYR	0.84	+++
GCYR	0.04	-
GSCR	0.98	+++
GSYC	0.01	-
GSYR	0.06	-
FSYR	0.89	+++

° See Table 1-1

SOD1 Aggregation Assay by Differential Extraction

The procedures used to assess SOD1 aggregation by differential detergent extraction and centrifugation were similar to previous descriptions (43). Spinal cords were homogenized with a probe sonicator (Microson XL2000; Misonix, Farmingdale, NY – 2W at 22.5 kHz) in 1:10 w/v of 1x TEN (10mM Tris, 1mM EDTA, 100mM NaCl). In cell culture experiments, cells were scraped from the culture dish in phosphate buffered saline (PBS) and centrifuged to pellet the cells before the pellets were resuspended in 100 µl 1xTEN. Spinal cord homogenates and resuspended cell culture pellets were then mixed with an equal volume of 2x extraction buffer 1 (10 mM Tris, 1 mM EDTA, 100 mM NaCl, 1% Nonidet P40, and 1x protease inhibitor cocktail) and sonicated as described above. The resulting lysate was centrifuged for 5 minutes at >100,000g in a Beckman AirFuge to separate a non-ionic detergent-insoluble pellet (P1) from

the supernate (S1). The supernate (S1) was decanted and saved for analysis. The pellet (P1) was resuspended in 200 μl of 1x extraction buffer 2 (10 mM Tris, 1 mM EDTA, 100 mM NaCl, 0.5% Nonidet P40, and 1x protease inhibitor cocktail) and sonicated to resuspend. The extract was then centrifuged for 5 minutes at >100,000g in a Beckman AirFuge to separate a pellet (P2) from the supernate. The P2 fraction was resuspended in buffer 3 (10 mM Tris, 1 mM EDTA, 100 mM NaCl, 0.5% Nonidet P40, 0.25% sodium dodecyl sulfate (SDS), 0.5% deoxycholic acid, and 1x protease inhibitor cocktail) by sonication and saved for analysis. Protein concentration was measured in S1 and P2 fractions by BCA method as described by the manufacturer (Pierce, Rockford, IL, USA) (Table 2-1).

Assay for Disulfide Cross-Linked SOD1

In variations of this procedure, buffer 1 was modified to include 100 mM iodoacetamide as noted in figure legends and the text. Additionally, in one set of experiments (see Fig. 2-8) SDS was substituted for NP40 in all extraction buffers; 2x SDS buffer (10 mM Tris, 1 mM EDTA, 100 mM NaCl, 1% SDS, and 1x protease inhibitor cocktail) was substituted for buffer 1, and a 1x SDS buffer (10 mM Tris, 1 mM EDTA, 100 mM NaCl, 0.5% SDS, and 1x protease inhibitor cocktail) was substituted for buffers 2 and 3.

Immunoblotting

Standard sodium dodecyl sulfate-polyacrylamide gel electrophoresis (SDS-PAGE) was performed in 18% or 4-20% Tris-Glycine gels (Invitrogen, Carlsbad, CA, USA). Samples were boiled for 5 minutes in Laemmli sample buffer prior to electrophoresis (148). In some experiments, reducing agent (5% β-mercaptoethanol- βME) was omitted from the sample buffer. Immunoblots were probed with rabbit polyclonal antibodies termed hSOD1 or m/hSOD1 at dilutions of 1:2500. The hSOD1 antibody is a peptide antiserum that binds to amino acids 24-36

(not conserved between mouse and human SOD1 proteins), and m/h SOD1 antibody is a peptide antiserum that recognizes amino acids 124-136 (conserved between mouse and human SOD1 proteins) (24).

Quantitative Analysis of Immunoblots

Quantification of the SOD1 protein in detergent-insoluble and detergent-soluble fractions was performed by measuring the band intensity of SOD1 in each lane using a Fuji Imaging system (FUJIFILM Life Science, Stamford, CT USA). The untransfected control served as background. SOD1 aggregation propensity was a function of the ratio of the band intensity in the detergent-insoluble fraction to that of the detergent-soluble fraction. The mean and standard error of the mean (SEM) were calculated for the aggregation propensity of each sample in each experiment. A homoscedastic student's T-test was used to calculate significance.

Results

Our initial study focused on examining known FALS mutations at cysteine residues to determine whether loss of any single cysteine residue diminishes SOD1 aggregation. This initial study also provided a reference point to which to compare our next set of studies when these mutations were experimentally combined in recombinant SOD1 proteins. FALS-linked SOD1 cysteine mutants (C6G, C6F, C111Y, and C146R) were expressed in HEK293-FT cells, and the cell lysates were separated into detergent-soluble and detergent-insoluble fractions following previously established protocols (43). All four mutants produced detergent-insoluble, sedimentable forms of mutant protein. In this assay, the detergent-soluble fractions (Fig. 2-1B) are representative of the steady-state levels of each mutant (an indication of the efficiency of transfection and level of expression). These experiments and those that follow include the G85R mutant as a positive control; this mutant exhibits anomalous migration in SDS-PAGE, migrating slightly faster than expected for its molecular weight. The aggregation potential, a measure

comparing the band intensity of the detergent-insoluble fraction (Fig. 2-1A) to the detergent-soluble fraction (Fig. 2-1B), for each of the cysteine mutants was significantly different from WT protein (Fig. 2-1C).

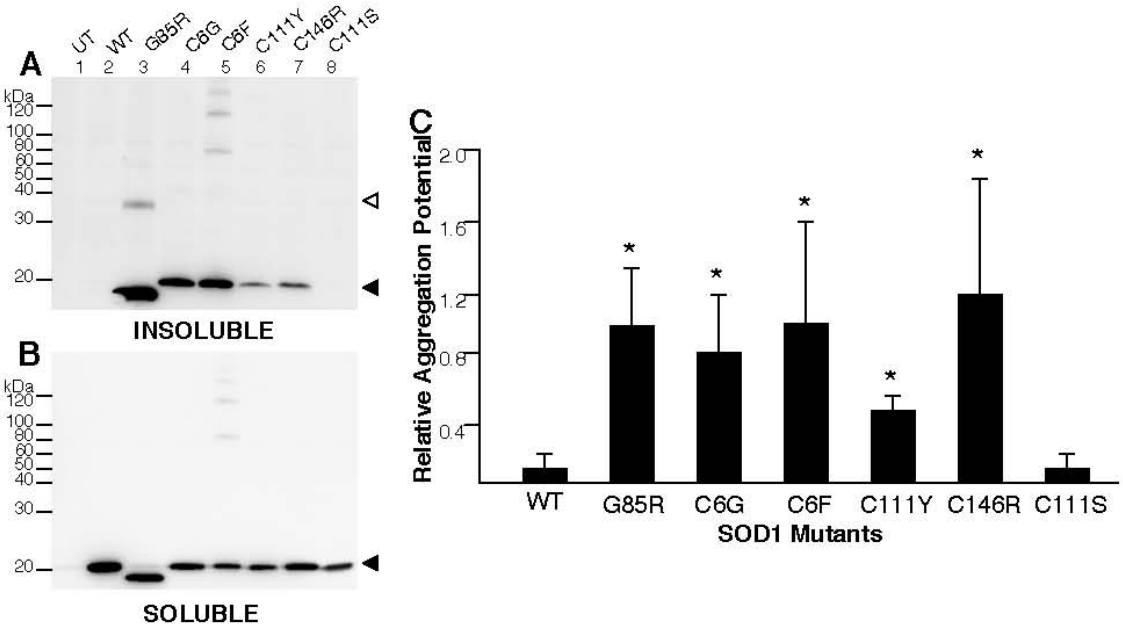

Figure 2-1. SOD1 aggregation of FALS cysteine mutants in transfected cells. Mutants were expressed in HEK293-FT cells and aggregate levels were determined as described in Methods. UT, untransfected cells. WT, cells transfected with vectors for WT SOD1. SOD1-G85R, a robustly aggregating FALS mutant, provides a positive control. SDS-PAGE was performed in the presence of a reducing agent in an 18% Tris-Glycine gel. Immunoblots were probed with an antiserum specific for human SOD1 (hSOD1). A) Detergent-insoluble protein fraction (20 ⌈g). B) Detergent-soluble protein fraction (5 ⌈g). C) Relative aggregation is a function of the amount of SOD1 found in the pellet fraction as compared to the supernatant (see Methods). The graph represents the mean (±SEM – error bars) of at least three different experiments. All FALS mutants were statistically different from WT SOD1: (*) $p<0.001$. C111S was not statistically different from WT SOD1. Open arrowhead; dimer-sized SOD1 molecules. Closed arrowhead; monomeric SOD1 molecules.

The detergent-insoluble fractions from cells transfected with SOD1-G85R often contained a form of the protein that migrates at a size expected for a dimer. Interestingly, lysates from cells that expressed the C6F mutant (alone or in combination with other mutations – see below) invariably contained forms of mutant SOD1 that migrated at higher-molecular-weight; often a

laddering effect was noted, indicative of the assembly of some type of repeating structure. These structures persist despite boiling in the presence of SDS and βME; thus, they are presumably either molecules that are covalently cross-linked by mechanisms other than disulfide or are assemblies of mutant SOD1 that are resistant to denaturation. In the case of C6F, these multimer-like structures were also detected in detergent-soluble fractions. The origin and relative importance of these structures is presently unclear.

In analyzing the data from the cysteine mutants, we noted variability in the amount of aggregated mutant protein produced from one experiment to the next, possibly due to variation in transfection efficiency between experiments. For example, the immunoblot shown in Fig. 2-1A suggests that the C146R mutant produces less detergent-insoluble protein than the C6G or C6F mutants. However, when measurements of multiple immunoblots from replicate experiments were compared, then the C146R mutant was not reproducibly different from the other cysteine mutants (Fig. 2-1C). The mutation of cysteine 111 to serine, a non-FALS mutation, did not produce a SOD1 protein that spontaneously aggregates (Fig. 2-1A, lane 8; Fig. 2-1C). In the analysis of these mutants and in the studies that follow, the principal outcome measure was whether the amount of mutant protein in the detergent-insoluble fraction at ~24 hours post-transfection was statistically different from WT SOD1, an indication of aggregation. More subtle differences in aggregation levels between mutants (e.g. C6F vs. C111Y, aggregation potentials of 1.08 and 0.51, respectively) are difficult to interpret and were not the focus of this study. The only measure of interest was that both mutants score as statistically different from wild-type protein. Overall, we can conclude that FALS mutations at cysteine residues 6, 111, or 146 induce, possibly to varying degrees, aggregation of the protein.

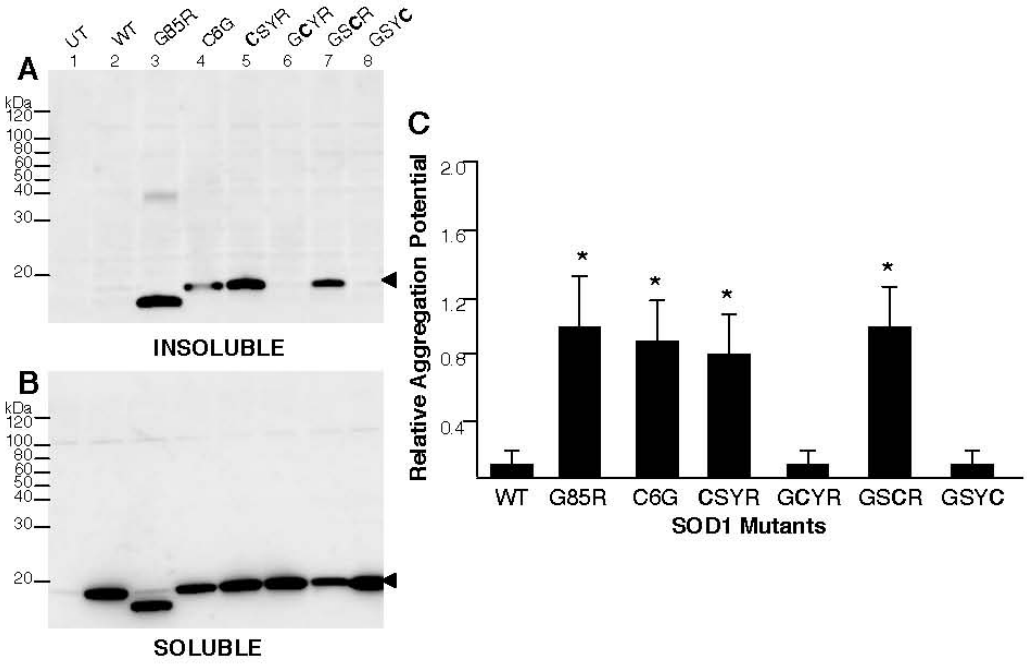

Figure 2-2. Role of cysteines 6 and 111 in SOD1 aggregation. Mutants were expressed in HEK293-FT cells and aggregate levels were determined as described in Methods. SDS-PAGE was performed in the presence of a reducing agent in an 18% Tris-Glycine gel. Immunoblots were probed with m/hSOD1 antiserum. A) Detergent-insoluble protein fraction (20 μg). B) Detergent-soluble protein fraction (5 μg). C) Quantification of the ratio of SOD1 in pellet fractions relative to supernatant was assessed as a measure of relative aggregation. The data represents the mean (±SEM – error bars) of at least three different experiments. Mutants where the ratios were statistically different from WT SOD1 were marked by (*): $p<0.0001$. Some mutants were not statistically different from WT SOD1: GCYR, GSYC, GSYR. CSYR=C6/C57S/C111Y/C146R, GCYR=C6G/C57/C111Y/C146R, GSCR=C6G/C57S/C111/C146R, GSYC=C6G/C57S/C111Y/C146. Closed arrowhead; monomeric SOD1 molecules.

To assess the roles of individual cysteine residues in mutant SOD1 aggregation, four SOD1 constructs were created, each of which contained one intact cysteine residue with the other three cysteines mutated (C6G, C57S, C111Y, or C146R). In this experiment, the C57S mutation is an experimental mutation. When we began this work, no FALS mutations at cysteine 57 were known, and the C57S mutation serves only as a means to eliminate the cysteine residue. These mutants were expressed in HEK293-FT cells and cell lysates were assayed for

aggregate formation as described above. When cysteine 6 (C57S/C111Y/C146R; labeled CSYR) or cysteine 111 (C6G/C57S/C146R; labeled GSCR) were intact, detergent-insoluble mutant protein was consistently detected within 24 hours (Fig. 2-2A, lanes 5 and 7). In all mutants, a considerable fraction of the mutant protein was soluble in detergent (Fig. 2-2B), an indicator of the overall level of expression of the different mutants. From replicate experiments, the aggregation potentials for mutants with cysteine 6 or cysteine 111 intact were determined to be significantly different from WT SOD1 protein (Fig. 2-2C). Much less aggregated SOD1 was detected when cysteine 57 (C6G/C111Y/C146R; labeled GCYR) or cysteine 146 (C6G/C57S/C111Y; labeled GSYC) were the only cysteines intact (Fig. 2-2A, lanes 6 and 8). Neither of these later two mutants differed from the aggregation potential for WT SOD1 (Fig. 2-2C). Notably, the two mutants that failed to form aggregates (C6G/C111Y/C146R and C6G/C57S/C111Y) produced detergent-soluble forms of these proteins at levels equivalent to those that produced aggregates (Fig. 2-2B, lanes 6 and 8), indicating that similar levels of expression were achieved. These results indicate that cysteine 6 and cysteine 111 play important roles in inducing the aggregation of human SOD1.

Because our studies indicate that proteins containing only a single cysteine at 6 or 111 alone will rapidly aggregate, we sought to determine if these residues are required for SOD1 aggregation. Two constructs were generated in which all four cysteine residues (C6G or F, C57S, C111Y, C146R) were mutated and expressed in HEK293-FT cells for assessment of aggregation. One of these constructs in which cysteine 6 was mutated to glycine in the context of three other mutants (C6G/C57S/C111Y/C146R) failed to produce aggregates within 24 hours (Fig. 2-3A, lane 4). However, when cysteine 6 was mutated to phenylalanine (C6F/C57S/C111Y/C146R), the detergent-insoluble fraction contained significant amounts of

aggregated protein (Fig. 2-3A, lane 5). The aggregation potential for the C6F version of the four-cysteine variant (C6F/C57S/C111Y/C146R) was significantly different from WT SOD1 and roughly equivalent to the natural FALS mutant SOD1-G85R (Fig. 2-3C). The difference in the propensity of the two 4-Cys mutants to aggregate did not appear to be due to a lower expression of the C6G version, as the level of this mutant protein in the detergent-soluble fraction was similar to that of the C6F version (Fig. 2-3B, lanes 4 and 5). Thus, while cysteine 6 and 111 may play a role in modulating the rate or propensity of mutant human SOD1 to aggregate, the presence of a cysteine residue is not required for rapid aggregate formation.

To further explore the role of cysteine residues 6 and 111 in aggregation, we produced a series of constructs in which these two cysteine residues were manipulated. Using the cell aggregation assay described above, we observed that when the C111S mutation was added to C6G, C6F, or G85R, less detergent-insoluble protein was formed as compared to the FALS mutants alone (Fig. 2-4A, lanes 4, 6, 8, and 9). The level of aggregated protein in cells transfected with C6G/C111S and G85R/C111S double mutants was not different from that of cells transfected with WT SOD1 (Fig. 2-4C). Next, the FALS mutation at cysteine 111 (C111Y) was combined with the FALS mutant at cysteine 6 (C6G). Although each of these FALS mutants aggregated when mutated alone (see Fig. 2-1A), when combined the amount of detergent-insoluble SOD1 detected was not different from WT SOD1 (Fig. 2-4A and C). All combination mutants were detected in the detergent-soluble fraction at similar levels, indicating that the protein was stably expressed and only a fraction of the total mutant SOD1 protein aggregates (Fig. 2-4B). These data provide evidence that cysteines 6 and 111 play a role in the formation of SOD1 aggregates with the rate of aggregation slowing significantly when cysteine 111 was mutated to serine.

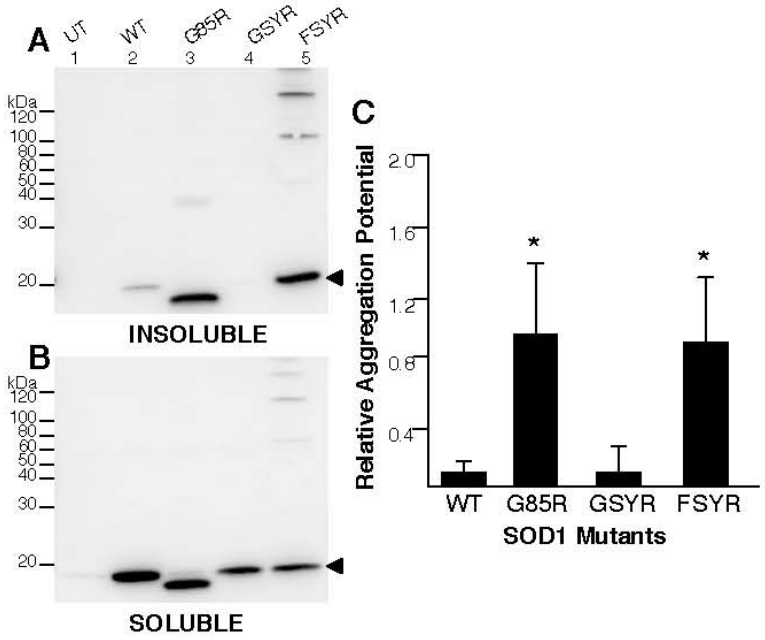

Figure 2-3. Cysteine residues are not required for SOD1 aggregate formation. Mutants were expressed in HEK293-FT cells and aggregate levels were determined as described in Methods. SDS-PAGE was performed in the presence of a reducing agent in an 18% Tris-Glycine gel. Immunoblots were probed with m/hSOD1 antiserum. A) Detergent-insoluble protein fraction (20 μg). B) Detergent-soluble protein fraction (5 μg). C) Quantification of relative aggregation potential (mean ratio ±SEM). Mutants G85R and FSYR were significantly different from the aggregation potential of WT SOD1: (*) $p<0.0009$. GSYR=C6G/C57S/C111Y/C146R. FSYR=C6G/C57S/C111Y/C146R. Open arrowhead; monomeric SOD1 molecules.

Although the foregoing studies implicate a role for cysteines 6 and 111 in promoting aggregation, with the mutation of cysteine 111 to serine appearing to strongly suppress aggregation [also see (144) and (145)], it is noteworthy that mouse SOD1 naturally encodes serine at position 111 and possesses only 3 cysteine residues in total (equivalent to positions 6, 57, 146 in human protein). If the mutation of cysteine 111 to serine reduces aggregation, then the prediction would be that mouse SOD1 encoding FALS mutations should not be prone to aggregate. Previous studies have established a transgenic mouse model of FALS by the expression of mouse SOD1 encoding the equivalent to the human G85R mutation (121). These mice exhibit a rapidly progressing paralytic disorder. To determine the importance of cysteine

111 *in vivo*, spinal cord tissue from symptomatic SOD1-G86R mice was assayed for SOD1 aggregation and found to accumulate detergent-insoluble SOD1 (Fig. 2-5A). Compared to mice expressing high levels of WT human SOD1, the symptomatic G86R mice contained high levels of detergent-insoluble mouse SOD1. In the spinal cords of the WT human SOD1 mice, the vast majority of the SOD1 was soluble in detergent, whereas in the G86R spinal cord tissue it appeared as though the majority of accumulated SOD1 was insoluble in detergent (compare Figs. 2-5A and B). This finding demonstrates that encoding a serine at 111 does not block the aggregation of mouse SOD1.

Because our assessment of the experimental mutation of human SOD1 (G85R/C111S) in which aggregation was slowed relied on the HEK293-FT cell model, we examined the aggregation of mouse SOD1-G86R in cell culture. The WT and G86R variants of mouse SOD1 were compared to the G85R variant of human SOD1. Both mouse SOD1-G86R and human SOD1-G85R formed detergent-insoluble aggregates at similar propensities (Fig. 2-6A). Similar to human WT SOD1 (Fig. 2-1A), mouse WT SOD1 was not readily detected in the detergent-insoluble fraction (Fig. 2-6A). As expected, all three SOD1 variants were detected in the detergent-soluble fraction (Fig. 2-6B). These data indicate that amino acid sequence differences between human and mouse SOD1 modulate the requirement for cysteine at 111 in promoting aggregation. In the context of the mouse protein, a cysteine at 111 is not required and the presence of serine does not reduce aggregation.

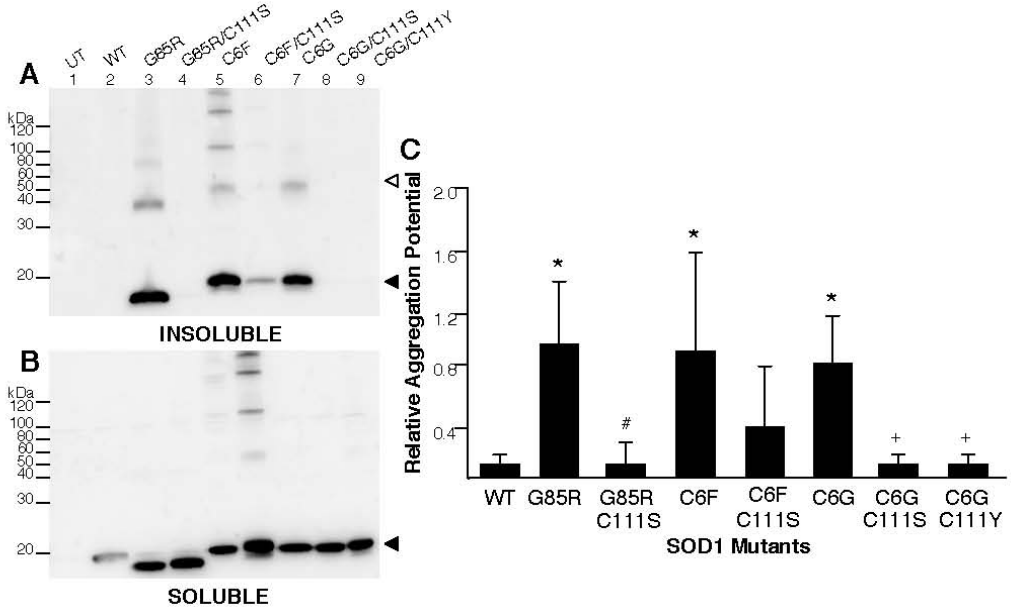

Figure 2-4. Role of cysteine 111 in mutant SOD1 aggregation. Mutants were expressed in HEK293-FT cells and aggregate levels were determined as described in Methods. SDS-PAGE was performed in the presence of a reducing agent in an 18% Tris-Glycine gel. Immunoblots were probed with m/hSOD1 antiserum. A) Detergent-insoluble protein fraction (20 μg). B) Detergent-soluble protein fraction (5 μg). C) Relative aggregation ratios are graphed (mean ratio ±SEM) of at least three different experiments. All FALS mutants were statistically different from wild-type SOD1: (*) $p<0.0005$. The ratios of insoluble to soluble SOD1 for all FALS mutants that were combined with mutated C111 were not statistically different from WT SOD1: G85R/C111S, C6F/C111S, C6G/C111S, C6G/C111Y. (+) C6G was significantly different from C6G/C111S and from C6G/C111Y $p<0.009$. C6F did not differ from C6F/C111S. (#) G85R was statistically different from G85R/C111S $p<0.004$. Open arrowhead; dimer-sized SOD1 molecules. Closed arrowhead; monomeric SOD1 molecules.

To determine the extent to which disulfide-linked multimers occur in lysates from HEK293-FT cells expressing human SOD1 with the A4V, G85R, and G93A natural FALS mutations, detergent extraction buffers were supplemented with iodoacetamide, a non-reversible sulfhydryl-blocking agent, as detergent-soluble and detergent-insoluble fractions were isolated. When these fractions were analyzed by SDS-PAGE in the absence of reducing agents, most of the detergent-insoluble protein migrated at the size expected for monomeric SOD1 (Fig. 2-7A,

lanes 3, 4, and 5). To a variable degree, a portion of the detergent-insoluble SOD1 in each cell lysate migrated at a higher than expected molecular weight (Fig. 2-7A). Distinct bands were detected at 40kDa, which are a size (in this gel system) that is consistent with disulfide-linked dimers of SOD1. When the mutants expressed in cell culture were prepared in the absence of iodoacetamide and examined by SDS-PAGE with reducing agent, nearly all mutant protein detected in the detergent-insoluble and detergent-soluble fractions migrated at a position expected of monomeric protein (Fig. 2-7C and D). Collectively, these data indicate that in the HEK293-FT cell culture model, a portion of the detergent-insoluble protein forms intermolecular disulfide bonds, forming primarily structures dimeric in size, but a large portion of the SOD1 in the detergent-insoluble fraction is not involved in intermolecular disulfide bonding.

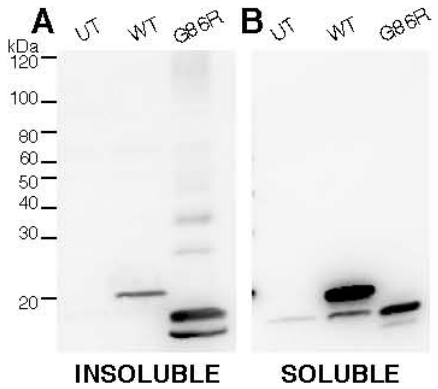

Figure 2-5. Symptomatic G86R mice form detergent insoluble species in spinal cord tissue. Spinal cords from WT and G86R mice were extracted in buffers containing NP40 as described in Methods. SDS-PAGE was performed in the presence of a reducing agent in an 18% Tris-Glycine gel. Immunoblots were probed with m/hSOD1 antiserum. Experiments were replicated twice; a representative example is shown. A) Detergent-insoluble protein fraction (20 μg). B) Detergent-soluble protein fraction (5 μg).

In a previous study, Furukawa and colleagues (141) noted that extraction of tissues from symptomatic G93A mice in 0.5% SDS solubilized disulfide cross-linked forms of mutant SOD1. To determine whether 0.5% SDS solubilizes all aggregated forms of mutant SOD1 in these mice, we used our extraction/centrifugation protocol, substituting 0.5% SDS for 0.5% NP40 (see

Methods). Extraction of spinal cord tissues from asymptomatic WT and symptomatic G93A transgenic mice in buffers with 0.5% SDS and iodoacetamide, which irreversibly blocks free sulfhydryl residues, completely solubilized all mutant SOD1 that accumulated (Fig. 2-8A). No protein was detected in the high-speed pellet after centrifugation (the detergent-insoluble fraction) (Fig. 2-8A, middle panel). In SDS-PAGE of these samples in the absence of reducing agent, high-molecular-weight SOD1 proteins were detected in the G93A tissue but not WT-SOD1 mice (Fig. 2-8A, left panel). When the detergent-soluble fraction was treated with reducing agent before SDS-PAGE, all of the disulfide bonds were broken and only monomeric SOD1 was detected (Fig. 2-8A, right panel). As a positive control, the same spinal cord homogenates were extracted with buffers containing 0.5% NP40 and were run in the presence of reducing agent (without iodoacetamide). As expected, the tissues from the symptomatic G93A mouse contained large amounts of mutant protein in the detergent-insoluble fraction (Fig. 2-8B, right panel – P2) with both WT and G93A SOD1 present in the detergent-soluble fractions (Fig. 2-8B, left panel – S1). Together, these data indicate that in a setting in which disulfide cross-links are preserved, ionic detergents are sufficient to disrupt aggregate structure. Hence disulfide cross-linking alone is not responsible for the maintenance of detergent-insoluble structures that are distinguished by sedimentation upon ultracentrifugation.

Discussion

Our study sought to examine how disulfide bonds, formed between specific cysteine residues of mutant SOD1, may mediate the formation of detergent-insoluble, sedimentable structures (termed aggregates). From our findings, we conclude that disulfide-cross-linking of mutant SOD1 is not critical in aggregate formation nor do these cross-links appear to be a sufficient bonding force in maintaining aggregate structure. By yet to be defined mechanisms,

cysteine residues 6 and 111 were found to exert significant influence over mutant protein aggregation.

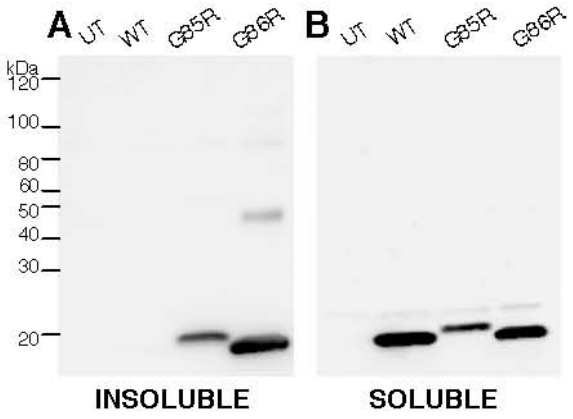

Figure 2-6. Mouse SOD1-G86R aggregates in cell culture. Mutants were expressed in HEK293-FT cells and aggregate levels were determined as described in Methods. SDS-PAGE was performed in the presence of a reducing agent in an 18% Tris-Glycine gel. Immunoblots were probed with m/hSOD1 antiserum. Experiments were replicated three times; a representative example is shown. A) Detergent-insoluble protein fraction (20 μg). B) Detergent-soluble protein fraction (5 μg).

A critical element in considering our work is how protein aggregates are defined. In histological studies of tissues, aggregates are usually defined by the formation of discernable inclusion-body structures. However, in FALS mice, such structures are not necessarily prominent pathologic features (43, 149). Biochemically, aggregates isolated from tissues and cells are defined by several criteria (for review see (150)). In general, aggregates are derived from assemblies of monomeric protein that attain relatively high-molecular-weight (examples include filamentous aggregates as well as smaller oligomeric structures). In many cases, pathologic protein aggregates resist dissociation in detergent, and larger aggregates are of a size that allows for sedimentation upon centrifugation. In the FALS mice, previous work from our laboratory has shown that spinal cord tissues of symptomatic mice accumulate substantial levels of detergent-insoluble, sedimentable, mutant SOD1 (43, 115, 151). Thus, our study focused on the biochemistry of these sedimentable aggregates.

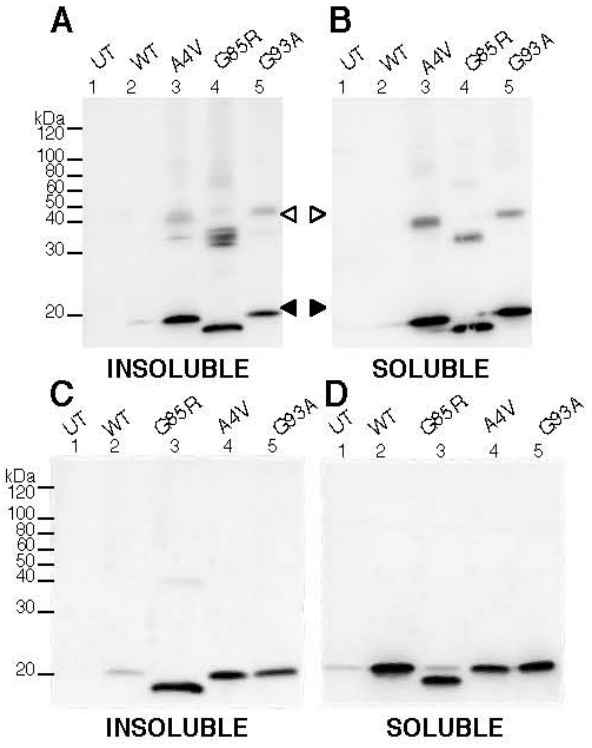

Figure 2-7. Intermolecular disulfide bonding by SOD1 mutants in expressed cultured cells. FALS mutants (A4V, G85R, G93A) were expressed in HEK293-FT cells and detergent extracted in buffers containing iodoacetamide (see Methods). A) and B). SDS-PAGE was performed in the absence of reducing agent in a 4-20% Tris-Glycine gel. Immunoblots were probed with m/hSOD1 antiserum. Experiments were replicated four times; a representative example is shown. A) Detergent-insoluble protein fraction (20 μg). B) Detergent-soluble protein fraction (5 μg). C) and D) The same sets of samples as depicted in panels A and B were analyzed by SDS-PAGE in the presence of a reducing agent. C) Detergent-insoluble protein fraction (20 μg). D) Detergent-soluble protein fraction (5μg). Open arrowhead; dimer-sized SOD1 molecules. Closed arrowhead; monomeric SOD1 molecules.

Previous work, from our group and others, has established that detergent-insoluble aggregates of mutant SOD1 that accumulate in spinal cords of FALS mice are extensively cross-linked by disulfide bonds (23, 141). Recent studies have investigated the role of disulfide bonding in SOD1 aggregation, and data reported to date have been interpreted as evidence that disulfide bond formation between mutant SOD1 proteins could either initiate oligomerization or provide the major bonding force to stabilize aggregate structures (141, 144, 145). Indeed, one of

the authors of the present study participated in a study suggesting a role for disulfide linkage in mutant SOD1 aggregation (23). However, through examination of multiple mutants and combinations of mutations, the present study demonstrates that the role of cysteine residues in SOD1 in modulating the aggregation of mutant SOD1 is complex and likely to involve mechanisms other than disulfide cross-linking.

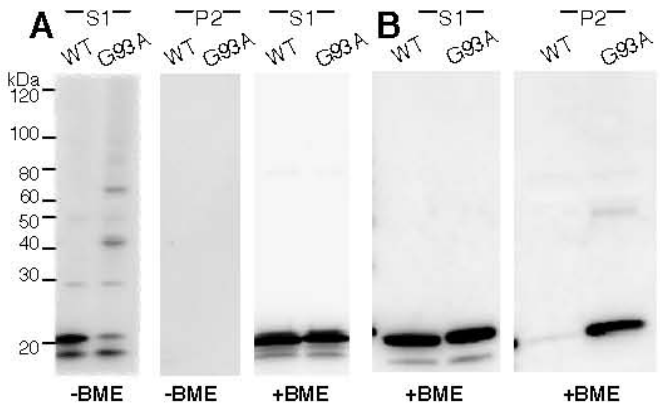

Figure 2-8. Disulfide bonds are not sufficient to maintain SOD1 aggregate structure. A) Spinal cord tissue from asymptomatic WT and symptomatic G93A SOD1 transgenic mice was extracted in 0.5% SDS detergent and iodoacetamide. B) Standard extraction in NP40 and centrifugation of the same tissues utilized in panel A. Samples were run in the presence or absence of reducing agent (βME), as noted, in 4-20% Tris-Glycine gels. Immunoblots were probed with m/hSOD1 antiserum. S1, detergent-soluble (5 μg). P2, detergent-insoluble (20 μg).

First, we found that SOD1 encoding FALS-linked mutations at cysteine residues 6, 111, or 146 aggregate when expressed in cell culture, indicating that the loss of any one of these cysteines does not block mutant protein aggregation. These findings, regarding cysteine 6 and 111, are in agreement with a study by Cozzolino and colleagues (144). Second, we noted that cysteines 6 and 111 appear to play important roles in promoting SOD1 aggregate formation as mutant proteins that possess either one of these residues retain the ability to rapidly aggregate while proteins that retained only cysteines 57 or 146 did not rapidly aggregate [also see (144)]. Similar to Cozzolino, we found that elimination of both cysteine 6 and 111 (most specifically by

mutating cysteine 111 to serine) reduced or dramatically slowed aggregation. However, we now demonstrate that this outcome is unique to human SOD1. Mouse SOD1 encoding the equivalent of the human G85R mutation, and which naturally encodes serine at position 111, retains a high propensity to aggregate in cell and mouse models. We also identified experimental mutants that retained only one cysteine residue while retaining high propensity to aggregate; these mutants are incapable of forming disulfide-linked structures larger than dimers (Fig. 2-9) and hence extensive cross-linking by disulfide bonding cannot be critical for aggregate formation or stability. Finally, and most importantly, we identify an experimental SOD1 mutant lacking all cysteine residues (3 of 4 replaced by FALS-linked mutations) that retained capacity to rapidly aggregate. From this body of evidence, we conclude that if disulfide cross-linking has any role in promoting or stabilizing mutant SOD1 aggregation, such cross-linking is not required and may not be of major importance.

Although one could argue that these experimental mutants and the cell culture system do not reflect natural events, we demonstrate that aggregates of SOD1-G93A found in the spinal cords of symptomatic mice dissociate completely in 0.5% SDS, despite extensive preservation of disulfide cross-linking. Collectively, these data demonstrate that disulfide cross-linking is not responsible for the structure adopted by mutant SOD1 that accounts for sedimentation upon ultracentrifugation; a hallmark feature of SOD1 aggregates.

Cysteines 6 and 111 Modulate Aggregation of Mutant SOD1

Similar to a recent series of studies (141, 143-145), we find that cysteines 6 and 111 in human SOD1 play important roles in modulating mutant SOD1 aggregation. However, the C6G, C6F, and C111Y mutants each rapidly formed aggregates in our cell model, indicating that neither of these residues is indispensable. Although we identified experimental mutants in which the need for cysteine at any of the natural positions is obviated, some of our experimental

mutants suggested important roles for cysteines 6 and 111 in promoting aggregation. Combining C6G and C111Y mutations (C6G/C111Y), or C6G and C6F with C111S (C6G/C111S and C6F/C111S), produced mutants with low propensities to aggregate. One of the most striking effects on aggregation was noted when the cysteine 111 to serine mutation was combined with the G85R mutation in human SOD1, producing a double mutant that failed to aggregate within 24 hours; similar to WT SOD1. Cozzolino recently demonstrated that combining a C111S mutation with the A4V, G93A, and C146R FALS mutations produced similar reductions in aggregation (144). Collectively, these studies implicate cysteine 111 as a potentially crucial residue in promoting aggregation. However, in mouse SOD1, position 111 is serine. Thus, the mouse SOD1-G86R animal, which develops motor neuron disease marked by hindlimb paralysis, possesses an equivalent of our experimental human G85R/C111S mutant. In contrast to human SOD1, mouse SOD1-G86R readily forms detergent-insoluble, sedimentable species in both cell culture models and most importantly in the spinal cords of symptomatic mouse SOD1-G86R mice. Hence, the effect of serine versus cysteine at position 111 on SOD1 aggregation appears to be dependent upon the species from which the protein is derived (mouse and human SOD1 differ in sequence at 25 positions).

Another key observation that leads us to believe that structural features of cysteines 6 and 111 modulate aggregation, rather than disulfide bonding, derives from the comparison of our two experimental mutants that alter all four cysteine residues. The C6G/C57S/C111Y/C146R variant showed an aggregation potential no different from WT SOD1, whereas the C6F/ C57S/C111Y/C146R variant rapidly aggregated similar to SOD1-G85R. The simplest explanation for this outcome is that the phenylalanine at position 6 imparts an important structural feature to the protein that restores its ability to rapidly aggregate.

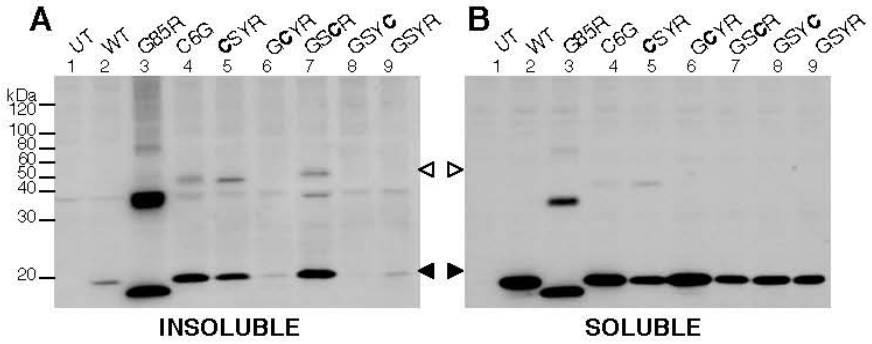

Figure 2-9. Intermolecular disulfide bonding by SOD1 mutants in expressed cultured cells. SOD1 mutants, each with only one cysteine residue intact, were expressed in HEK293-FT cells and were treated with iodoacetamide to irreversibly block free sulfhydryl groups before extraction in detergent and high speed centrifugation. SDS-PAGE was performed in the absence of reducing agent in a 4-20% Tris-Glycine gel. Immunoblots were probed with m/hSOD1 antiserum. Experiments were replicated four times; a representative example is shown. The labels above lanes 5-9 use the same nomenclature as is used in Figure 2-2. A) Detergent-insoluble protein fraction (20 μg). B) Detergent-soluble protein fraction (5 μg). Small amounts of SOD1 migrating at a size consistent with dimeric enzyme is visible when mutants encoded cysteine at position 6 or 111 (lanes 4, 5 and 7). Open arrowhead; dimer-sized SOD1 molecules. Closed arrowhead; monomeric SOD1 molecules. A nonspecific protein band that migrates just below the dimer-sized SOD1 band (MW ~37 kDa) is visible in all lanes.

Structural Features of Cysteine 111

In most species, the amino acid homologous to position 111 is serine rather than cysteine: humans and chickens are the only species in which position 111 is occupied by cysteine (23). In crystal structures of human SOD1, position 111 is located in the Greek-key loop near the dimer interface (38). Cysteine 111 is not obviously involved in crucial structural elements of the enzyme, but it is notable that serine is highly conserved at this position with the two exceptions noted above. Recent studies have demonstrated that cysteine 111 may strongly bind metal ions, including copper (152). Cysteine 111 may also bind other ligands such as glutathione, thioredoxins, or other molecules that utilize disulfide linkages to mediate binding (153, 154). A recent study by Fujiwara (155) reported that cysteine 111 is a target for oxidative modification

and that some of the mutant SOD1 that accumulates in pathologic structures in G93A mice is oxidatively modified at this position. Notably, Cozzolino et al (144) reported that modulating the redox potential of NSC-34 cells influenced mutant SOD1 aggregation. It is possible that mechanisms involving a modification of the cysteine residues, particularly 111, impart structural alterations in the protein to promote aggregation.

Disulfide Bonding in Mutant SOD1 Aggregation

Our analysis of mutant SOD1 aggregates formed in both cell culture and the G93A mouse model indicates that aggregates of SOD1-G93A in symptomatic mice appear to be dissociated (converted from structures that sediment upon ultracentrifugation to structures that do not) in 0.5% SDS, despite retaining significant disulfide cross-linking. Thus, whatever role disulfide bonding plays in aggregate formation, such bonds are not sufficient to maintain the aggregate structure as a sedimentable entity.

We were initially surprised to find that 0.5% SDS was sufficient to solubilize (fractionate to high speed supernate) mutant SOD1. In previous studies, using a filter-trap assay, we had interpreted the retention of significant fractions of mutant SOD1 in 0.22 μm cellulose acetate filters as evidence that mutant SOD1 aggregates are SDS-resistant (114). In light of our current study, and the study by Furukawa and colleagues described above (141), we now interpret the retention of mutant SOD1 in these filters as entrapment of disulfide cross-linked lattices that persist after solubilization in SDS rather than retention of structures that are identical to the sedimentable species of mutant protein described here. In this latter scenario, the disulfide cross-links maintain an extended network of intermolecular interactions, some of which would be large enough to be retained in the filter. Importantly, a disulfide cross-linked network is distinct from

the structures that are distinguished by resistance to solubilization in non-ionic detergent and sedimentation upon ultracentrifugation.

Prior studies of mutant SOD1 in tissues from G93A mice had identified high-molecular-weight structures in denaturing SDS-PAGE that were interpreted to represent SDS-resistant complexes (117, 156, 157). The SDS-resistant high-molecular-weight SOD1 seen in SDS-PAGE generally ranges in size from dimers to molecules of a mass no larger than relatively small oligomers (no more than 10-20 subunits). Such structures do not appear to possess sufficient mass to sediment in ultracentrifugation (see Fig. 2-9). We propose that these SDS-resistant structures that have been described in SDS-PAGE may largely represent covalently-linked adducts to SOD1, formed by modifications such as ubiquitination or sumolyation, or may represent SOD1 proteins that are covalently cross-linked by mechanisms other than disulfide linkages (43). We have previously demonstrated high-molecular-weight forms of mutant SOD1 in denaturing SDS-PAGE analysis of detergent-insoluble, sedimentable structures (43). These high-molecular-weight, SDS-resistant, SOD1 proteins are a relatively minor fraction of total detergent-insoluble protein. Notably, a recent study of mutant SOD1 that fractionates into the NP40 insoluble fraction demonstrated that the majority of the detergent-insoluble SOD1 display a mass consistent with an unmodified monomer; which is in some manner assembled into higher order sedimentable structures (151).

Conclusions

We conclude that disulfide bonding is likely to be of limited importance in maintaining the structure of aggregated forms of mutant SOD1. Instead, it appears that the aggregates are stabilized by molecular interactions that are dissociable by ionic detergent. We note that β-strand elements are a prominent feature of SOD1 and that these elements in the core β-barrel

structure of the protein are aligned adjacent to one another forming numerous hairpin folds (38). The stacking of β-sheets is a characteristic feature of amyloids (158-162). In previous studies, we have noted the appearance of amyloid-like structures (stained with Thioflavin-S) in tissues of some but not all FALS mouse models (43, 115). Whether FALS mutant SOD1 assembles into amyloid-like structures *in vivo* is, however, unclear. Notably, *in vitro*, amyloid-like structures that are detergent-sensitive have been demonstrated for the H46R and S134N FALS mutants (163).

We are convinced by our data and that of others (141, 143-145) that cysteines 6 and 111 participate in some crucial component of human SOD1 aggregation, however we believe that our study provides abundant evidence that the mechanism does not require disulfide cross-linking. Instead, we propose that some other structural feature of these residues is critical in promoting aggregate formation. Whether modifications to cysteine residues, particularly cysteine 111, are critical in promoting human SOD1 aggregation is clearly a topic deserving further study. Similarly, a better understanding of the structural features of human SOD1 aggregates and the role cysteine residues play in maintenance of such structures is required.

CHAPTER 3
AGGREGATION MODULATING ELEMENTS IN HUMAN SOD1 PROTEIN

Introduction

Normally folded SOD1 forms a homodimer of two 153-amino acid subunits. Each subunit contains eight β-strands, copper bound in the active site, zinc binding site, an electrostatic loop, and an intramolecular disulfide bond between cysteine 57 and cysteine 146 (38). The majority of FALS mutations are point mutations that occur predominantly in β-strand regions. However, a subset of FALS mutations produce reading frameshifts and early termination codons. The effects of FALS mutations on enzyme activity, turnover, and folding of the SOD1 protein vary considerably (24-26). Enzyme activity ranges from undetectable to normal (24, 27-30), and many mutants increase the susceptibility of SOD1 to disulfide reduction (31). However, all FALS mutants that have been studied in cell culture share a propensity to form detergent-insoluble SOD1 species in cell culture, which are defined as aggregates (43)(Prudencio M, Hart PJ, Borchelt DR, Andersen P, submitted). It is possible that FALS mutations in SOD1 alter structural aspects of the protein that enhance aggregation, and it is possible that specific regions within the protein mediate misfolding.

Considerable attention has been placed on the role of disulfide cross-linking in the formation of SOD1 aggregates (see Chapters 2 and 4) (23, 46, 141, 144). In symptomatic SOD1 transgenic mice, high-molecular-weight, disulfide cross-linked forms of SOD1 are prominent in the detergent-insoluble protein fraction, which become more abundant as mice approach disease endstage (23, 141)(Karch CM, Prudencio M, Winkler D, Hart PJ, Borchelt DR, In Press). However, in Chapter 2, we demonstrate that SOD1 aggregates are not stabilized by disulfide cross-linking alone (46). Studies *in vitro* and in cell culture suggest that cysteine residues 6 and

111 are important for modulating mutant SOD1 aggregation (46, 128, 144). However, my studies found that no single cysteine residue is required for aggregation (46)(see Chapter 2).

In this study, we examined the role that specific regions in the protein might play in the formation of SOD1 aggregates using a mutagenesis approach and cell culture assay for aggregation. The FALS mutation G85R and the mouse SOD1 G86R mutation have similar aggregation propensities. However, we discovered that chimeric human-mouse proteins with the FALS mutation (G85R) have strikingly different aggregation propensities. We exploited this finding to develop a system to identify sequences in human SOD1 that are important for the formation of aggregates. We found that amino acids 42-50 and 109-123 in human SOD1 are important for aggregation and that species-specific interaction is required between these two regions for aggregation to occur. Thus, it is likely that aggregation occurs by global misfolding of the protein and that aggregation is enhanced by several regions normally adjacent in the folded structure as opposed to a single residue in the human protein.

Methods

Construction of SOD1 Expression Vectors

FALS and experimental mutations were created in the cDNA of human SOD1, mouse SOD1, and chimeric proteins of human and mouse sequence (wild type (WT) chimeric proteins were generated by Genscript, Piscataway, NJ, USA) using standard PCR strategies with oligonucleotides that introduce the specific point mutations (Table 3-1). All mutant cDNAs created in this manner were sequenced in their entirety to verify the presence of the desired mutations and the absence of undesired mutations. SOD1 mutants were expressed in the pEF-BOS vector (146).

Table 3-1. Aggregation propensity of chimeric SOD1 mutants

SOD1 mutants	Average aggregation propensity	Production of aggregates°
H G85R	1.36	++
M/H WT	0.00	-
M/H G85R	0.64	++
M/H G85R/C111S	0.38	++
H/M WT	0.01	-
H/M G85R	0.06	-
H/M G85R/S111C	0.41	++
H/MG85R/S111C/G90D	0.32	++
H/M G85R/S111C/R102S	0.33	++
H/M G85R/Δ90-102	0.13	-
H/M G85R/Δ109-123	1.91	+++
H/M G85R/S111C/M117L	0.23	-
H/M G85R/S111C/E109D	0.05	-
H/M G85R/Δ40-52	0.09	-
H/M G85R/Δ1-40/Δ90-102	0.08	-
H/M G85R/S111C/Q123A	0.07	-
H/M G85R/Δ40-52/Δ109-123	0.15	-
H A4V	0.99	+++
M A4V	0.29	++
H/M A4V	0.35	++
H/M A4V/Δ109-123	1.82	+++
H V148G	0.79	+++
M V148G	0.04	-
H/M V148G	0.11	-
H/M V148G/Δ109-123	0.50	++

° See Table 1-1

Tissue Culture Transient Transfection

HEK 293-FT cells were cultured in 60-mm poly-D lysine coated dishes. Upon reaching 95% confluency, cells were transfected with Lipofectamine 2000 (Invitrogen, Carlsbad, CA, USA) and then harvested after 24 hours as previously described (46).

SOD1 Aggregation Assay by Differential Extraction

The procedures used to assess SOD1 aggregation by differential detergent extraction and centrifugation were similar to previous descriptions (43, 46). Protein concentration was measured in S1 and P2 fractions by BCA method as described by the manufacturer (Pierce, Rockford, IL, USA) (Table 3-1).

Immunoblotting

Standard sodium dodecyl sulfate-polyacrylamide gel electrophoresis (SDS-PAGE) was performed in 18% or 4-20% Tris-Glycine gels (Invitrogen, Carlsbad, CA, USA). Samples were boiled for 5 minutes in Laemmli sample buffer prior to electrophoresis (148). Immunoblots were probed with a rabbit polyclonal antibody termed m/hSOD1 at dilutions of 1:2500. The m/h SOD1 antibody is a peptide antiserum that recognizes amino acids 124-136 (conserved between mouse and human SOD1 proteins) (24).

Quantitative Analysis of Immunoblots

Quantification of the SOD1 protein in detergent-insoluble and detergent-soluble fractions was performed by measuring the band intensity of SOD1 in each lane using a Fuji Imaging system (FUJIFILM Life Science, Stamford, CT USA). The untransfected control served as background. SOD1 aggregation propensity was a function of the ratio of the band intensity in the detergent-insoluble fraction to that of the detergent-soluble fraction. The mean and standard error of the mean (SEM) were calculated for the aggregation propensity of each sample in each experiment. A homoscedastic student's T-test was used to calculate significance.

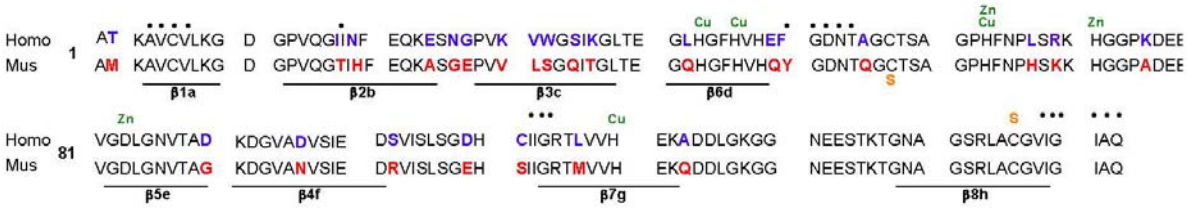

Figure 3-1. Human and mouse SOD1 differ at 25 amino acids. Alignment of human and mouse SOD1. Unconserved amino acids are marked in bold. Blue, human residues. Red, mouse residues. *, residues that form the dimer interface. Green, metal binding sites. Gold S, residues forming the intramolecular disulfide bond.

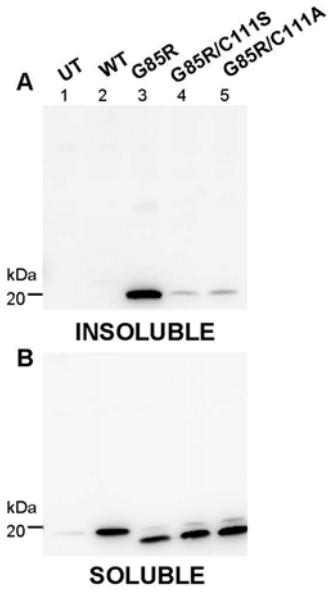

Figure 3-2. Cysteine 111 plays a role in SOD1 aggregation. Mutants were expressed in HEK293-FT cells, and aggregate levels were measured as described in Methods. UT, untransfected cells. WT, cells transfected with vectors containing WT SOD1 protein, which does not aggregate. G85R is a robustly aggregating FALS mutant. SDS-PAGE was performed in the presence of reducing agent in an 18% Tris-Glycine gels. Immunoblots were probed with an antiserum recognizing a conserved region in mouse and human SOD1 (m/hSOD1). A) Detergent-insoluble protein fraction (20 μg). B) Detergent-soluble protein fraction (5 μg). Image is representative of 3 repetitions of this experiment.

Results

SOD1 aggregation is a pathologic hallmark of FALS. We have demonstrated that the cysteine encoded at amino acid 111 is important in modulating SOD1 aggregation; however, we also showed that we could create a SOD1 recombinant protein in which all four cysteine residues were mutated (C6F/C57S/C111Y/C146R) that still retains a high propensity to aggregate (46)(see Chapter 2). These findings lead us to search for other regions of the SOD1 protein that enhance mutant SOD1 aggregation. To examine regions of the protein that may enhance aggregation, SOD1 mutants were expressed in HEK293-FT cells, and the cell lysates were separated into detergent-insoluble and detergent-soluble fractions.

The human FALS G85R mutation and the mouse G86R mutation have similar aggregation propensities in cell culture and both mutants cause hindlimb paralysis when the protein is overexpressed in mice (46, 113, 121). Human and mouse SOD1 differ at 25 amino acids (Fig. 3-1). Human SOD1 encodes a cysteine at amino acid 111. Alternatively, mouse SOD1 encodes a serine at amino acid 111. In human SOD1, when amino acid 85 encodes an arginine and amino acid 111 encodes a serine (G85R/C111S), the aggregation potential is similar to WT protein (46)(see Chapter 2)(Fig. 3-2). However, in mouse SOD1, when amino acid 85 encodes an arginine and amino acid 111 encodes a serine, the protein aggregates robustly (46). Because a serine encoded at amino acid 111 has different effects in mouse SOD1 and in human SOD1, we exploited this finding to develop a system to identify sequences in human SOD1 that are important for the formation of aggregates in FALS mutants.

When the cysteine at amino acid 111 is substituted for a serine in the highly aggregating FALS mutant G85R, SOD1 aggregation is reduced to near wild-type (WT) SOD1 levels, which is considered non-aggregating (46)(see Chapter 2)(Fig. 3-2A). To determine if this effect is unique to the serine, cysteine 111 was mutated to an alanine in the context of the G85R mutation. Vectors containing SOD1 with intergenic mutations at amino acids 85 (an FALS mutation) and 111 (an experimental mutation) were expressed in HEK293-FT cells, and cell lysates were extracted in non-ionic detergent to isolate detergent-insoluble and detergent-soluble protein fractions. Note that a serine encoded at amino acid 111 is highly conserved, with the exception of human and chicken SOD1 (23). An alanine encoded at amino acid 111 is a structurally conservative mutation. The G85R/C111S and the G85R/C111A mutants had similarly low levels of SOD1 in the detergent-insoluble fraction (Fig. 3-2A). The amount of detergent-soluble material, representing stably folded protein, was similar in all mutants (Fig. 3-2B). Thus,

substituting the cysteine residue at amino acid 111 in the context of a FALS mutation has a dramatic effect on aggregation.

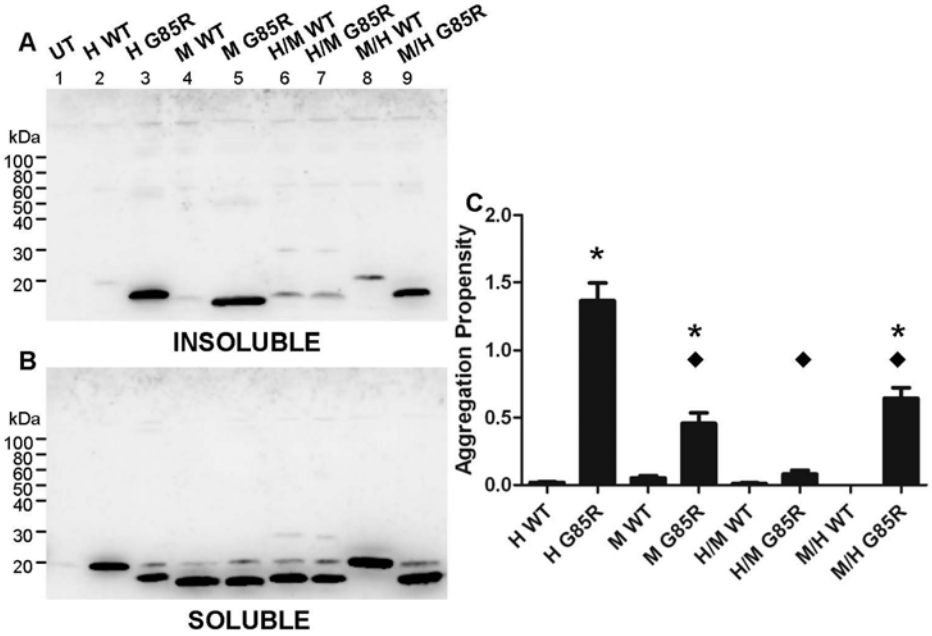

Figure 3-3. Differences in aggregation propensity between mouse and human SOD1 chimeric proteins. Mutants were expressed in HEK293-FT cells, and aggregate levels were measured as described in Methods. UT, untransfected cells. WT, cells transfected with vectors containing WT SOD1 protein, which does not aggregate. H/M, human SOD1 between amino acids 1-80 and mouse SOD1 between 81-153. M/H, mouse SOD1 between amino acids 1-80 and human SOD1 between 81-153. G85R is a robustly aggregating FALS mutant. SDS-PAGE was performed in the presence of reducing agent in 18% Tris-Glycine gels. Immunoblots were probed with m/hSOD1 antiserum. A) Detergent-insoluble protein fraction (20 μg). B) Detergent-soluble protein fraction (5 μg). C) Relative aggregation propensity is a function of the amount of SOD1 found in the detergent-insoluble fraction compared to the detergent-soluble fraction. The graph represents the mean (±SEM (error bars)) of at least three different experiments. *, Statistically different from all WT variants (H WT, H/M WT, M/H WT): $p<0.05$. °, Statistically different from H/M G85R: $p<0.05$. ◆, Statistically different from human G85R: $p<0.05$.

Chimeric proteins were created to identify the residues that mediate human SOD1 aggregation. In the H/M SOD1 protein, amino acids 1-80 were encoded as human SOD1 and amino acids 81-153 were encoded as mouse SOD1. In the M/H SOD1 protein, amino acids 1-80 were encoded as mouse SOD1 and amino acids 81-153 were encoded as human SOD1.

Chimeric SOD1 proteins were expressed in HEK293-FT cells and extracted in non-ionic detergent. Chimeric proteins that encode WT sequence of human and mouse SOD1 (H/M WT and M/H WT) had an aggregation propensity that was similar to the human WT protein (Fig. 3-3C, lanes 2, 6, 8). Thus, the fusion of mouse and human sequence did not overtly alter protein folding. When the highly aggregating FALS mutant G85R was introduced into the H/M and M/H chimeric proteins, the aggregation propensities for both constructs were significantly less than human G85R (Fig. 3-3C). The H/M G85R mutant had very little detergent-insoluble protein (Fig. 3-3A) and did not differ from WT protein in its propensity to aggregate (Fig. 3-3C); however, the M/H G85R mutant formed detectable amounts of detergent-insoluble protein (Fig. 3-3A). The M/H G85R mutant had an aggregation propensity that was significantly different from WT protein (Fig. 3-3C). Thus, the M/H G85R mutant aggregates but at lower levels than the human protein. Despite the differences in aggregation propensity, the levels of detergent-soluble SOD1 remained consistent (Fig. 3-3B). These chimeric proteins demonstrate that differences occur in human and mouse sequences that alter the propensity of the FALS-G85R mutant to misfold and aggregate.

Due to the apparent importance of amino acid 111 in human SOD1 aggregation, we used chimeric proteins to understand how this residue mediates aggregation. The chimeric protein H/M G85R encodes a serine at amino acid 111, which results in an aggregation propensity that is similar to human G85R/C111S (compare Figs. 3-2A and 3-3A). To more closely examine the role of cysteine 111 in SOD1 aggregation, amino acid 111 was altered to encode either cysteine or serine in the presence of the FALS-G85R mutant in the H/M and M/H chimeric proteins (termed H/M G85R/S111C and M/H G85R/C111S). Encoding a cysteine at amino acid 111 in the H/M G85R mutant (H/M G85R/S111C) resulted in a slight increase in aggregation (Fig. 3-

4A). A cysteine encoded at amino acid 111 produced a protein with an aggregation propensity that was significantly different from H/M G85R; however, it was also different from human G85R (Fig. 3-4C). Thus, restoring a cysteine to amino acid 111 enhanced mutant SOD1 aggregation; however, it was not sufficient to restore aggregation to the levels of human G85R. Alternatively, when amino acid 111 encoded a serine (the mouse residue) in the M/H G85R mutant (M/H G85R/C111S), the aggregation levels of this mutant decreased only slightly (Fig. 3-4A). A serine encoded at amino acid 111 produced a protein with an aggregation propensity that was not significantly different from M/H G85R (Fig. 3-4C). Thus, the presence of a cysteine at amino acid 111 in either chimeric protein does not have robust restorative effects on aggregation. Together, these findings are consistent with evidence from our group, which suggests that cysteine 111 is important but not required for SOD1 aggregation (46).

It is possible that cysteine 111 works in concert with other neighboring residues to mediate aggregation. To determine if residues between amino acids 81 and 153 are capable of enhancing SOD1 aggregation, we focused on the H/M SOD1 protein by humanizing specific amino acids or blocks of sequence. Humanizing the region encoding amino acids 109-123 (E109D, S111C, M117L, and Q123A) in the H/M G85R mutant (termed H/M G85R/Δ109-123) resulted in a protein that robustly aggregated in cell culture (Fig. 3-5A). When amino acid 109-123 encoded human residues, the aggregation propensity was similar to human G85R (Fig. 3-5C). Thus, this region appears to be important for aggregation. To determine if individual residues between amino acids 109-123 are responsible for enhancing aggregation, each residue was substituted for the corresponding human residue (eg: H/M G85R/E109D/S111C, H/M G85R/S111C/M117L, H/M G85R/S111C/Q123A). Each of these mutants had an aggregation propensity similar to H/M G85R/S111C (Fig. 3-5C). Thus, individual amino acids encoding human SOD1 do not

enhance the effect of cysteine 111 on aggregation. With the exception of H/M G85R/Δ109-123, all mutants had similar levels of SOD1 in the detergent-soluble fraction (Fig. 3-5B). The H/M G85R/Δ109-123 protein was less stable than other mutants used in this study. Together, this evidence suggests that no single residue is responsible for aggregation but that the region of amino acids 109-123 may be important for enhancing human SOD1 aggregation.

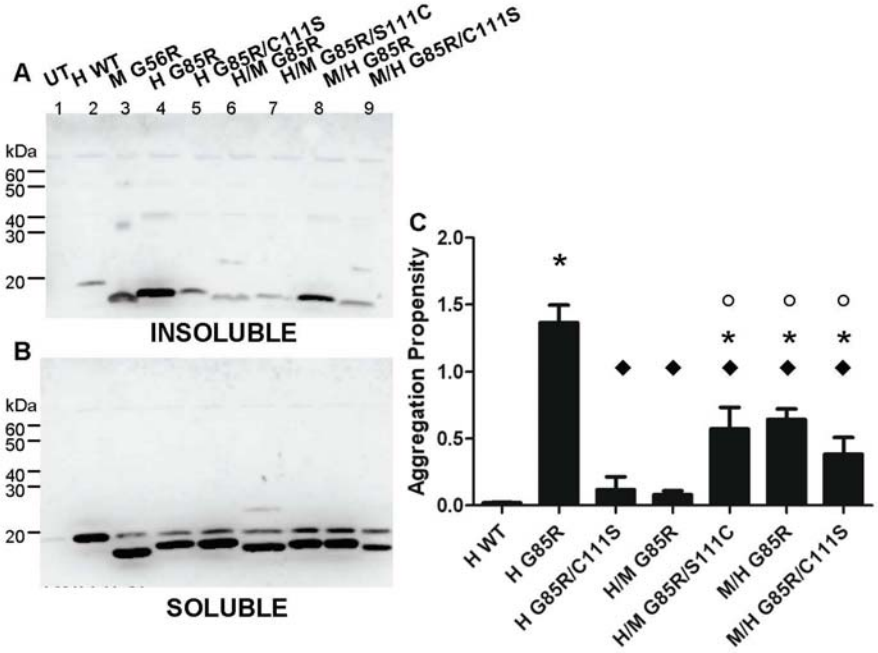

Figure 3-4. Amino acid 111 does not predict aggregation alone. Mutants were expressed in HEK293-FT cells, and aggregate levels were measured as described in Methods. UT, untransfected cells. WT, cells transfected with vectors containing WT SOD1 protein, which does not aggregate. H/M, human SOD1 between amino acids 1-80 and mouse SOD1 between 81-153. G85R is a robustly aggregating FALS mutant. SDS-PAGE was performed in the presence of reducing agent in 18% Tris-Glycine gels. Immunoblots were probed with m/hSOD1 antiserum. A) Detergent-insoluble protein fraction (20 μg). B) Detergent-soluble protein fraction (5 μg). C) Relative aggregation propensity is a function of the amount of SOD1 found in the detergent-insoluble fraction compared to the detergent-soluble fraction. The graph represents the mean (±SEM (error bars)) of at least three different experiments. *, Statistically different from all WT variants (H WT, H/M WT, M/H WT): $p<0.05$. °, Statistically different from H/M G85R: $p<0.05$. ◆, Statistically different from H G85R: $p<0.05$.

Upon closer examination of the normally folded SOD1 protein, we confirmed that residues 109-123, which reside in β-strand 7, are in close proximity to the unconserved region of residues 42-50, which reside in β-strand 6 (38). In the H/M G85R mutant, β-strands 6 and 7 are not homologous and the highly aggregating H/M G85R/Δ109-123 mutant restores homology in β-strands 6 and 7. To determine if β-strands 6 and 7 undergo species-specific interactions that are required for aggregation, residues 42-50 were substituted for amino acids encoding mouse SOD1 (L42Q, E49Q, and F50Y) in the context of the H/M G85R/Δ109-123, creating a mutant in which β-strands 6 and 7 differed in species (termed H/M G85R/Δ42-50/Δ109-123). Encoding mouse SOD1 at amino acids 42-50, when human SOD1 was encoded at amino acids 109-123 results in little detergent-insoluble SOD1 (Fig. 3-5A) and an aggregation propensity similar to WT (Fig. 3-5C). If β-strands 6 and 7 undergo species-specific interactions for aggregation to occur in FALS mutants, we predicted that substituting residues 42-50 for amino acids encoding mouse SOD1 in the context of H/M G85R would enhance SOD1 aggregation (termed H/M G85R/Δ42-50). H/M G85R/Δ42-50, in which β-strands 6 and 7 encoded mouse SOD1, had a low propensity to aggregate, similar to WT (Fig. 3-5C). The amount of detergent-soluble SOD1 was similar in all the mutants examined (Fig. 3-5B). Thus, our evidence suggests that SOD1 aggregation is enhanced when β-strands 6 and 7 encode human SOD1 in the context of the mutant protein.

To determine if amino acids 109-123 are universally important for aggregation of mutant SOD1, two FALS mutations located at the beginning of the protein (A4V) and at the end of the protein (V148G) were introduced into the chimeric H/M SOD1 protein. H/M A4V produced significantly less aggregates than human A4V (Fig. 3-6C); however, the aggregation propensity of H/M A4V was also different from WT protein. Humanizing amino acids 109-123 in the H/M A4V protein (termed H/M A4V/Δ109-123) produced a robustly aggregating mutant that was

significantly different from H/M A4V; yet, similar in its propensity to aggregate to human A4V (Fig. 3-6C). A similar pattern of aggregation was observed with the V148G mutation, whereby the H/M variant aggregated at low levels and humanizing 109-123 enhanced aggregation to human levels (Fig. 3-6C). Thus, the effect of amino acids 109-123 on aggregation is shared among a variety of FALS mutants.

Discussion

This study was designed to identify regions in the human SOD1 protein that enhance mutant SOD1 aggregation. We utilized chimeric SOD1 proteins that combine human and mouse SOD1 sequence and found that amino acids 109-123 of human SOD1 are important for enhancing mutant SOD1 aggregation. Additionally, we provide evidence that species-specific interactions between β-strand 6 (including amino acids 42-50) and β-strand 7 (including amino acids 109-123) result in high levels of human SOD1 aggregation. This effect is similar in FALS mutants that occur at the beginning, middle, and end of the protein. Thus, we suggest that aggregation occurs by global misfolding of the protein and is enhanced by specific regions in the human protein.

Our results demonstrate that regions 42-50 and 109-123 are important for enhancing mutant human SOD1 aggregation (Fig. 3-7). These residues reside within β-strands 6 and 7, respectively. In the normally folded SOD1 protein, these two elements neighbor one another. Normal structural components of β-strand 6 and 7 are critical to structures that support aggregation. Residues within this region form the dimer interface (Fig. 3-1). Additionally, three of the four copper binding sites are located between amino acids 42-50 and 109-123. These copper binding sites are well conserved. Interestingly, dimer formation and copper binding promote stability in the WT protein, which accounts for a protein that is stable in 1% SDS and

8M urea (39). Thus, it may be possible that FALS mutations disrupt these important interactions, destabilize the protein, and promote aggregation.

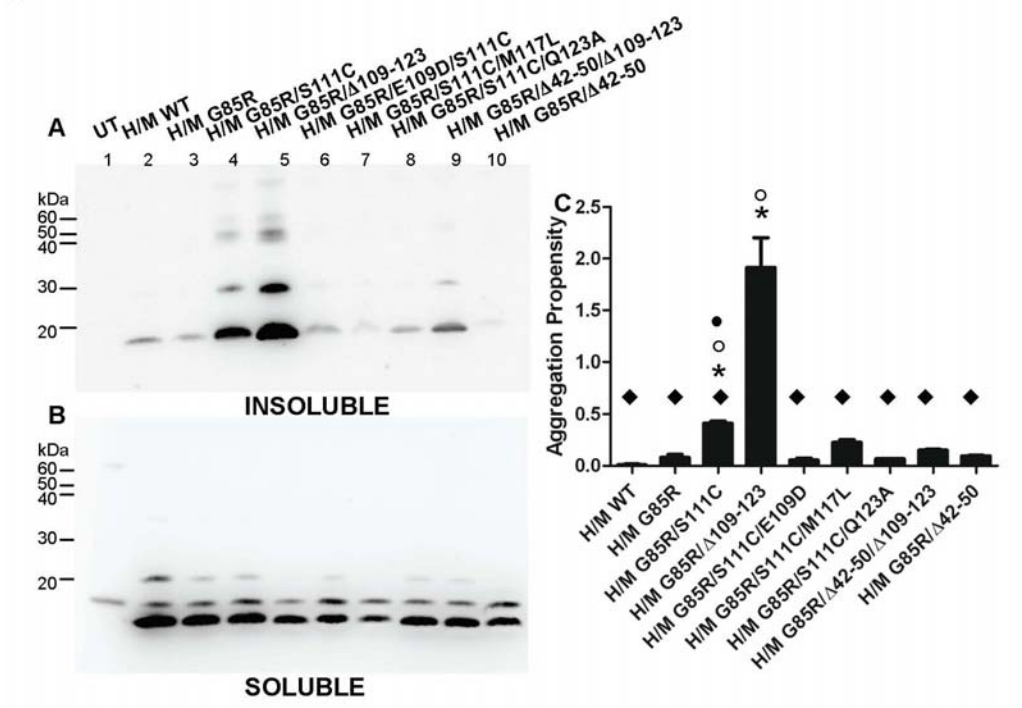

Figure 3-5. Amino acids 42-50 and 109-123 in human SOD1 are important for aggregation. Mutants were expressed in HEK293-FT cells, and aggregate levels were measured as described in Methods. UT, untransfected cells. WT, cells transfected with vectors containing WT SOD1 protein, which does not aggregate. H/M, human SOD1 between amino acids 1-80 and mouse SOD1 between 81-153. G85R is a robustly aggregating FALS mutant. SDS-PAGE was performed in the presence of reducing agent in 18% Tris-Glycine gels. Immunoblots were probed with m/hSOD1 antiserum. A) Detergent-insoluble protein fraction (20 μg). B) Detergent-soluble protein fraction (5 μg). C) Relative aggregation propensity is a function of the amount of SOD1 found in the detergent-insoluble fraction compared to the detergent-soluble fraction. The graph represents the mean (±SEM (error bars)) of at least three different experiments. *, Statistically different from all WT variants (H WT, H/M WT, M/H WT): $p<0.05$. °, Statistically different from H/M G85R: $p<0.05$. ◆, Statistically different from human G85R: $p<0.05$. •, Statistically different from H/M G85R/Δ109-123: $p<0.05$.

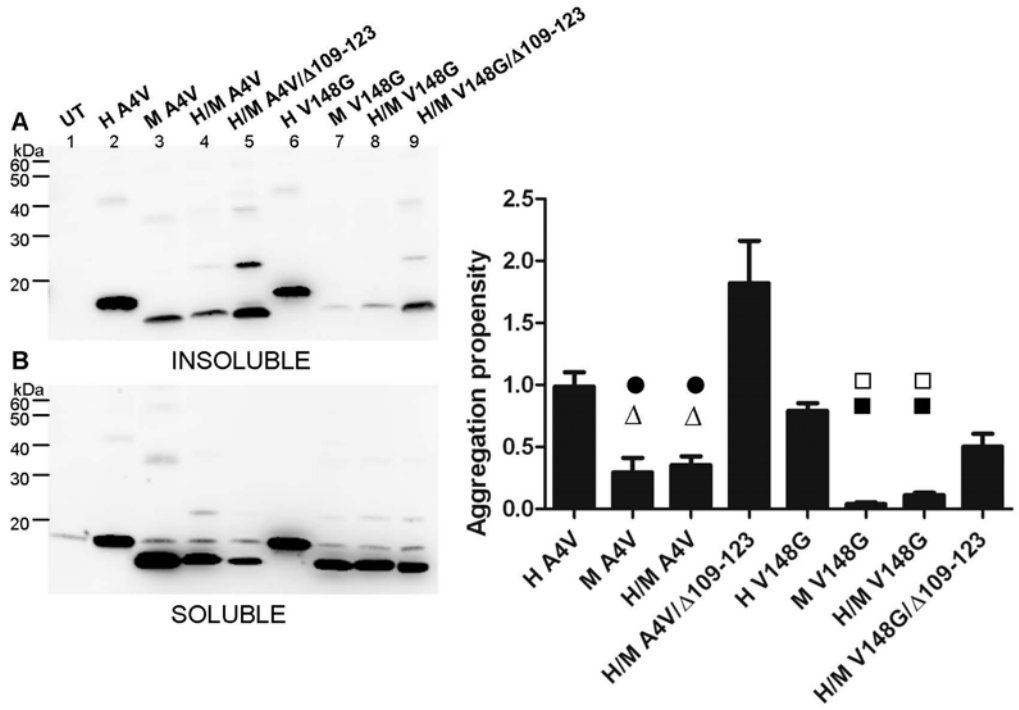

Figure 3-6. Human amino acids 109-123 enhance aggregation in FALS mutants throughout the protein. Mutants were expressed in HEK293-FT cells, and aggregate levels were measured as described in Methods. UT, untransfected cells. A4V and V148G are robustly aggregating FALS mutants. SDS-PAGE was performed in the presence of reducing agent in 18% Tris-Glycine gels. Immunoblots were probed with m/hSOD1 antiserum. A) Detergent-insoluble protein fraction (20 μg). B) Detergent-soluble protein fraction (5 μg). C) Relative aggregation propensity is a function of the amount of SOD1 found in the detergent-insoluble fraction compared to the detergent-soluble fraction. The graph represents the mean (±SEM (error bars)) of three different experiments. ●, Statistically different from H A4V: $p<0.05$. Δ, Statistically different from H/M A4V/Δ109-123: $p<0.05$. □, Statistically different from H V148G: $p<0.05$. ■, Statistically different from H/M V148G/Δ109-123: $p<0.05$.

If strong interactions are required between β-strands 6 and 7 for mutant human SOD1 aggregation to occur, we would predict that FALS mutants within this region would disrupt interactions between β-strands 6 and 7. Disrupted interactions between β-strands 6 and 7 might then result in lower aggregation propensity. Because aggregation inversely correlates with disease duration in FALS patients (Prudencio M, Hart PJ, Borchelt DR, Andersen P, submitted), we would predict that FALS mutants occuring between amino acids 42-50 and 109-123 would

produce a long disease duration. However, FALS mutations between amino acids 42-50 and 109-123 are moderate to highly aggregating in cell culture and have short disease duration (with 2 exceptions of long disease duration: G41D and H46R)(see also Table 1-1)(Prudencio M, Hart PJ, Borchelt DR, Andersen P, submitted). Thus, it is possible that a single mutation in one of these regions does not alter interaction or that tight binding is not required for aggregation.

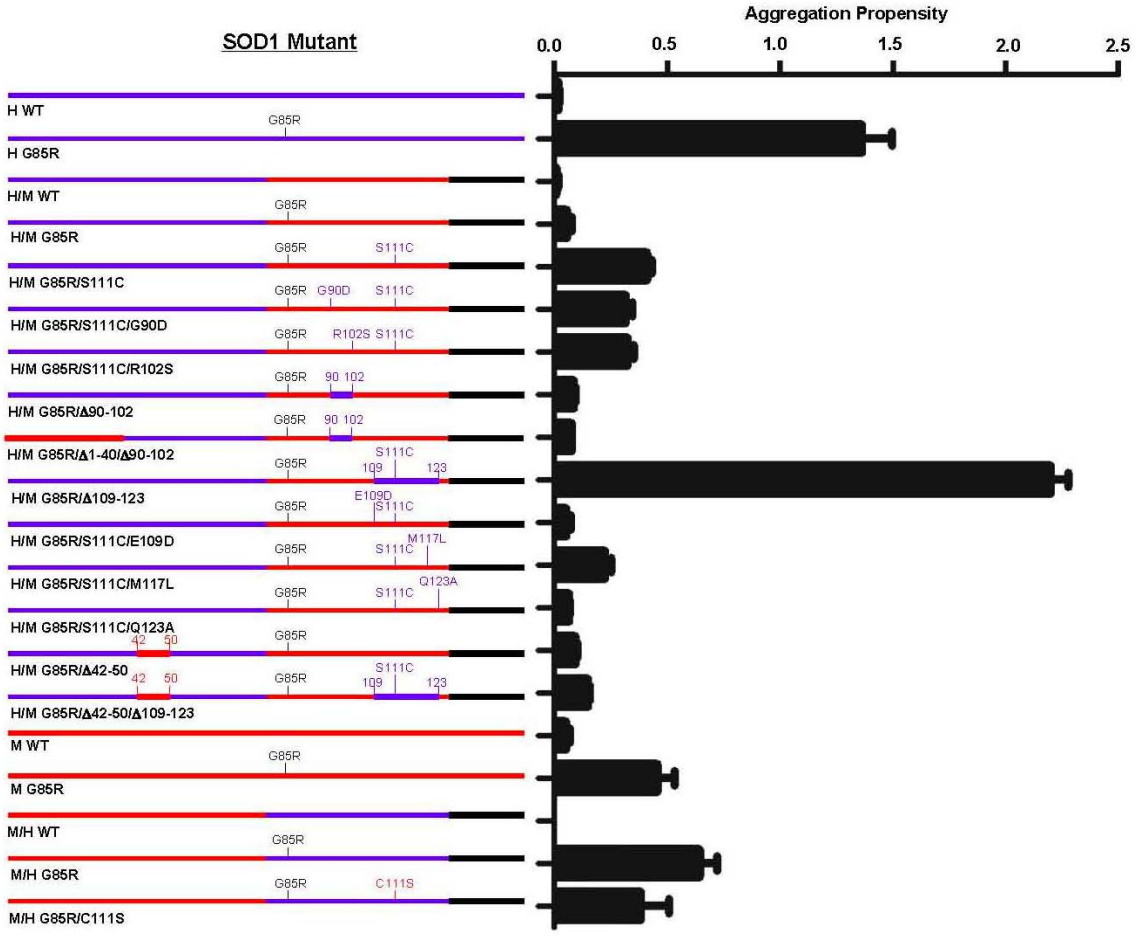

Figure 3-7. Chimeric proteins have differential aggregation propensities. Diagrams of the chimeric proteins used in this study are represented on the left panel. Blue, human SOD1. Red, mouse SOD1. Black, highly conserved between human and mouse (amino acids 124-153). Relative aggregation propensity is a function of the amount of SOD1 measured in the detergent-insoluble fraction compared to the detergent-soluble fraction. The graph represents the mean (±SEM (error bars)) of at least three different experiments.

Our study identifies sequences in β-strand 6 (residues 40-52) and β-strand 7 (residues 109-123) of SOD1 that appear to modulate aggregation of the human protein. Shaw and colleagues report similar findings, using hydrogen exchange and SOD1 peptides, that a portion of the dimer interface (residues 50-53) and a region containing β-strand 7, loop VII, and a portion of β-strand 8 (residues 117-144) are destabilized (164). Together, these studies suggest that mutant ions in SOD1 promote destabilization in the β-strand regions to enhance SOD1 aggregate formation. However, the mechanisms by which these residues enhance aggregation are yet to be determined.

CHAPTER 4
THE ROLE OF MUTANT SOD1 DISULFIDE OXIDATION AND AGGREGATION IN THE PATHOGENESIS OF FAMILIAL ALS•

Introduction

One proposed gain of toxic property is the propensity of SOD1 to misfold and for these misfolded SOD1 proteins to interact to form increasingly high-molecular-weight oligomers (105). Mutations in SOD1 destabilize the native state protein and possibly promote aggregation by diminishing metal binding and altering the secondary, tertiary, or quaternary structures (106-111). SOD1 immunoreactive inclusions are detected in tissues from FALS patients (112) and from SOD1 transgenic mice (113). Aggregated forms of mutant SOD1 can also be detected in SOD1 transgenic mice and cell culture based on detergent insolubility or size exclusion filtration (23, 43, 114, 115).

All mouse models of FALS that overexpress variants of mutant human SOD1 share a similar phenotype of motor neuron loss, muscle wasting, and hindlimb paralysis. FALS-linked SOD1 mutants that have been expressed in mice include: G93A (119), G37R (120), G85R (113), L126Z (115), G86R (121), D90A (123), Gins127TGGG (123), and H46R (166). Mouse models have also been developed to express forms of mutant SOD1 that combine disease-linked mutations and include experimental mutations to study the mechanism of SOD1 toxicity: H46R/H48Q (104) and H46R/H48Q/H63G/H120G (43). FALS-linked SOD1 mutant mice are predominantly characterized by the loss of motor neurons and the presence of aggregates in the spinal cord and brainstem (119, 124, 125). In all SOD1 transgenic mice, the appearance of symptoms is associated with an accumulation of sedimentable structures that are detergent-insoluble, which is diagnostic for protein aggregation (43, 104, 114, 115, 117, 123, 131, 132).

• This work is adapted from a manuscript published in the *Proceedings of the National Academy of Sciences*, In Press.

Together, this evidence illustrates that SOD1 aggregates are a prominent pathological feature in ALS mice and are possible mediators of the disease.

Several groups have described the appearance of SOD1 positive inclusions (130, 167) and high-molecular-weight, detergent-insoluble SOD1 protein complexes (23, 117, 123, 127, 142) in SOD1 transgenic mice prior to the onset of paralysis. These studies have also documented an increase in the abundance of these species as the mice age. A number of recent studies have examined the role of aberrant intermolecular disulfide cross-linking in the formation and stabilization of mutant SOD1 aggregates (23, 46, 141, 144, 145)(see Chapter 2). Mutant protein isolated from transgenic mouse models form aberrant intermolecular disulfide bonds that generate extensively cross-linked high-molecular weight proteins (23, 46, 123, 141) (see Chapter 2). However, the role of disulfide bonding in aggregate formation is unclear. Several studies have suggested that such cross-linking is crucial to aggregate formation (141, 143), whereas we recently demonstrated that, in cell culture models, aggregated forms of mutant SOD1 can be generated in the absence of disulfide cross-linking (see Chapter 2) (46).

In the present study, we have examined the solubility and extent of disulfide cross-linking through the course of disease in four different mutant SOD1 mouse models (G37R, G93A, and H46R/H48Q, L126Z). The questions asked were the following: 1) Do disulfide-cross-linked forms of mutant SOD1 accumulate prior to the formation of aggregates; 2) Is there a correlation between the formation of disulfide cross-linked SOD1 and the appearance of other pathologic or symptomatic features of disease; 3) What is the status of the normal intramolecular disulfide bond of SOD1 (C57 to C146) in aggregated forms of the protein. Using a highly sensitive detergent extraction assay coupled to immunoblot analysis, we traced the appearance and abundance of detergent-insoluble and disulfide-cross-linked SOD1 species throughout the

disease course of SOD1 transgenic mice. Our findings demonstrate that the accumulation of disulfide cross-linked mutant protein is co-incident with the accumulation of detergent-insoluble aggregates of mutant protein, with both of these events occurring well after the appearance of multiple pathologic abnormalities but concurrent with the onset of symptoms. Though aggregates formed *in vivo* are extensively disulfide cross-linked, complete reduction of disulfide cross-linkages does not dissociate SOD1 aggregates. In both cell culture and the mouse models, we find that mutant protein lacking any type of disulfide linkage, including its normal intramolecular disulfide bond, is the major component of the detergent-insoluble SOD1 aggregates. Because formation of the intramolecular disulfide bond is associated with maturation of SOD1, including acquisition of metal cofactors, it appears that mutant SOD1 that fails to mature may be disproportionately prone to aggregation.

Methods

Transgenic Mice

The SOD1 transgenic mice used in this study have been previously characterized: the G93A variant [B6SJL-TgN (SOD1-G93A)1Gur; disease onset 4-5 mo; Jackson Laboratory, Bar Harbor, ME, USA] (31), the G37R variant [line 29 (disease onset at 7-8 mo)] (147), the H46R/H48Q variant [line 139 (disease onset at 6-7 mo)] (104), the L126Z variant [line 45 (disease onset at 8-9 mo)] (115), and the wild type (WT) variant (line 76) (147).

SOD1 Aggregation Assay by Differential Extraction

The procedures used to assess SOD1 aggregation by differential detergent extraction and centrifugation in cell culture and mouse models were similar to previous descriptions (see Chapter 2) (43, 46). Spinal cords are homogenized with a probe sonicator (Microson XL2000; Misonix, Farmingdale, NY – 2W at 22.5 kHz) in 1:10 w/v of 1x TEN (10mM Tris pH 7.5, 1mM EDTA, 100mM NaCl). A crude supernate was isolated by centrifugation at 800g in an HS-4

rotor. A fraction of the spinal cord homogenate (100 μl) was then extracted in 0.5% NP40 as described previously (46).

Assay for Disulfide Cross-Linked SOD1

In variations of the extraction, samples were extracted in the presence of 100 mM iodoacetamide (as noted in the figure legends and text). SDS was substituted for NP40 in all extraction buffers: 10x SDS buffer (10 mM Tris pH 7.5, 1 mM EDTA, 100 mM NaCl, 10% SDS, and 1x protease inhibitor cocktail) was substituted for buffer 1, and 1x SDS buffer (10 mM Tris, 1mM EDTA, 100 mM NaCl, 1% SDS, and 1x protease inhibitor cocktail) was substituted for buffers 2 and 3. Protein concentration was measured in both fractions by BCA method as described by the manufacturer (Pierce, Rockford, IL, USA).

Immunoblotting

Standard sodium dodecyl sulfate-polyacrylamide gel electrophoresis (SDS-PAGE) was performed in 18% Tris-Glycine gels (Invitrogen, Calsbad, CA, USA). Samples were boiled for 5 minutes in Laemmli sample buffer prior to electrophoresis (148). Immunoblots were probed with rabbit polyclonal antibodies termed hSOD1 and m/hSOD1 at dilutions of 1:2500. The hSOD1 antiserum was raised against a synthetic peptide that is specific to human SOD1 (aa 24-36) (113). The m/hSOD1 antiserum was raised against a synthetic peptide conserved between mouse and human SOD1 (aa 124-136) (24).

Assay for Detection of Reduced and Oxidized SOD1

In some experiments, the reducing agent (5% β-mercaptoethanol [βME]) was omitted from the sample buffer. In experiments requiring in-gel reduction, prior to electrotransfer to nitrocellulose membranes, gels were incubated in transfer buffer in the presence of 2% βME for 10 minutes. Immunoblots were probed as described above.

Quantitative Analysis of Immunoblots

Quantification of SOD1 protein in detergent-insoluble and detergent-soluble fractions was performed by measuring the band intensity of SOD1 in each lane using a Fuji imaging system (FUJIFILM, LifeScience, Stamford, CT, USA) (see chapter 2).

Results

Previous studies of mice that model SOD1-linked FALS have established that the brainstems and spinal cords of symptomatic mice contain relatively high levels of detergent-insoluble mutant SOD1 mice (46, 114, 117, 141, 142). A substantial fraction of the detergent-insoluble mutant SOD1 that accumulates in these tissues is aberrantly cross-linked via intermolecular disulfide linkages (46, 114, 117, 141, 142).

In the present study, we determined the relative presence of disulfide cross-linked and detergent-insoluble mutant SOD1 through the course of disease in four models of SOD1-linked FALS (G93A, G37R, H46R/H48Q, and L126Z). Spinal cords were taken at time points throughout the lifespan of these transgenic SOD1 mice, and spinal cord homogenates were extracted in non-ionic detergent (0.5% NP40). In this assay, the detergent-insoluble fraction represents aggregated SOD1 protein. In the first 3 months of disease course, in SOD1-G93A mice, the levels of detergent-insoluble SOD1 remained low (Fig. 4-1A, lanes 2, 3, and 4) and roughly equivalent to the level of detergent-insoluble SOD1 in control mice expressing WT SOD1 (Fig. 4-1A, lane 1); rising only after 120 to 150 days (Fig. 4-1A, lanes 5 and 6), at which time the mice were paralyzed. Throughout the lifespan of the SOD1-G93A mice, the amount of detergent-soluble SOD1, which is presumed to represent the fraction of mutant protein that acquires a near normal conformation, remained constant (Fig. 4-1B). Similarly to SOD1-G93A mice, SOD1 aggregates were detected only near the endstage of disease in SOD1-G37R, SOD1-H46R/H48Q, SOD1-L126Z mice, which have similar ages of disease onset (Fig. 4-1C, lanes 3

and 4; Fig. 4-1E, lanes 5 and 6; Fig 4-1F, lanes 4 and 5; respectively). Prior to the presence of overt symptoms for these mutant lines of mice, the levels of detectable detergent-insoluble SOD1 were not different from that of control WT SOD1 mice (Fig. 4-1C, lanes 1 and 2; Fig. 4-1E, lanes 1-4; Fig. 4-1F, lanes 1 and 2). The levels of G37R and H46R/H48Q SOD1 in the detergent-soluble fraction remained constant as the mice aged (Figs. 4-1D and F). SOD1-L126Z has a short half-life; so, little detergent-soluble SOD1 accumulates throughout the disease course (Fig. 4-1 H). Thus, each SOD1 variant illustrated similar aggregation profiles throughout their lifespans in that the levels of detergent-insoluble SOD1 aggregates rise only near the endstage of disease.

Because all SOD1 variants illustrate similar aggregate accumulation over time, we sought to compare the variants at presymptomatic and symptomatic stages of the disease. At a pre-symptomatic time point, the spinal cords of each line of SOD1 transgenic mice (G93A, G37R, H46R/H48Q, and L126Z) contained no greater level of detergent-insoluble SOD1 than mice expressing WT SOD1, with the exception of SOD1-L126Z (Fig. 4-2A). Thus, at the early stages of the disease, the levels of detergent-insoluble SOD1 are low with the vast majority of the protein found in the detergent-soluble fraction (Fig. 4-2B). At disease endstage for each of these mutants, detergent-insoluble SOD1 was readily detected (Fig. 4-2C, lanes 2-9). While the degree of accumulation of detergent-insoluble SOD1 was similar in the G93A and H46R/H48Q mice, the levels of detergent-insoluble SOD1 in endstage G37R mice were consistently lower than the other two lines (Fig. 4-2C). SOD1 in the detergent-soluble fraction at disease endstage (Fig. 4-2D) was similar to that present at the presymptomatic stage (Fig. 4-2B), which indicates that overall SOD1 levels do not change as the mice age. It is interesting to note that the amount of detergent-insoluble SOD1 detected at disease endstage (Fig. 4-2C) may be related to the age

that the mouse develops paralysis. SOD1-G37R mice, which develop symptoms between 210 and 240 days, have the lowest amount of detergent-insoluble SOD1 species (Fig. 4-2C, lanes 2 and 3). These findings indicate that the levels of accumulated SOD1 aggregates at endstage disease vary to some degree among the different lines of mice.

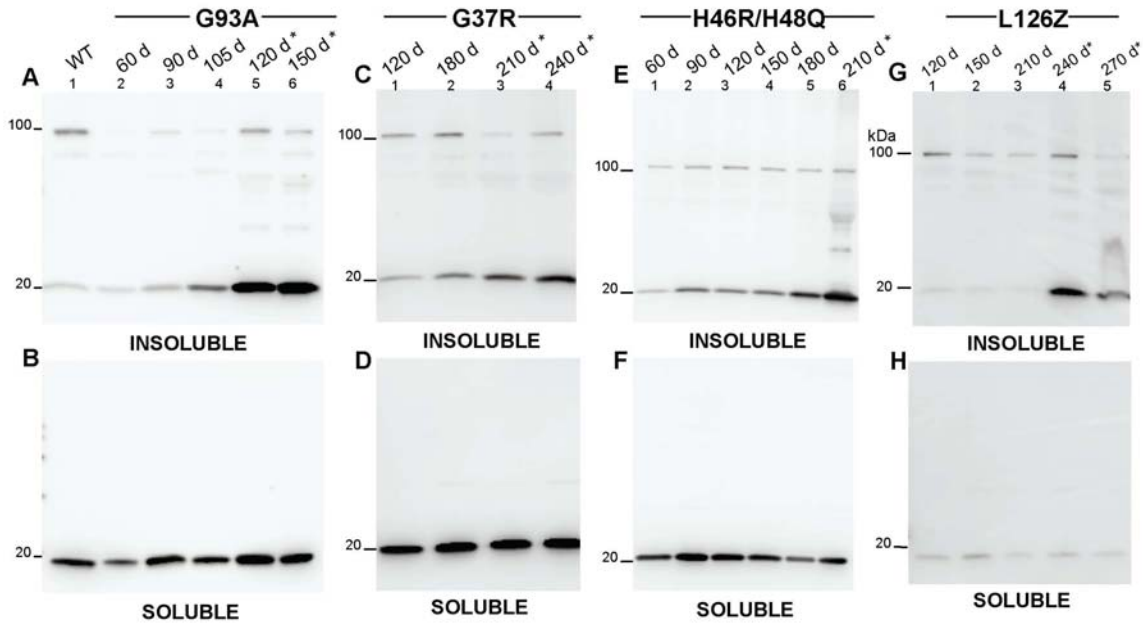

Figure 4-1. The levels of detergent-insoluble SOD1 increase dramatically late in the course of disease in SOD1 transgenic mice. Detergent (NP40) insoluble (20 μg) and soluble proteins (5 μg) were isolated from spinal cord as described in Methods and then electrophoresed in the presence of reducing agent before immunoblotting (hSOD1 antiserum). A, B) G93A detergent-insoluble (A) and soluble (B) proteins. C, D) G37R detergent-insoluble (C) and soluble (D) proteins. E,F) H46R/H48Q detergent-insoluble (E) and soluble (F) proteins. G,H) L126Z detergent-insoluble (G) and soluble (H) proteins. WT, 180 days. * Denotes mice harvested at disease endstage (paralysis).

In SOD1 transgenic mice, extensive pathological abnormalities have been described prior to the onset of paralysis. For each SOD1 variant, aggregation was quantified and expressed as a percentage of the amount of detergent-insoluble SOD1 at disease endstage. In SOD1-G93A mice, aggregation dramatically increased as the mice approach disease endstage (Fig. 4-3A). When comparing the aggregation potential in these mice with other pathology that has been previously described, it was clear that a number of abnormalities occur prior to the accumulation

of aggregated SOD1 (Fig. 4-3A). Similarly, in SOD1-G37R mice, significant pathology, including vacuole formation and gliosis, occurred prior to the robust accumulation of detergent-insoluble SOD1 (Fig. 4-3B). Less is known about the progression of disease in SOD1-H46R/H48Q mice, but we have detected evidence of reactive gliosis in these mice as early as 60 days of age (Fig. 4-4B), well before the appearance of significant levels of aggregated mutant SOD1 (Fig. 4-3C). Similarly, in SOD1-L126Z mice, we have detected evidence of gliosis at 150 days (Fig. 4-5) prior to aggregate accumulation (Fig. 4-3D), and αB crystallin activation in astrocytes at 240 days (Fig. 4-6), at disease endstage. Note that variation in the age at which mice reach criteria for endstage (obvious hindlimb paralysis) introduces variability in the lifespan of the mice. For this reason, the animals sacrificed for timed harvest may be at different stages of disease, leading to variability in aggregate loads in tissues at pre-symptomatic ages. SOD1-G93A mice, which have the shortest lifespan, also had the most rapid increase in aggregate levels (Fig. 4-3A). Correspondingly, SOD1-H46R/H48Q mice, which have the longest lifespan, had the slowest increase in aggregate levels (Fig. 4-3C). Thus, it appears that the earlier the mice developed symptoms, the more quickly the levels of aggregated SOD1 rise. However, in all cases, significant pathologic abnormalities occurred in spinal cord prior to the accumulation of significant levels of mutant SOD1 aggregates.

It has been proposed that oxidative stress may enhance the formation of non-native, intermolecular disulfide bonds that contribute to the formation of high-molecular-weight disulfide cross-linked aggregates (141), a prominent feature in symptomatic SOD1 transgenic mice (123, 141, 142). We sought to determine if disulfide cross-linking between misfolded SOD1 species occurs as a precursor to aggregate formation. Spinal cords were taken at time points throughout the lifespan of SOD1-G93A transgenic mice and were extracted in 1% SDS in

the presence of iodoacetamide (IA), a thiol modifying agent that irreversibly prevents air oxidation and disulfide bond scrambling. Treating spinal cord homogenates with IA allows for a more accurate representation of the disulfide status of SOD1 in the spinal cord at the time of extraction, without experimental alteration. A high concentration of SDS (1%) was sufficient to solubilize most of the SOD1 protein (Fig. 4-7A), which allowed for the detection of the total amount of high-molecular-weight, disulfide cross-linked species in the spinal cord at each time point. High-molecular-weight, disulfide cross-linked SOD1 species were most prominent at disease endstage in SOD1-G93A mice (Fig. 4-7B, lanes 7 and 8). At 105 days, 2-3 weeks prior to the appearance of overt hindlimb weakness, high-molecular-weight disulfide cross-linked species were detectable (Fig. 4-7B, lane 6). These high-molecular-weight species correspond to SOD1 multimers, representing dimers, trimers, tetramers, and larger multimers. Prior to 105 days, high-molecular-weight species were virtually undetectable (Fig. 4-7B, lanes 3-5). Treating the SDS-solubilized fractions with reducing agent, prior to gel electrophoresis, produced SOD1 monomer (Fig. 4-7C), indicating that the high-molecular-weight species detected (Fig. 4-7B, lanes 6, 7, 8) were composed of disulfide cross-linked SOD1 species.

For comparison to the appearance of disulfide cross-linked mutant protein, we show the time course of the appearance of NP40-insoluble mutant SOD1 at the ages examined (Figs. 4-7D, E, and F). High-molecular-weight, disulfide cross-linked, SOD1-G93A was most abundant at disease endstage (Fig. 4-7D, lanes 7 and 8), with a smaller fraction of high-molecular-weight species present prior to paralysis at 105 days (Fig. 4-7D, lane 6). Before 105 days, virtually no detergent-insoluble, disulfide cross-linked, SOD1-G93A was detected (Fig. 4-7D, lanes 3-5). The detergent-soluble fraction contained only SOD1 monomer until disease endstage (120 and 150 days), when faint high-molecular-weight SOD1 immunoreactive bands were detected (Fig.

4-7E, lanes 7 and 8). Collectively, these data demonstrate that the levels of disulfide cross-linked mutant SOD1 rise in parallel with the levels of detergent-insoluble protein.

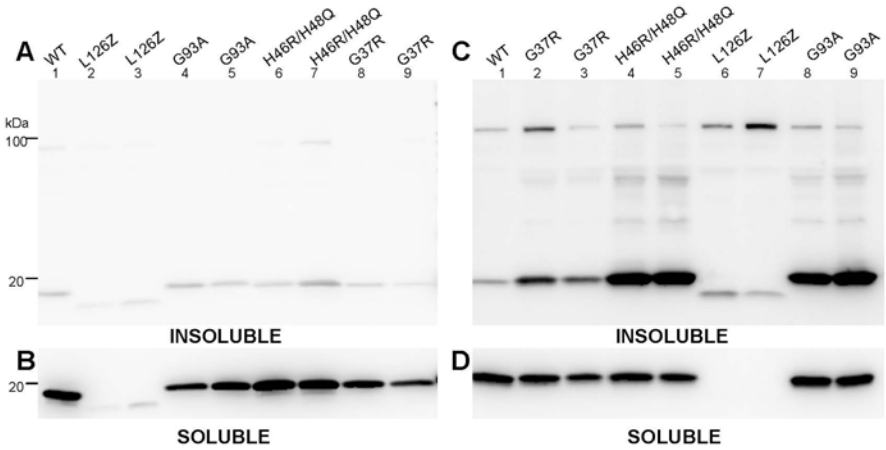

Figure 4-2. Variation in the levels of detergent-insoluble SOD1 in the spinal cords of paralyzed FALS mice. Spinal cords were extracted in buffers containing 0.5% NP40 to isolate detergent-insoluble and soluble protein fractions and analyzed by immunoblot as described in Figure 1. A) Detergent-insoluble SOD1 (20 μg total protein from insoluble fraction) from presymptomatic mice: L126Z (120 d), G93A (60 d), H46R/H48Q (60 d), G37R (120 d). B) Detergent-soluble SOD1 (5 μg total protein from soluble fraction). C) Detergent-insoluble SOD1 (20 μg total protein from insoluble fraction) from endstage (paralyzed) mice: G37R (240 d), H46R/H48Q (210 d), L126Z (270 d), and G93A (150 d). D) Detergent-soluble SOD1 (5 μg total protein from soluble fraction). WT, 180 days.

The logistics of harvesting tissues from multiple mice at different stages of disease requires storage of tissues, homogenates, or individual tissue extracts for some period of time. The studies here included tissues that had been in storage for extended intervals as well as tissues harvested and used within a few days. In our experience, storage of the tissues by flash freezing on dry ice followed by storage at -80ºC introduces the least artifact in analysis of mutant SOD1 aggregation. By this approach, tissues from different animals at different ages can be directly compared by side-by-side extraction and immunoblotting. We observed no obvious indication that tissues stored for longer intervals contained higher levels of disulfide cross-linked material. In one example, we compare the extraction of tissues from 60-day-old animals stored at -80ºC to

tissues that were harvested and extracted in the same day (Fig. 4-7, compare lanes 3 and 4 all panels). Freezing and storage did not induce the formation of disulfide cross-linked material. Thus we are confident that the storage of tissue at -80°C did not artificially reduce disulfide cross-links and that such cross-linking do not extensively occur prior to the appearance of detergent-insoluble mutant SOD1.

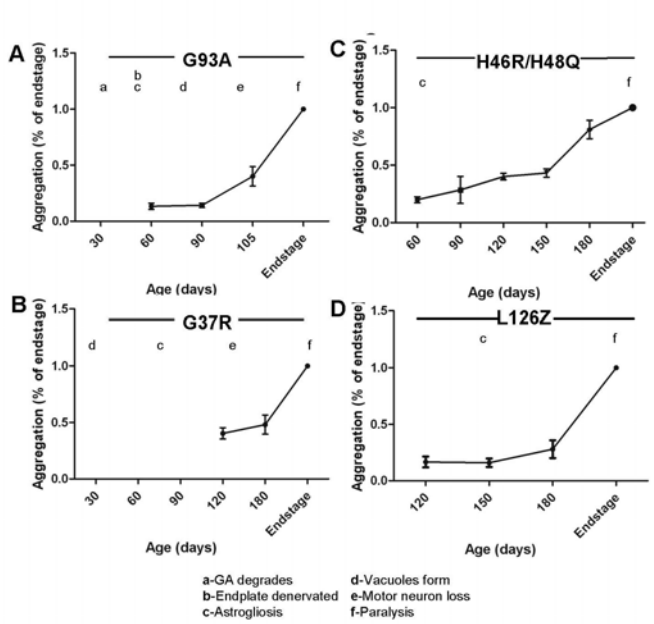

Figure 4-3. Detergent-insoluble SOD1 accumulates to high levels near disease endstage. The amount of SOD1 present in the detergent-insoluble protein fraction was quantified by measuring the band intensity of SOD1 in each lane using a Fuji imaging system (FUJIFILM, LifeScience, Stamford, CT, USA). Aggregation was quantified by calculating the ratio of band intensity in the insoluble fraction at each time point to the insoluble fraction at disease endstage (set at 1). The standard error of the mean (SEM) was calculated for aggregation of each sample and graphed (A) G93A; B) G37R; C) H46RH48Q; D) L126Z). Timelines of pathologic changes were graphed with aggregation.

Because high-molecular-weight, disulfide-linked SOD1 species were prominent at disease endstage in SOD1-G93A mice, we sought to determine whether the maintenance of structures that are detergent-insoluble is dependent upon disulfide cross-linking. Spinal cords from SOD1-G93A mice (at disease endstage) were extracted in 0.5% NP40 and in the presence

of varying concentrations of reducing agent (βME). In comparison to extractions performed in the absence of βME, extraction of the spinal cord tissue in 30% βME did not substantially change the amount of mutant SOD1 that partitioned into the detergent-insoluble fraction (Fig. 4-8A). Similarly, extraction in 30% βME did not alter the amount of mutant SOD1 that partitioned into the detergent-soluble fraction (Fig. 4-8B). Thus, while high-molecular-weight species of SOD1 are extensively disulfide cross-linked (Fig. 4-7D), these bonds are not responsible for maintaining the structure that induces detergent-insolubility, which we equate with aggregation.

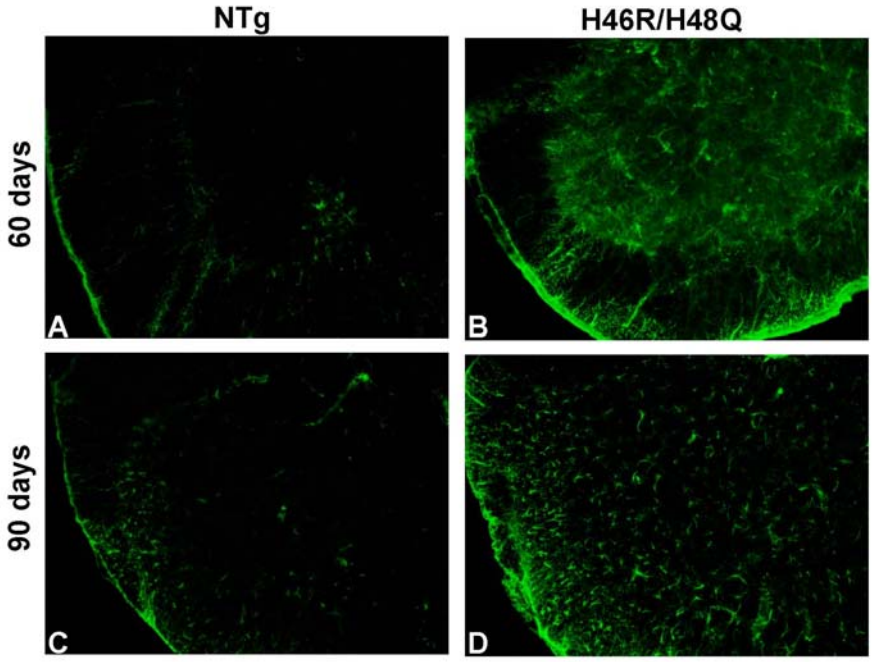

Figure 4-4. Astrogliosis occurs early in disease progression in SOD1-H46R/H48Q mice. At the ages specified, SOD1-H46R/H48Q mice were perfused with 4% paraformaldehyde. Tissue was stored in 30% sucrose prior to cryostat sectioning (14 microns). Sections were blocked in 5% normal goat serum (Invitrogen, Calsbad, CA), and tissue sections were stained with antibodies to GFAP (Chemicon) followed by secondary anti-mouse IgG antibodies conjugated to Alexafluor 488 $F(ab')_2$ fragment (green) (Invitrogen). NTg, age matched littermates. Ventral horn, spinal cord. Magnification of image at capture - 40x.

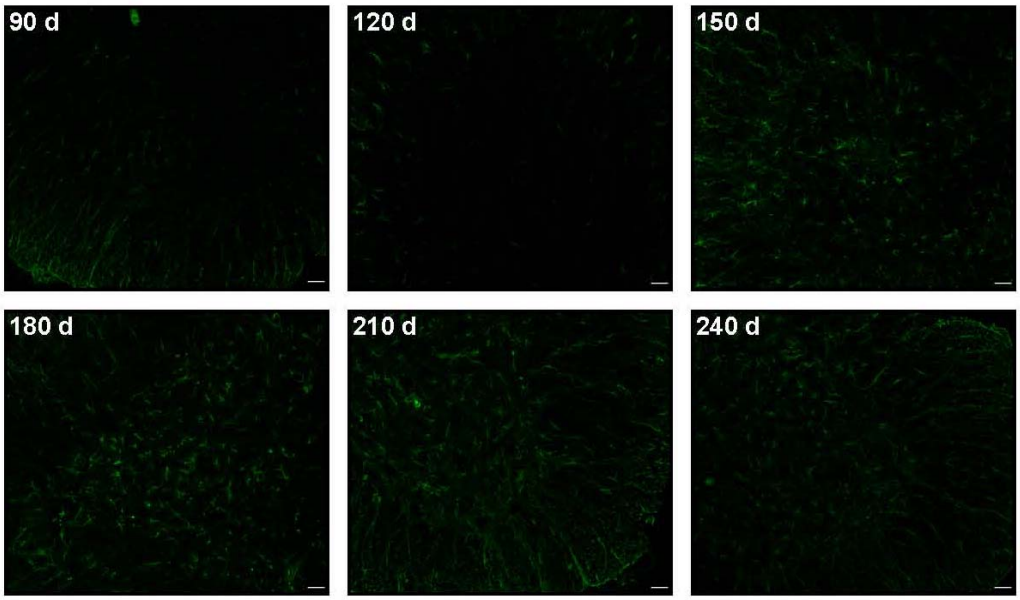

Figure 4-5. Astrogliosis occurs at 150 days in L126Z mice. At the ages specified, SOD1-L126Z mice were perfused with 4% paraformaldehyde. Tissue was stored in 30% sucrose prior to cryostat sectioning (14 microns). Sections were blocked in 5% normal goat serum (Invitrogen, Calsbad, CA), and tissue sections were stained with antibodies to GFAP (Chemicon) followed by secondary anti-mouse IgG antibodies conjugated to Alexafluor 488 $F(ab')_2$ fragment (green) (Invitrogen). Ventral horn, spinal cord. Magnification of image at capture - 40x. Scale bar – 10 microns.

Recent studies have demonstrated that SOD1 that has acquired its normal intramolecular disulfide bond can be distinguished from reduced forms by electrophoretic migration in SDS-PAGE (in the absence of reducing agents) (142, 168). The oxidized form of the enzyme migrates slightly faster than the reduced form; possibly as a result of the more compact structure of the oxidized form of the protein. In non-reducing SDS-PAGE of NP40-insoluble fractions from the spinal cords from endstage G93A mice, we detected a form of mutant protein that appeared to be completely reduced with an apparent molecular mass of about 20 kDa (see Fig. 4-7D, lanes 7 and 8). In the detergent-soluble fractions of mice across all ages, in these non-reducing gels, we observed mutant SOD1 proteins of 20 kDa and approximately 16 kDa (see Fig. 4-7E, lanes 2-8). This banding pattern matched that described by Jonsson et al, as reduced

(labeled – R) and disulfide-oxidized (labeled – O) SOD1 protein (142). The presence of the single higher-molecular-weight band in the detergent-insoluble fraction suggested that all of the monomeric SOD1 protein in this fraction is completely reduced. However, in the study by Zetterstrom et al, the authors demonstrated that the detection of oxidized forms of SOD1 by non-reducing SDS-PAGE and immunoblotting is greatly enhanced when the gels are incubated in reducing agent prior to electrophoretic transfer to immunoblotting membranes (168). Treating the SDS and NP40 solubilized fractions with reducing agent, prior to gel electrophoresis, produced a single SOD1 band that migrated at about 20 kDa (Fig. 4-7C, F). Therefore, we concluded that the spinal cords of G93A mice contained both reduced and oxidized forms of SOD1.

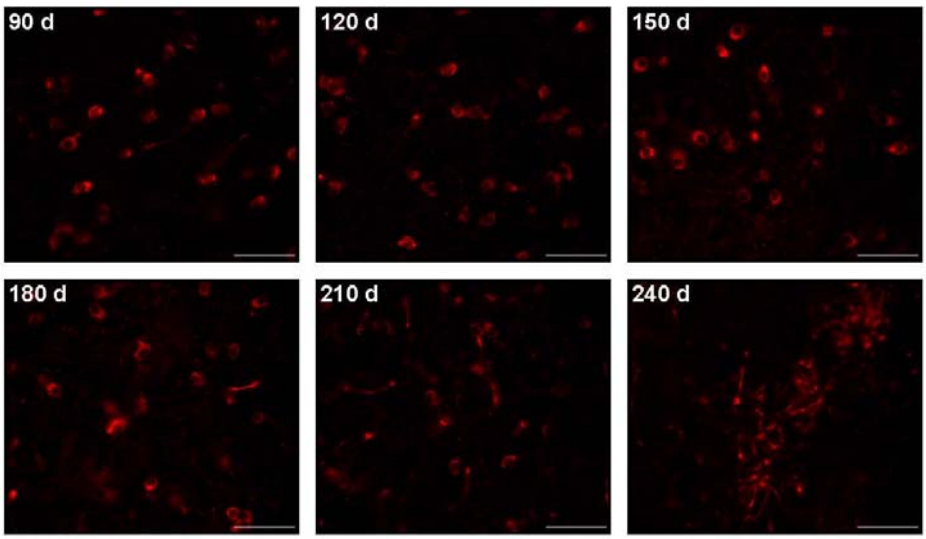

Figure 4-6. αB crystallin is upregulated in astrocytes at disease endstage in L126Z mice. At the ages specified, SOD1-L126Z mice were perfused with 4% paraformaldehyde. Tissue was stored in 30% sucrose prior to cryostat sectioning (14 microns). Sections were blocked in 5% normal goat serum (Invitrogen, Calsbad, CA), and tissue sections were stained with antibodies to αB crystallin (Stressgen) followed by secondary anti-mouse IgG antibodies conjugated to Alexafluor 568 $F(ab')_2$ fragment (green) (Invitrogen). Ventral horn, spinal cord. Magnification of image at capture - 40x. Scale bar – 40 microns.

To confirm this finding and eliminate any potential influence of sample preparation or storage, we sacrificed paralyzed animals and performed the detergent extraction and SDS-PAGE in the same day. We also included a treatment in which the gels were incubated in reducing agent prior to electrophoretic transfer to immunoblotting membranes. Zetterstrom and colleagues demonstrated that the detection of oxidized forms of SOD1 by non-reducing SDS-PAGE and immunoblotting is enhanced by in-gel reduction of disulfide bonds prior to immunoblot transfer (168). In detergent-soluble fractions of tissues from both WT and endstage G93A mice, we detected both reduced and oxidized forms of monomeric SOD1. In the detergent-soluble fractions, the oxidized form of the protein represented the vast majority of detectable SOD1 protein (Fig. 4-9B, lanes 2-4). In the detergent-insoluble fractions, no WT SOD1 was observed and the major detectable species of mutant G93A SOD1 migrated as expected for reduced protein (Fig. 4-9A, lanes 2-4). A second minor species of detergent-insoluble mutant SOD1 in these fractions migrated to size similar, but not identical to, oxidized SOD1. This species was not detected when in-gel reduction before transfer was omitted (Fig. 4-9C, lanes 3-4). Whether this apparently oxidized, detergent-insoluble form of mutant SOD1 possesses a disulfide bond between cysteines 57 and 146 is uncertain. It is possible that an intramolecular disulfide between other cysteine residues produced this species of mutant, detergent-insoluble SOD1. Similarly, we found significant levels of reduced mutant SOD1 in the detergent-insoluble fraction of tissues from endstage G37R and H46R/H48Q mice (Fig. 4-10A). For reasons that are unclear, in-gel reduction noticeably reduced the amount of high-molecular-weight SOD1 species detected in the detergent-insoluble fractions in these experiments. It appears that in-gel reduction increases either the transfer efficiency or antigenicity of SOD1 (with the normal 57 to 146 disulfide bond) for immunoblot detection (168);

however, this treatment reduces one or both of these parameters for high-molecular-weight SOD1 with abnormal intermolecular disulfide bonds. Whether the disulfide cross-linked high-molecular-weight mutant SOD1 possesses a normal 57 to 146 disulfide bond is unclear. Overall, we conclude that a portion of the mutant SOD1 that accumulates as detergent-insoluble is derived from protein that either never acquired or lost the normal intramolecular disulfide bond.

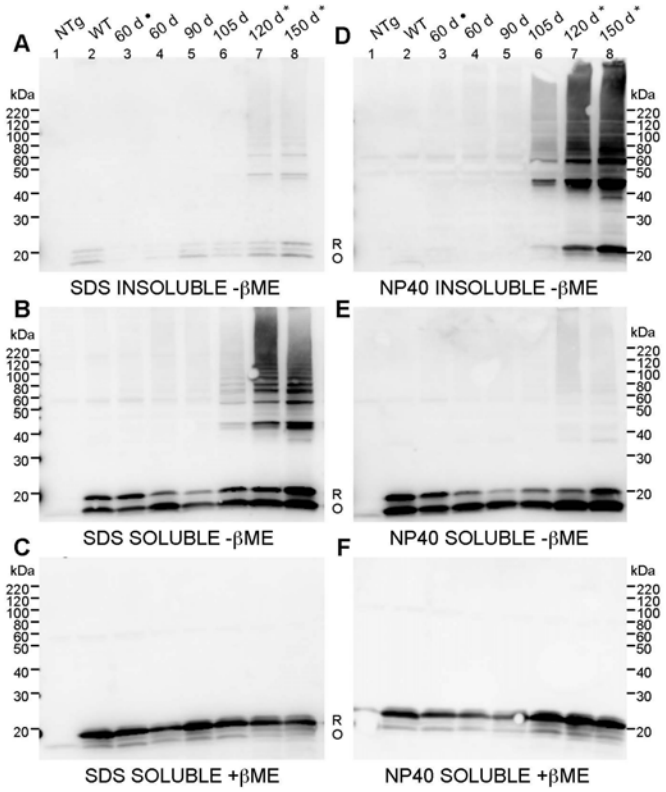

Figure 4-7. The appearance of disulfide cross-linked SOD1 is coincident with the accumulation of detergent-insoluble mutant protein. G93A spinal cords were extracted in 1% SDS (panels A,B,C) or in 0.5% NP40 (panels D,E,F) in the presence of 100 mM iodoacetamide. Fractions were electrophoresed in the presence (C, F) or absence (A,B,D,E) of βME. Immunoblots were probed with m/hSOD1 antiserum. NTg, nontransgenic. WT, WT SOD1. A) Insoluble in 1% SDS (20 μg). B) Soluble in 1% SDS (5 μg). C) Soluble in 1% SDS electrophoresed in the presence βME. D) Insoluble in 0.5% NP40. E) Soluble in 0.5% NP40. F) Soluble in 0.5% NP40 electrophoresed in the presence βME. R, reduced disulfide bond (C57-C146). O, oxidized disulfide bond (C57-C146). * Denotes disease endstage (paralysis). • Denotes fresh spinal cord tissue. Ntg, 90 days. WT, 180 days.

We re-examined the detergent-insoluble forms of mutant SOD1 that accumulate in the spinal cords of G93A, G37R, and H46R/H48Q mice using the in-gel reduction procedure to enhance detection of oxidized forms of SOD1. In spinal cords of endstage mice that express each of these three mutants, in the detergent-insoluble fraction we detected both reduced and oxidized forms of monomeric SOD1 (Fig. 4-10A, lanes 3-5). The relative ratio of reduced to oxidized was reproducibly in favor of the reduced form being most prominent. By contrast, in the detergent-soluble fractions, the ratio of reduced to oxidized protein was far in favor of the oxidized form in mice that express WT, G93A, and G37R SOD1 (Fig. 4-10B, lanes 2-5). However, in mice that express H46R/H48Q SOD1, the ratio of reduced to oxidized protein in the detergent-soluble fraction remained in favor of the reduced form of the protein (Fig. 4-10B, lane 5). Thus, these results are consistent with the cell culture findings in that, with regard to forms of detergent-insoluble mutant SOD1 that migrate near the position expected for monomeric enzyme, reduced forms of mutant SOD1 appear to preferentially acquire detergent-insolubility.

To further explore the role of reduced and oxidized mutant SOD1 in aggregation, we turned to a cell culture model of aggregation that utilizes HEK293-FT cells (23, 43, 46). The high levels of expression that are achieved in these cells induced rapid aggregation of mutant SOD1 (A4V, G37R, G93A) and the formation of detergent-insoluble, sedimentable forms of the protein (Fig. 4-11) [also see (23, 43, 46)]. When we applied the non-reducing SDS-PAGE, with or without, in-gel reduction prior to transfer, we noted a number of interesting features of the cell culture model. First, we determined that in the cell culture model, the majority of detergent-insoluble mutant SOD1 that accumulates appears to be completely reduced (compare Figs. 4-11A and C). In these gels we included purified dimeric, metallated, WT human SOD1 (isolated

from yeast) as a control (lanes 1 and 8 of each gel – these proteins were not subjected to detergent extraction or centrifugation). Reduction and denaturation of this purified protein produced a single band that migrated at approximately 20 kDa (Fig. 4-11A, lane 1), where as denaturation and SDS-PAGE in the absence of reducing agent produced a single band that migrated at approximately 16 kDa (Fig. 4-11A, lane 8). Note that the oxidized form of purified WT SOD1 was not as readily detected when the in-gel incubation with reducing agent was omitted prior to transfer (compare Figs. 4-11A and C, lane 8 in each) [also see (168)].

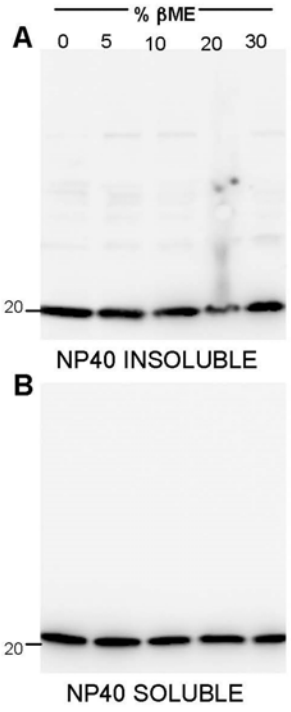

Figure 4-8. SOD1 aggregates resist dissociation in high concentrations of reducing agents. Spinal cord tissue from a symptomatic G93A transgenic mouse was extracted in 0.5% NP40 and increasing concentrations of βME (noted on Figure). Immunoblots were probed with hSOD1 antiserum. A) Detergent-insoluble (20 μg). B) Detergent-soluble (5 μg).

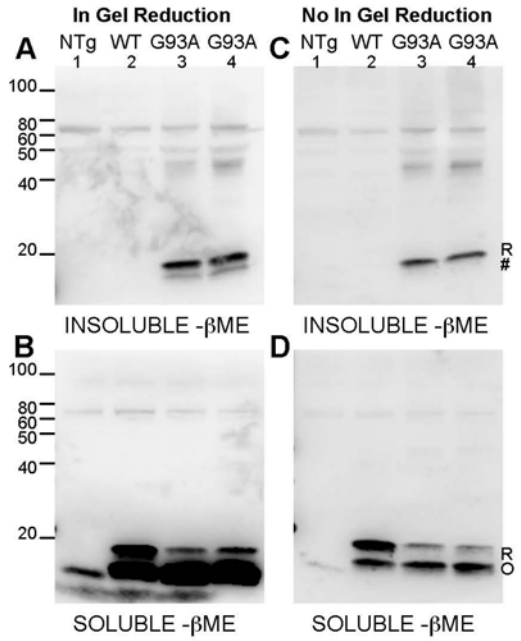

Figure 4-9. SOD1 aggregates are largely composed of disulfide-reduced forms of SOD1 in fresh spinal cord tissue. Spinal cords from freshly harvested mice were extracted in non-ionic detergent and iodoacetamide. A and B) Gels were incubated in reducing buffer prior to transfer. C and D) Gels were processed without reducing agent. A and C) Detergent insoluble (40 μg protein). B and D) Detergent soluble (40 μg protein). Immunoblots were probed with m/hSOD1 antiserum. R, reduced. O, oxidized. #, Possible non-natively oxidized bond.

Applying this technique to the detergent-insoluble forms of the A4V, G37R, G93A, and H46R/H48Q mutants produced in cell culture demonstrated an electrophoretic migration to a size closer to the reduced forms of purified WT SOD1 (Figs. 4-11A and C). Note that the relative detection of reduced and oxidized mutant protein in these fractions was similar between gels that were or were not incubated in reducing agents prior to transfer. In these cell culture experiments and similar to previous studies (43), the H46R/H48Q mutant produced less detergent-insoluble protein in cell culture. By contrast in the detergent-soluble fractions of these cell extracts, we detected both reduced and oxidized forms of SOD1 (Fig. 4-11B, lanes 3-7). Omission of the in-gel reduction demonstrated the upper band to be the reduced forms of SOD1 (Fig. 4-11D, lanes

3-7). In analyzing the detergent-soluble fractions in the blots that included the in-gel reduction, we noted that the relative ratio of reduced to oxidized protein differed between the mutant and WT SOD1 proteins. In a very reproducible pattern, the predominant form of WT SOD1 in these transfected cells migrated to the same position as purified oxidized SOD1 (Fig. 4-11B, lanes 3 and 8). By contrast, for each of the mutants, the predominant form of detergent-soluble protein migrated to the position of reduced WT SOD1 (Fig. 4-11B, compare lane 1 to lanes 4-7). For the A4V and H46R/H48Q mutants, the majority of detergent-soluble protein migrated to the same position as reduced WT protein. Together, these findings demonstrate that reduced forms of mutant SOD1 (lacking the normal intramolecular disulfide bond – and presumably any other type of intramolecular disulfide linkage) are more prone to form detergent-insoluble complexes, which is consistent with evidence (see Chapter 2) which suggests that cysteine residues are important for aggregation via a mechanism alternative to disulfide cross-linking.

Discussion

High-molecular-weight, disulfide-linked SOD1 aggregates accumulate to high levels in paralyzed transgenic mice that express mutant forms of SOD1 linked to familial ALS (123, 141, 142). In the present study, we sought to trace the accumulation of these species throughout the lifespans of four lines of mutant SOD1 transgenic mice (G93A, G37R, H46R/H48Q, L126Z). We demonstrate, in four lines of mutant SOD1 transgenic mice (G93A, G37R, H46R/H48Q, L126Z), that the formation of SOD1 aggregates follows a similar time course. In all four lines of mice, SOD1 aggregates accumulate to high levels just prior to hindlimb paralysis but well after the appearance of several pathologic features in spinal cord. We also demonstrate that the appearance of disulfide cross-linked mutant SOD1 parallels the appearance of detergent-insoluble (NP40-insoluble) protein. We find no evidence that disulfide cross-linked forms of SOD1 are precursors to more highly structured aggregates. Moreover, we demonstrate that

disulfide cross-linking is not responsible for the maintenance of structures that induce insolubility in NP40 detergent. In both cell and mouse models, a significant fraction of the NP40-insoluble mutant SOD1 dissociates upon SDS and heat denaturation (in the absence of reducing agent) to what appears to be monomeric protein. These species of mutant SOD1 must be organized into high-molecular-weight structures, which results in their sedimentation upon centrifugation, that are bound via forces other than disulfide cross-linking. We demonstrate that the majority of these non-cross-linked forms of mutant protein in SOD1 aggregates appear to lack the normal intramolecular disulfide bond. Moreover, our work in cell culture models suggests that completely reduced forms of mutant protein are more prone to produce aggregates. This finding is in agreement with a recent study of the *in vitro* aggregation of purified mutant SOD1 (169). Collectively, our data supports a model in which the mutant SOD1 that fails to acquire the normal intramolecular disulfide bond (or suffers reduction of this bond) is prone to aggregate. These events seem to occur to the greatest extent late in disease progression. The implications of these data in regard to the role of aggregation in disease pathogenesis are discussed below.

Redox Chemistry and SOD1 Aggregation in SOD1 Transgenic Mice

High-molecular-weight, detergent-insoluble, SOD1 complexes (termed aggregates) have been repeatedly detected in spinal cords of transgenic mice that model SOD1-linked FALS (see Chapter 2) (23, 46, 117, 141, 142). Recently, several groups have published studies that implicate aberrant disulfide cross-linking between cysteine residues, particularly cysteines 6 and 111, of mutant SOD1 in the formation of these complexes (23, 46, 141, 144, 145). However, we have provided evidence to indicate that disulfide bonding is not the only force stabilizing these aggregates (46)(see Chapter 2). In this study, we sought to determine whether disulfide cross-linking precedes the formation of detergent-insoluble SOD1 aggregates. We determined that

disulfide cross-linked forms of mutant protein are detected concurrently with detergent-insoluble mutant SOD1, suggesting that it is unlikely that an oxidative event occurs early in the disease course to induce disulfide cross-linking, which then induces the formation of aggregates. This line of thinking is consistent with a previous study from our group that demonstrated that mutant forms of SOD1 that are incapable of forming disulfide cross-links retain the ability to aggregate into high-molecular-weight species (46)(see Chapter 2). We also demonstrate that these high-molecular-weight structures are dissociated by high levels of reducing agent (30% βME), leaving SOD1 monomer intact, which indicates that these aberrant disulfide cross-links are not directly involved in the formation or maintenance of these structures. Instead, it is likely that disulfide cross-links form after the mutant SOD1 proteins come into close proximity as a result of assembly into high-molecular-weight structures.

Post-Translational Modification of Mutant SOD1 and Aggregation

In addition to high-molecular-weight, disulfide cross-linked, forms of mutant SOD1, detergent-insoluble fractions also contain forms of mutant protein that migrate at the size expected for monomeric protein. Using a protocol developed by Jonsson and colleagues (142), we demonstrate that the majority of the mutant SOD1 from G37R, G93A, and H46R/H48Q mice that is NP40-insoluble but dissociable into monomeric species by heat and SDS denaturation shows the electrophoretic characteristics of completely reduced WT SOD1. This outcome is consistent with the study of Jonsson and colleagues (142); which demonstrated that a significant fraction of the total SOD1 expressed in transgenic mice producing D90A, G93A, and G127X variants of SOD1 lacks the normal intramolecular disulfide bond (C57-C146).

Our study of SOD1 aggregation in cell culture provided more definitive evidence for the contribution of reduced forms of mutant SOD1 in aggregation. In our cell model, the vast

majority of the NP40-insoluble mutant SOD1 that dissociates upon heat and SDS denaturation to a monomeric size protein exhibited electrophoretic mobilities consistent with reduced protein. Moreover, when we examined the mutant proteins that were NP40-soluble, we noted that the majority of the protein produced in these cells showed electrophoretic mobilities consistent with reduced protein, suggesting that in our cell culture model the high level expression of the mutant protein overwhelms the ability of the cells to provide the necessary factors to correctly fold most of this protein. In contrast, the majority of WT SOD1, even when overexpressed, displayed electrophoretic properties consistent with the presence of the normal intramolecular disulfide bond. These findings are informative in three ways. First, we can be confident that reduced forms of mutant SOD1 are prone to form NP40-insoluble aggregates. Second, we demonstrate that the failure to form the normal disulfide linkage is not sufficient to induce aggregation. Finally, a significant fraction of disulfide-reduced mutant SOD1 can achieve conformations that remain soluble in detergent.

In spinal cords of the WT, G37R, and G93A mice, we found that the majority of SOD1 that achieves a conformation that is soluble in detergent shows electrophoretic characteristics consistent with the presence of the normal intramolecular disulfide bond. Importantly, in these mice, the levels of expression, though high, are still an order of magnitude or more lower than what is achieved in cell culture. Moreover, the time scales in the mouse and cell systems are vastly different. Thus, in the animals, there is either sufficient capacity or sufficient time to allow some mutant SOD1 to achieve detergent-soluble conformations with normal disulfide linkages.

In the spinal cords of H46R/H48Q mice, the detergent-soluble forms of the protein appeared to be largely reduced. Evidence suggests that copper is required to form the

intramolecular disulfide bond (170); our data on the H46R/H48Q mutant, which does not bind Cu (171), is consistent with this hypothesis. Previous work has shown that FALS mutants of SOD1 are more susceptible to proteolytic digestion in the presence of reducing agents (31), suggesting that mutant SOD1 is destabilized under reducing conditions in the cell. Because reduced SOD1 monomers have lower stability and higher conformational freedom (172), these species are more likely to contribute to the formation of aggregates. WT SOD1 is less susceptible to disulfide reduction than mutant SOD1 (31), which may explain why WT SOD1 is less prone to misfold. A recent study of the aggregation of purified SOD1 *in vitro* demonstrated that completely reduced forms of mutant SOD1 were most prone to produce filamentous aggregates (169).

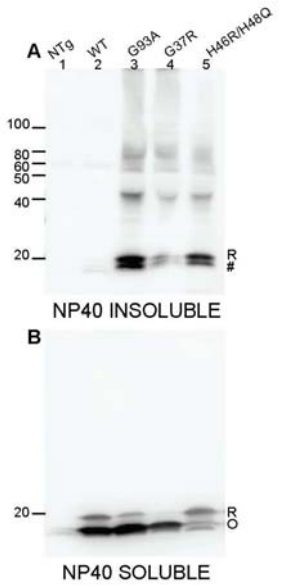

Figure 4-10. Reduced forms of mutant SOD1 are components of NP40-insoluble aggregates. Spinal cords from three lines of SOD1 mice at endstage were extracted in 0.5% NP40 in the presence of 100 mM iodoacetamide. Immunoblots were probed with m/h SOD1 antiserum. A) Detergent-insoluble (20 μg). B) Detergent-soluble (5 μg). To enhance detection of oxidized forms of hSOD1, gels were incubated in transfer buffer containing 2% βME for 10 min before electrotransfer to nitrocellulose membranes. R, reduced disulfide bond (C57-C146). O, oxidized disulfide bond (C57-C146). #, Possible non-natively oxidized disulfide bond.

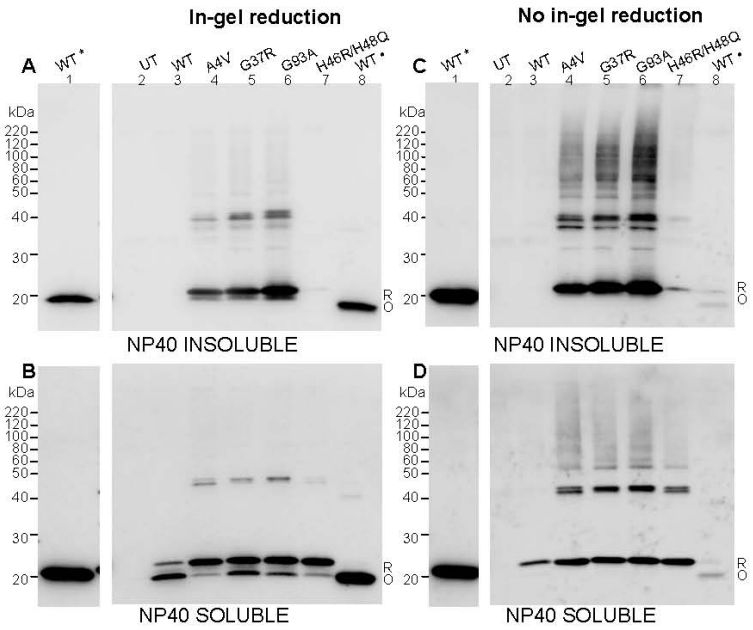

Figure 4-11. Reduced hSOD1 protein is preferentially incorporated into detergent-insoluble aggregates. HEK293-FT cells were transfected with vectors for WT, A4V, G37R, G93A and H46R/H48Q hSOD1 proteins, harvested after 48 hours, and extracted in buffers with 0.5% NP40 and 100 mM iodoacetamide. Detergent-insoluble (A, C) and soluble fractions (B, D) from cells transfected with each construct were electrophoresed in the absence of βME (lanes 2-8). Immunoblots were probed with m/h SOD1. Lane 1 of each panel contains purified WT SOD1 that was reduced prior to electrophoresis (*). This lane was separated from the remaining samples by a lane containing marker proteins and an empty space to prevent reducing agent from diffusing into other samples (these intervening lanes have been cropped out of the gel image). Lane 8 of each panel contains purified WT SOD1 that was verified to have an intact intramolecular disulfide bond (•). Purified WT SOD1 proteins were treated with 100 mM iodoacetamide prior boiling in Sample buffer and electrophoresis. To enhance detection of oxidized forms of hSOD1, gels were incubated in transfer buffer containing 2% βME for 10 min before electrotransfer to nitrocellulose membranes (A, B). UT, untransfected cells. R, reduced disulfide bond (C57-C146). O, oxidized disulfide bond (C57-C146). Image is representative of 3 repetitions of the experiment.

While a fraction of reduced SOD1 protein may remain soluble in non-ionic detergent, the presence of reduced SOD1 in aggregates produced in mouse and cell models supports the hypothesis that immature (with respect to acquisition of Cu or Zn cofactors and formation of intramolecular disulfide bonds) mutant SOD1 is more prone to misfold and produce conformations that support aggregation [reviewed in (173)].

We note that some of the tissues used in this study were stored at -80ºC for substantial intervals, which could have provided an opportunity for *ex-vivo* oxidation and artifactual generation of disulfide linkages. We did not observe an obvious pattern in which tissues stored for longer periods of time produce higher amounts of disulfide cross-linked forms of SOD1. It is possible, however, that some oxidation of cysteine residues occurs during tissue storage or sample preparation. We have no indication of disulfide reduction with storage or sample preparation. Thus, we can conclude that the reduced forms of mutant SOD1 we describe here represent the minimum levels of this form of SOD1 in tissues of symptomatic mice. The best estimation of the relative amount of completely reduced mutant SOD1 in detergent-insoluble fractions is obtained by analysis of the data in Fig. 4-7, in which we estimate that completely reduced protein may account for ~10% of total detergent-insoluble mutant protein in mouse tissues. However, we do not know what proportion of the mutant protein that is associated with high-molecular-weight, disulfide cross-linked species possesses a normal 57 to 146 disulfide linkage.

Mutant SOD1 Aggregation in Disease Pathogenesis

In this study, aggregates are defined as forms of mutant SOD1 that are insoluble in nonionic detergents (NP40) and sediment upon centrifugation. When exposed to heat, SDS, and reducing agents, these aggregates dissociate and predominantly show electrophoretic mobilities consistent with a monomeric protein. Mass spectrum analysis of NP40-insoluble SOD1 aggregates have recently demonstrated that unmodified mutant SOD1 proteins are major components of the aggregate (151). Notably, in this later study, aggregates were dissociated in guandinium isothiocyanate and DTT prior to analysis, which would have reduced all oxidized cysteine modifications. Our study here, along with several previous studies (23, 46, 141) demonstrates that intermolecular disulfide cross-linking is a major modification to mutant SOD1

in the aggregates. However, the timing of the appearance of this modification in mice, and the lesser degree of such modifications in cell culture models of aggregation, lead us to conclude that oxidative cross-linking of disulfide residues is likely to be a secondary event in the formation of the aggregate structures.

Several groups have described SOD1 aggregation in mutant SOD1 transgenic mice through various stages of the lifespans (117, 142). Our study builds on the current literature. In a previous study from our group, a filter trap assay was used to detect and measure the aggregation of SOD1-G37R in mutant mice-finding that aggregates are most abundant when mice are overtly paralyzed (210-240 days) with a lesser degree of SOD1 aggregation noted at ages prior to symptoms at 180 days (114). We have recently determined that the methods used in this study may have primarily detected the disulfide cross-linked forms of mutant protein (46)(Chapter 2). However, the outcome of the study is essentially unchanged in regards to the timing of the appearance of mutant SOD1 aggregates. In G93A mice, detergent-insoluble protein complexes have been described to increase linearly through the lifespan of the animal and were detected as early as 30 days of age (117). In this particular study, aggregates were defined as high-molecular-weight species that were resistant to heat, SDS, and reducing agents, and they were unique to mice expressing SOD1-G93A (117). Recently, however, we have established that these forms of mutant SOD1 are distinct from the NP40-insoluble protein we have studied here (46)(Chapter 2). It is unclear whether the high-molecular-weight species of mutant SOD1 that are resistant to SDS, heat, and reducing agents represent forms of mutant protein which are covalently cross-linked to other proteins (such as ubiquitin (43, 104)) or some type of highly stable oligomeric structure. However, it is clear that these SDS, heat, reducing

agent resistant species of mutant protein are ultimately components of NP40-insoluble aggregates (43, 46, 104).

The study that most closely resembles our present report examined mice expressing G93A, G127X, and G85R FALS variants of SOD1 (142). In this study, spinal cords were extracted in low concentrations of non-ionic detergent (0.1% NP40), which resulted in the detection of detergent-insoluble species of mutant SOD1 as early as 50 days (123, 142). However, similar species were detected in WT SOD1 mice at all time points (142). At terminal stages of disease, the levels of mutant protein that were NP40-insoluble increased dramatically, including forms of mutant protein that were resistant to SDS, heat, and reducing agent (142). Moreover, in mice expressing WT SOD1 at very advanced ages (400 to 600 days), the levels of NP40-insoluble WT SOD1 were observed to increase with the appearance of high-molecular-weight species were SDS, heat, and reducing agent resistant (142). Thus, the methodology employed in the Jonsson study indicates that both mutant and WT SOD1 adopt similar conformations as a function of age.

While our assay is similar to Jonsson and colleagues (142, 168), it differs in several significant ways. First, we use 5-fold higher concentrations of NP40 in our extraction buffers (0.5%), with a 20 to 1 ratio of buffer to tissue (vol to wt). The Jonsson method uses 0.1% NP40 (the volume is not specified). Second, we centrifuge tissue extracts at >100,000 xg in an Airfuge for 5 minutes followed by one wash step in which the pellet is resuspended in buffer with NP40, disrupted by sonication, and then centrifuged at >100,000 xg to produce the final pellet. The Jonsson method uses 20,000 xg for 30 minutes, followed by 5 washes in double the original extraction volume with 20,000 xg centrifugation to separate detergent-insoluble material. Comparison of these methods is difficult because of uncertainty regarding some of the details of the protocols. We use sonication to disrupt the tissue in the absence of detergent, whereas

Jonsson describes homogenization of the tissue in detergent as the method of tissue disruption. After initial disruption of the tissue, we use a low speed centrifugation to remove tissue fragments that have not been completely disrupted. This step is absent from the Jonsson protocol. Because we use higher detergent concentrations, we conclude that we extract the tissues at higher detergent to protein ratios than that of the Jonsson method. We conclude that this difference in methodology, alone or in conjunction with other differences, allows us to distinguish the forms of mutant SOD1 that are most distinct from WT protein.

Despite the methodological differences between our approach and that of comparable studies, it appears to us that the general consensus is that the levels of NP40-insoluble mutant SOD1 increase rapidly towards the terminal stages of disease. All variants of SOD1 transgenic mice (G93A, G37R, H46R/H48Q, L126Z) examined here illustrated a similar time course of SOD1 aggregate accumulation, where aggregates were most prominent when mice developed hindlimb paralysis. Our inclusion of the G93A mice provides a point of reference with other published studies (117, 142). In all of these studies, the levels of conformationally distinct forms of G93A SOD1 increase dramatically as paralysis develops. What is less clear is the nature and abundance of stable, misfolded, mutant protein earlier in disease. The identification of SDS, heat, and reducing agent resistant forms of high-molecular-weight SOD1-G93A by Johnston and colleagues as early as 30 days of age implies that conformational abnormalities in mutant SOD1 occur early in disease pathogenesis (117).

The effects of FALS mutations on the normal enzyme activity, turnover, and folding of SOD1 vary considerably (24, 26). In cell culture and *in vitro* models, enzyme activity ranges from undetectable to near normal (24, 27-30); most mutations accelerate the rate of protein turnover (24, 29); and many mutations increase the susceptibility of SOD1 to disulfide reduction

(31). The G93A variant has an activity similar to WT SOD1 protein (174) and has a half-life similar to WT SOD1 protein (175); the G37R variant also has an activity similar to WT SOD1 (24, 147) and a half-life that is estimated to be half of that of WT SOD1 (24); and the H46R/H48Q variant has no activity (104, 171). Despite this vast range of biophysical properties, all of the mutants, in mice and in humans, produce a similar phenotype of paralysis (104, 119, 147). Here, we demonstrate that SOD1 mutants with different properties also show a similar time course of SOD1 aggregate formation in relation to the development of hindlimb paralysis.

SOD1 Aggregation and Toxicity

Previous studies have established that FALS mice develop significant pathology prior to the appearance of hindlimb paralysis. In SOD1-G93A mice, approximately 40% of the motor endplates are denervated at 47 days, 80 days before the appearance of hindlimb paralysis and SOD1 aggregation (176). At this early time point, motor unit loss [40 days (177)] and a decline of contractile force in fast twitch muscles [40 days (178)] also occur, illustrating that dramatic loss of muscle function and motor neuron innervation may occur early in the disease course. Similarly, SOD1-G37R mice show vacuolar changes in spinal cord [36 days (179)], motor neuron loss [133 days (125)], and reactive astrogliosis [77 days (125)] before these mice develop hindlimb paralysis (210 days). The SOD1-H46R/H48Q mice that were included in this study are less well characterized, but we have noted the appearance of astrogliosis in spinal cord as early as 60 days (Fig. 4-4). Our data indicate that at time points when each of these mice have significant pathologic abnormalities, including astrogliosis, motor neuron loss, denervation, and vacuolation, only low levels of detergent-insoluble SOD1 can be detected. This outcome implies that other forms of mutant SOD1 may mediate toxic events at early stages of disease or that very low levels of aggregates are sufficient to mediate toxicity.

It is difficult to discard SOD1 aggregation as entirely secondary to disease pathogenesis. In a study of mice that express SOD1-G37R via the mouse PrP vector, we created a line of mice in which expression of the mutant protein, when animals were heterozygous for the transgenes, was below the threshold for inducing disease (114). However, upon mating to homozygousity, which resulted in a 2-fold increase in mutant protein expression, ALS symptoms were observed to occur by 9 months of age (149). In the homozygous paralyzed mice, we detected NP40-insoluble forms of mutant SOD1 whereas in the disease-free heterozygous mice there was no evidence of aggregated SOD1. More recently, Jaarsma and colleagues generated mice that express SOD1-G93A via a vector generated from the Thy1.2 promoter (133). In the heterozygous state, these animals do not develop disease and do not develop detergent-insoluble aggregates of mutant SOD1. When crossed to homozygousity, disease is produced at about 20 months of age, and paralyzed mice accumulate detergent-insoluble forms of mutant protein (133). A third example involves matings of mice that express mutant SOD1-A4V at levels too low to induce disease with mice that express high levels of WT SOD1 (134). Mice expressing the low level of SOD1-A4V do not accumulate detergent-insoluble SOD1 aggregates, but such aggregates along with paralytic disease are produced in mice that co-express A4V and WT SOD1 (134). Jaarsma and colleagues reported similar outcomes when Thy1.2-G93A mice were crossed to mice expressing high levels of WT SOD1 (133). Collectively, these studies provide a compelling argument for the notion that the threshold of SOD1 burden (mutant alone or mutant with WT) that is required to induce disease is similar to the threshold required to induce aggregation.

The late appearance of high-molecular-weight SOD1 aggregates in the progression of disease in FALS mice leaves open three possibilities for SOD1 aggregate function in ALS

pathology. First, it is possible that the accumulation of SOD1 aggregates mediates all aspects of toxicity with early pathologic events mediated by very low levels of aggregates (below the level of detection). Under this scenario, some of the early pathology described in FALS transgenic mice prior to aggregate formation could be the result of overexpression of mutant SOD1. For example, the early vacuolar pathology is a major feature of mice expressing high levels of G93A and G37R variants of mutant SOD1, but much less apparent in mice expressing C-terminal truncation mutants or inactive mutants (104, 115, 119, 147). There is one example in transgenic mice where mutant SOD1 induces disease without a concurrent accumulation of SOD1 aggregates: coexpression of human copper chaperone for SOD1 (CCS) with SOD1-G93A, hastens the onset of disease and blocks aggregate formation (157). In these animals, vacuolar degeneration of the spinal cord is the primary pathology. It remains to be established whether CCS overexpression accelerates disease in mice that normally lack the vacuolar pathology. Second, all toxic events are mediated by detergent-soluble forms of mutant SOD1 (monomeric or oligomeric). In this scenario aggregates form because the toxic processes that occur in affected cell types leave them less able to properly modify nascent mutant SOD1 by loading structure stabilizing metal cofactors, which induce normal intramolecular disulfide bonding. These immature SOD1 proteins then become the building blocks of aggregates. Under this scenario, the aggregates are simply biomarkers for extreme cell stress. Lastly, some unidentified toxic event mediated by detergent-soluble forms of mutant SOD1 (monomeric or oligomeric) triggers early pathologic abnormalities (gliosis, vacuolation, denervation, etc) with the resulting stress on the cell inducing the formation of SOD1 aggregates, which impart additional toxicity and induce paralytic phenotypes. Although there is one example in which aggregation and toxicity of mutant SOD1 are clearly separated (157), it is not entirely clear whether this example extends to

other FALS mutants of SOD1 or involves toxic mechanisms relevant to human disease. Ultimately, unraveling the true nature of SOD1 aggregation in SOD1-linked FALS may require the identification of small molecules that selectively inhibit SOD1 aggregation.

Conclusions

The present study demonstrates that the accumulation of detergent-insoluble aggregates of mutant SOD1 increases dramatically as FALS mice develop paralysis. Extensive disulfide cross-linking occurs in these aggregates, but we do not find evidence that such cross-linking is a prerequisite to aggregation or is critical to aggregate stability (see also Chapter 2). We also provide evidence that SOD1 that fails to acquire the normal disulfide linkage is most prone to aggregation. Overall, these data suggest that oxidative stresses, which diminish cellular redox potential, are unlikely to provide the trigger that induces mutant SOD1 aggregation. Instead, it appears that failure of mutant SOD1 to mature is more critical. The fact that high-molecular-weight forms of detergent-insoluble mutant SOD1 do not accumulate to high levels until very late in disease limits the role of such structures in disease pathogenesis.

CHAPTER 5
αB CRYSTALLIN IS A MODEST MODIFIER OF DISEASE PROGRESSION IN MOUSE MODELS OF ALS

Introduction

All mouse models of FALS that overexpress mutant human SOD1 share a similar phenotype of motor neuron loss, muscle wasting, and hindlimb paralysis (180). In mouse models of FALS, mutant SOD1 is ubiquitously expressed; however, cell death is largely restricted to motor neurons. In all SOD1 transgenic mice, the appearance of symptoms is associated with an accumulation of sedimentable structures that are detergent-insoluble, which is diagnostic for protein aggregation (43, 104, 114, 115, 117, 123, 131, 132)(Karch CM, Prudencio M, Winkler D, Hart PJ, Borchelt DR, In Press) (Chapter 4). SOD1 aggregates are selectively detected in the spinal cord, and these aberrant structures are absent in muscle and other tissues (114). While SOD1 aggregation is absent in muscle tissue, muscle pathology, including denervation of the motor endplate (181), has been reported to occur early in the disease in FALS mice.

Previous studies suggest that heat shock proteins may be important in modulating SOD1 aggregation (182). It has been proposed that a common feature of FALS-linked SOD1 mutants is an increased propensity to misfold (26, 106-111). An *in vitro* study of aggregation demonstrated that αB crystallin inhibits mutant SOD1 aggregation (23). This small heat shock protein binds to exposed hydrophobic surfaces on denatured or misfolded proteins (183-186), which allows αB crystallin to inhibit protein aggregation (187, 188). Oligomerization of αB crystallin is associated with its activation as a chaperone (189). In spinal cords of FALS mice (G37R, G85R, G93A, H46R/H48Q, Quad, L126Z), increased levels of detergent-insoluble αB crystallin are detected after the onset of symptoms (43, 115). In symptomatic L126Z mice, mutant SOD1 appears to specifically accumulate in motor neurons where αB crystallin

expression is absent (115). Together, this evidence suggests that, *in vivo*, αB crystallin may suppress SOD1 aggregation in select cell types. αB crystallin is unique in that it is highly expressed in select tissues: skeletal muscle and oligodendrocytes (190, 191). αB crystallin knock-out mice have been developed in which αB crystallin gene and a portion of the HSPB2 gene are removed (HSPB2 was unidentified at the time of development) (192). HSPB2 (also termed myotonic dystrophy kinase bind protein) is highly expressed in the heart and muscle, specifically in Z membranes and neuromuscular junctions, and is ubiquitously expressed at lower levels (193, 194). HSPB2 acts as a molecular chaperone for myotonic dystrophy protein kinase (193). αB crystallin knock-out mice have no overt pathology until 40 weeks of age, at which time they develop muscular degeneration, kyphosis, and osteoarthritis (192). However, mice that retain one αB crystallin allele do not develop an adverse phenotype (192).

In this study, we used three lines of SOD1 transgenic mice to study the effect of αB crystallin on disease course, aggregate accumulation, and aggregate localization. Two of the models used, Gn.G37R and Gn.L126Z mice, have mutations in human genomic SOD1 and are under the control of the human SOD1 promoter (23, 115, 147), producing ubiquitous expression of human SOD1. Both mice develop the characteristic ALS phenotype of hindlimb paralysis, motor neuron loss, and accumulation of detergent-insoluble SOD1 in the spinal cord. In both lines of mice, misfolded forms of mutant SOD1 appear to accumulate selectively in motor neurons (115, 125, 147). Gn.L126Z mice differ from Gn.G37R mice in that the L126Z mutant has a short half-life: SOD1 protein that is not immediately degraded is converted into aggregates (43, 115). PrP.G37R mice have mutations in the human SOD1 cDNA and are under the control of the mouse prion promoter, which is predominantly expressed in neuronal and muscle tissue (149). Mice that are heterozygous for PrP.G37R do not develop pathology by two years of age

and do not form SOD1 aggregates; however, mice that are homozygous for PrP.G37R develop hindlimb paralysis, motor neuron loss, and detergent-insoluble SOD1 species, indicating that threshold levels of mutant SOD1 expression are required to induce disease in this mouse model (149).

To study the role of αB crystallin in SOD1 pathology, we crossed the three models of SOD1 transgenic mice described above to αB crystallin knock-out mice and asked the following questions: (1) does the elimination of αB crystallin alter the clinical appearance of disease in mutant SOD1 transgenic mice; (2) does elimination of αB crystallin alter the abundance and tissue distribution of detergent-insoluble SOD1 species; and (3) does the elimination of αB crystallin alter the cellular localization of pathologic lesions. The αB crystallin knock-out mice develop a late onset muscular degeneration and to our surprise the presence of this second insult had little impact on progression of neurologic phenotypes of SOD1 mice. The levels and tissue distribution of detergent-insoluble SOD1 species, which represent aggregated mutant SOD1, did not change in mice lacking αB crystallin. Finally, the distribution of pathologic features was not changed by the elimination of αB crystallin. We conclude that αB crystallin is not normally involved in modulating the rate or subcellular distribution of mutant SOD1 aggregation or pathologic accumulation.

Methods

Tissue Culture Transfection and Transgenic Mice

SOD1 mutants have been previously characterized (43). αB crystallin cDNA (Clontech, Mountain View, CA, USA) was expressed in the pEF-BOS vector (146). GFP cDNA (Clontech, Mountain View ,CA, USA) was expressed in the pcDNA3.1(A)-Myc vector (Invitrogen,

Carlsbad, CA, USA). Transient transfection was performed in HEK293-FT cells as previously described (43, 46).

The SOD1 transgenic mice used in this study have been previously characterized. Three mice were created in genomic SOD1 sequence under the control of the human SOD1 promoter: the G37R variant [line 29 (onset at 7-8 mo)] (147), the L126Z variant [line 45 (onset at 7-9 mo)](149), and the wild type (WT) variant (line 76) (147). One SOD1 transgenic mouse was created using SOD1 cDNA under the control of the mouse prion promoter: G37R [line 39 (asymptomatic)] (149). Mice homozygous null for αB crystallin were obtained from Dr. Eric Wawrousek at the National Eye Institute and have been described previously (192). Mice were identified by PCR of tail DNA using primers described previously (115, 147, 149, 192). All procedures involving mice were reviewed an approved by the University of Florida Institutional Animal Care and Use Committee.

SOD1 Aggregation Assay by Differential Extraction

The procedures used to assess SOD1 aggregation by differential detergent extraction and centrifugation in spinal cords and muscle were similar to previous descriptions (see Chapter 2) (43, 46). Protein concentration was measured in the detergent-insoluble and detergent-soluble fractions by BCA method as described by the manufacturer (Pierce, Rockford, IL, USA).

Immunoblotting

Standard sodium dodecyl sulfate-polyacrylamide gel electrophoresis (SDS-PAGE) was performed in 18% Tris-Glycine gels (Invitrogen, Calsbad, CA, USA). Samples were boiled for 5 minutes in Laemmli sample buffer prior to electrophoresis (148).

Quantitative Analysis of Immunoblots

Quantification of SOD1 protein in detergent-insoluble and detergent-soluble fractions was performed by measuring the band intensity of SOD1 in each lane using a Fuji imaging system

(FUJIFILM, LifeScience, Stamford, CT, USA). Aggregation propensity was measured by comparing the ratio of band intensity in the detergent-insoluble fraction to the band intensity in the detergent-soluble fraction. The standard error of the mean (SEM) was calculated for aggregation of each sample in each experiment. Statistical significance was measured using an unpaired t-test.

Antibodies

Immunoblots were probed with rabbit polyclonal antibodies termed hSOD1 and m/hSOD1 at dilutions of 1:2500. The hSOD1 antiserum was raised against a synthetic peptide that is specific to human SOD1 (aa 24-36) (113). The m/hSOD1 antiserum was raised against a synthetic peptide conserved between mouse and human SOD1 (aa 124-136) (24). Immunoblots were also probed with a mouse polyclonal antibody-αB crystallin (Stressgen, Ann Arbor, MI, USA) at dilutions of 1:1000; rabbit polyclonal antibody-Hsp40 (Stressgen, Ann Arbor, MI, USA) at dilutions of 1:2000; and rabbit polyclonal antibody-Hsp70 (Stressgen, Ann Arbor, MI, USA) at dilutions of 1:1000.

Tissue was stained with antibodies to hSOD1 (1:2500), GFAP (1:500 - Chemicon, Billerica, MA, USA), NeuN (1:500-Chemicon, Billerica, MA, USA), and αB crystallin (1:1000-Sressgen, Ann Arbor, MI, USA). Secondary antibodies used included goat-anti-mouse AlexaFluor 488 (Invitrogen, Calsbad, CA) and goat-anti-rabbit AlexaFluor 568 (Invitrogen, Calsbad, CA).

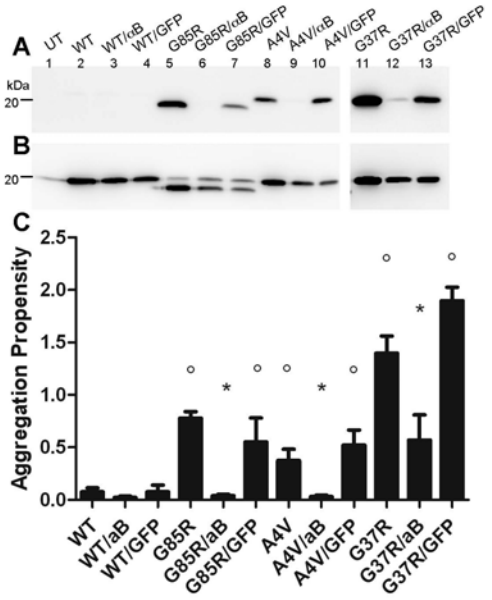

Figure 5-1. αB crystallin reduces mutant SOD1 aggregation in cell culture. HEK293-FT cells were transfected with mutant SOD1 (4 μg) alone, with mutant SOD1 (2 μg) and αB crystallin (2 μg), or with mutant SOD1 (2 μg) and GFP (2 μg). Cell lysates were extracted in non-ionic detergent and run on 18% Tris-Glycine gels. Immunoblots were probed with m/hSOD1 antiserum. A) Detergent-insoluble (20 μg). B) Detergent-soluble (5 μg). C) Quantification of aggregation propensity measured as a ratio of detergent-insoluble to soluble and expressed as SEM. *, significantly different from mutant SOD1 ($p<0.05$). °, significantly different from WT SOD1 ($p<0.05$). The image shown is representative of 3 repetitions of the experiment. Data from at least 3 experiments were used to quantify aggregation propensities in panel C. Note: due to low expression levels at 24 hours, cells expressing G37R, G37R/αB, and G37R/GFP were harvested 48 hours after transfection.

Histology

After inducing deep anesthesia, mice were transcardially perfused with cold PBS and then 4% paraformaldehyde in 1x PBS. After 48 hours of post-fixation, tissues were transferred to 30% sucrose for at least 48 hours prior to cryostat sectioning (Microm HM550). Coronal sections of spinal cord (14 microns) were cut and stored in anti-freeze solution (100 mM sodium acetate, 250 mM polyvinyl pyrolidone, 40% ethylene glycol, pH 6). Sections were stored at -20°C. To stain tissue, sections were washed in PBS prior to blocking in 5% normal goat serum

(Invitrogen, Calsbad, CA). Sections were then incubated in primary and secondary antibodies with PBS, 5% normal goat serum, and 1% triton. Images were captured using an Olympus IX81-DSU Spinning Disk confocal microscope.

Results

Small heat shock proteins, such as αB crystallin, aid in the folding of misfolded protein in the cell (195). Because mutations in SOD1 predispose the protein to misfold and form aggregates, we believed that a small heat shock protein such as αB crystallin could reduce the aggregation of mutant SOD1 protein. Additionally, there is evidence *in vitro* that αB crystallin can modulate mutant SOD1 aggregation (23). To assess the effect of αB crystallin on mutant SOD1 aggregation, vectors encoding FALS mutants (G85R, A4V, G37R) were transfected alone, with vectors encoding αB crystallin (ratio of 1:1), or with vectors encoding GFP (ratio of 1:1) in HEK293-FT cells. The cell lysates were fractionated into detergent-insoluble and detergent-soluble fractions by sonication and high speed centrifugation in non-ionic detergent (46). In this study, SOD1 aggregates are defined as protein that is insoluble in non-ionic detergent and sediments upon centrifugation. All FALS-linked SOD1 mutants formed detergent-insoluble species (Fig. 5-1A, lanes 5, 8, 11) and had aggregation propensities significantly different from WT protein (Fig. 5-1C). The co-expression of αB crystallin with each SOD1 mutant (G85R, A4V, G37R) reduced aggregation (Fig. 5-1A, lanes 6, 9, 12) to levels that were not significantly different from WT (Fig. 5-1C). To control for non-specific effects on mutant SOD1 expression that could be caused by co-transfection of the αB-crystallin expression vectors, vectors expressing mutant SOD1 were co-transfected with vectors expressing GFP cDNA. There was a slight reduction in mutant SOD1 protein in the detergent-insoluble protein fraction due to the reduced amount of mutant SOD1 starting material (2 μg versus 4μg) (Fig. 5-1A, lanes

7, 10, 13); however, the aggregation propensity of mutant SOD1 (ratio of soluble to insoluble protein) expressed with GFP was similar to mutant SOD1 expressed alone (Fig. 5-1C). Under all conditions, a significant amount of mutant SOD1 was found in the detergent-soluble fraction, which likely represents the protein that is folded in a normal or near normal conformation (Fig. 5-1B). Thus, αB crystallin specifically reduces mutant SOD1 aggregation in cell culture.

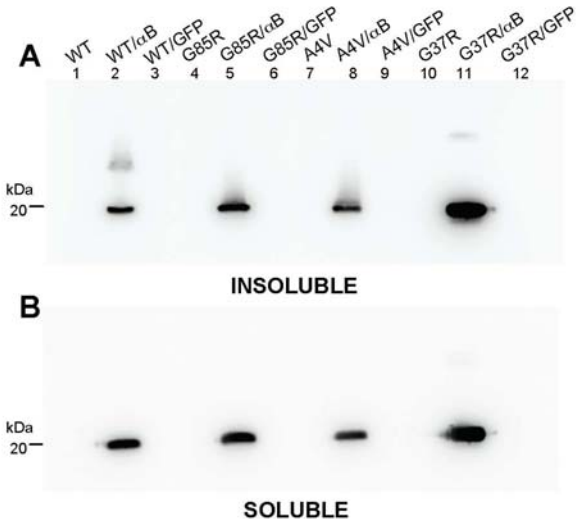

Figure 5-2. Overexpressed αB crystallin is upregulated in response to mutant SOD1 in cell culture. Detergent-insoluble protein fractions and detergent-soluble protein fractions from Figure 1 were run on 18% Tris-Glycine gels and immunoblotted with αB crystallin antiserum. A) Detergent-insoluble (20 μg). B) Detergent-soluble (5 μg). Note: due to low expression levels at 24 hours, cells expressing G37R, G37R/αB, and G37R/GFP were harvested 48 hours after transfection.

The active form of αB crystallin is oligomeric and insoluble in detergent (189). Cell lysates used to measure SOD1 aggregation were also immunoblotted with a polyclonal antibody to human αB crystallin. In cells co-transfected with vectors expressing mutant SOD1 (G85R, A4V, and G37R) and αB crystallin, αB crystallin was highly expressed in the detergent-soluble protein fraction (Fig. 5-2B, lanes 4, 7, 10) and in the detergent-insoluble protein fraction (Fig. 5-2A, lanes 4, 7, 10). However, αB crystallin was undetectable in cells transfected with vectors expressing mutant SOD1 alone or in cells co-transfected with vectors expressing mutant SOD1

and GFP (Fig. 5-2). Thus, the robust expression and oligomerization of αB crystallin accounts for the low levels of mutant SOD1 aggregates in HEK293-FT cells. Also note, HEK293-FT cells do not constitutively express αB crystallin nor can these cells be induced to express αB crystallin in response to mutant SOD1 expression. To more extensively assess the heat shock response in HEK293-FT cells, we incubated the cells at 42°C for 30 minutes and collected cells at multiple times points post heat shock. Immunobloting for Hsp70 and Hsp40 revealed that Hsp70 was highly induced prior to heat shock and remained highly induced 24 hours post-heat shock (Fig. 5-3). Hsp40 was constitutively induced at levels slight lower than Hsp70 (Fig. 5-3). In spite of high levels of Hsp70 and Hsp40 in this cell culture system, mutant SOD1 robustly aggregates.

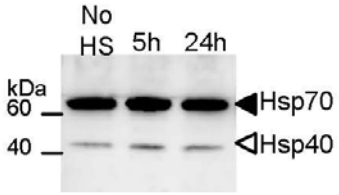

Figure 5-3. Hsp40 and Hsp70 are constitutively induced in HEK293-FT cells. Cells were not exposed to heat shock or heat shocked at 40°C for 30 minutes and harvested at 5 hours or 24 hours post heat shock. Cell lysates were sonicated in PBS and run on an 18% Tris-Glycine gel. Immunoblots were probed with Hsp40 and Hsp70 antibodies. Image is representative of 3 repetitions of the experiment.

Using available mice with the targeted deletion of αB crystallin, we asked whether reducing or eliminating αB crystallin in mutant SOD1 transgenic mice would alter the disease course and, or, change the location of SOD1 aggregates. Because αB crystallin null mice develop myopathy at 40 weeks (192), we asked whether muscle degeneration could compound the ALS phenotype in mice overexpressing mutant SOD1. Denervation of the motor endplate occurs early in the disease course (176), prior to SOD1 aggregation and hindlimb paralysis (Karch CM, Prudencio M, Winkler D, Hart PJ, Borchelt DR, In Press). Mutant SOD1 transgenic

mice (Gn.G37R, Gn.L126Z, PrP.G37R) were crossed to mice that were homozygous null for αB crystallin (termed αB crystallin knockout (KO) mice here after) to produce mutant SOD1 mice in which αB crystallin was reduced (heterozygous; +/-) or eliminated (KO: -/-). In all three lines of mutant SOD1 transgenic mice (Gn.G37R, Gn.L126Z, PrP.G37R), the reduction (+/-) or the elimination (-/-) of αB crystallin resulted in a modest change in disease course (Fig. 5-4). Gn.G37R and Gn.L126Z mice developed characteristic hindlimb paralysis. Gn.G37R mice with reduced αB crystallin (n=17, mean: 204 days) and no αB crystallin (n=12, mean: 195 days) had lifespans significantly different from Gn.G37R mice with WT levels of αB crystallin (n=15, mean: 214.5 days; $p<0.0001$, $p=0.001$, respectively) (Fig. 5-4A). The lifespans of Gn.G37R mice with reduced αB crystallin were not different from Gn.G37R mice with no αB crystallin ($p=0.6919$). Gn.L26Z mice with reduced αB crystallin (n=8, mean: 225 days) had lifespans similar to Gn.L126Z mice expressing WT levels of αB crystallin (n=8, mean: 210 days; $p= 0.5552$) (Fig. 5-4B). Gn.L126Z mice without αB crystallin (-/-) died earlier than Gn.L126Z mice expressing WT levels of αB crystallin and Gn.L126Z mice expressing reduced levels of αB crystallin (n=8, mean: 180 days; $p<0.0001$, $p=0.0145$, respectively) (Fig. 5-4B). Thus, reduction or elimination of αB crystallin is capable of altering disease course in SOD1 transgenic mice; however, this was not a robust effect. It is possible that αB crystallin is only a minimal modifier in disease course.

To more stringently test the role of αB crystallin in FALS disease course, we used mice that express G37R under the control of the mouse prion promoter (PrP.G37R). Mice that are heterozygous for the PrP.G37R transgene do not develop FALS symptoms, whereas a 2-fold increase in expression by generating homozygous animals produces disease (149). Eliminating αB crystallin in heterozygous PrP.G37R mice did not induce FALS symptoms (mice were

harvested at 40 weeks due to symptoms associated with loss of αB crystallin). Thus, in PrP.G37R mice, the second insult provided by the elimination of αB crystallin did not create enough of a burden to alter the disease progression in asymptomatic mutant SOD1 mice. We conclude that αB crystallin may play a role as one modifier of mutant SOD1 misfolding and toxicity, but it does not appear to be a critical modifier.

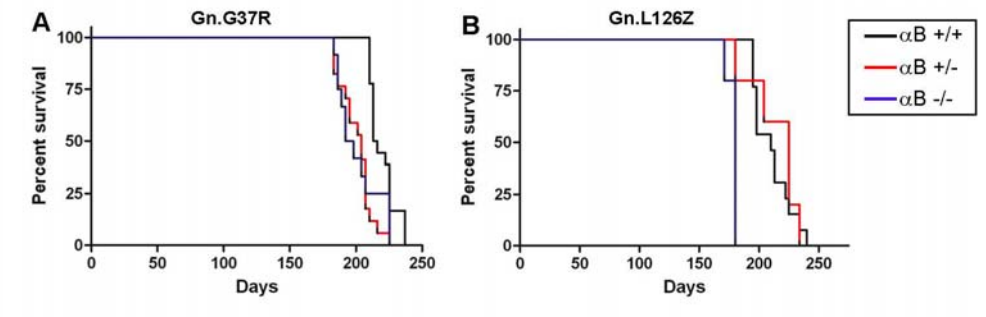

Figure 5-4. Reduction or elimination of αB crystallin in mutant SOD1 transgenic mice does not substantially alter survival. Kaplan-Meier survival curves of mutant SOD1 transgenic mice with WT (black), heterozygous (red), or homozygous null (blue) αB crystallin. A) Gn.G37R mice. B) Gn.L126Z mice. Note: PrP.G37R mice did not develop symptoms (n=10 per condition).

Because the elimination of αB crystallin altered the disease course, we were interested in the effects of αB crystallin on aggregate accumulation and aggregate location *in vivo*. In mutant SOD1 mice, SOD1 aggregates are absent in muscle and are only detected in the spinal cord and brainstem (Fig. 5-5, lanes 2 and 3) (115, 147, 149). We hypothesized that the high level of expression of αB crystallin in muscle could protect this tissue from the accumulation of SOD1 aggregates. To test this hypothesis, hindlimb muscle from Gn.G37R, Gn.L126Z, and PrP.G37R (αB +/+, αB +/-, αB -/-) was extracted in non-ionic detergent and centrifuged at 100,000xg to isolate detergent-insoluble and detergent-soluble fractions. In muscle from symptomatic mice (Gn.G37R and Gn.L126Z), SOD1 was not detected in the detergent-insoluble fraction when αB crystallin was reduced (+/-) or eliminated (-/-) (Fig. 5-6A, lanes 3-4, 7-8). In these tissues, all

mutant SOD1 was found in the detergent-soluble fraction (Fig. 5-6B, lanes 3-6); however, only faint bands were apparent for Gn.L126Z, due to the short half-life of this protein (Fig. 5-6B, lanes 7-8). In asymptomatic mice, (PrP.G37R), SOD1 was not detected in the detergent-insoluble fraction when αB crystallin was reduced (+/-) or eliminated (-/-) (Fig. 5-6A, lanes 5-6); however, detergent-soluble SOD1 was present in muscle tissue (Fig. 5-6B, lanes 5-6). Thus, the reduction or elimination of αB crystallin in SOD1 transgenic mice does not alter the tissue specific accumulation of detergent-insoluble SOD1.

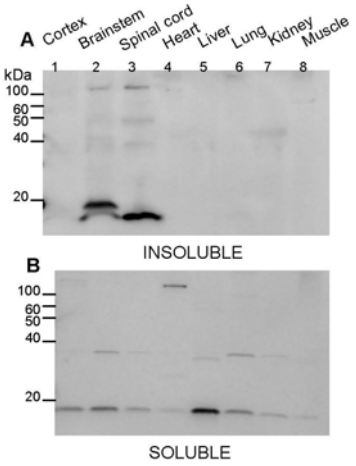

Figure 5-5. SOD1 aggregation is restricted to the brainstem and spinal cord in Gn.L126Z mice. Organs and nervous tissues were extracted in non-ionic detergent and run on 18% Tris-Glycine gels. Immunoblots were probed with hSOD1 antiserum. A) Detergent-insoluble (20 μg). B) Detergent-soluble (5 μg). Image is representative of 2 repetitions of the experiment.

Because the disease course was slightly accelerated without a change in localization of mutant SOD1 aggregates, it was still possible that the reduction or elimination of αB crystallin could alter the abundance of SOD1 aggregates in the spinal cord tissue. The spinal cord is the prominent site of pathology in mutant SOD1 transgenic mice (115, 147, 149). In symptomatic mutant SOD1 transgenic mice, detergent-insoluble SOD1 aggregates are detected exclusively in the brainstem and spinal cord (180) (Fig. 5-5A, lanes 2 and 3). We measured detergent-insoluble SOD1 in spinal cord tissue in each variant using the detergent extraction assay described above.

Gn.G37R and Gn.L126Z, which normally form detergent-insoluble SOD1, showed little change in the overall levels of detergent-insoluble SOD1 when αB crystallin was reduced (+/-) or eliminated (-/-) (Fig. 5-7A, lanes 3-5 and 9-11, respectively). PrP.G37R, which does not form aggregates when heterozygous for the transgene, produced levels of detergent-insoluble SOD1 similar to or less than WT SOD1 (Fig. 5-7A, compare lanes 1 and 6-8). Aggregation propensity of the mutant SOD1 did not differ among αB crystallin genotypes in all three lines of mice (Fig. 5-8; Fig. 5-9). SOD1 WT mice and αB crystallin KO mice contained little or no detectable SOD1 in the detergent-insoluble fraction (Fig. 5-7A, lanes 1 and 2). Levels of detergent-soluble protein were detected at slightly varying levels in Gn.G37R and PrP.G37R in all αB crystallin variants; however, no consistent change was detected when αB crystallin was reduced or eliminated (Fig. 5-7B, lanes 3-8). Levels of detergent-soluble SOD1 in Gn.L126Z mice were virtually undetectable due to the short half-life of this variant (115) (Fig. 5-7B, lanes 9-11). Thus, the reduction or elimination of αB crystallin does not alter the abundance of detergent-insoluble SOD1 in the spinal cords of mutant SOD1 transgenic mice.

When αB crystallin is activated, it forms a large complex that is insoluble in detergent (43, 115, 196) (Fig. 5-2). Using the detergent extraction assay described above, detergent-insoluble and detergent-soluble protein was isolated and immunoblotted to detect the presence of αB crystallin in spinal cord tissue. In all three lines of mice, αB crystallin was predominantly detected in the detergent-insoluble fraction when wild-type (+/+) or reduced (+/-) levels of αB crystallin were present in the tissue (Fig. 5-10A, lanes 3-4, 6-7, 9-10). Only in the presence of wild-type levels of αB crystallin could αB crystallin be prominently detected in the detergent-soluble fraction (Fig. 5-10B, lanes 3,6,9). The levels of αB crystallin were the highest in Gn.G37R mice, despite similar loading levels (Fig. 5-10A, lanes 3,4). This is consistent with

previous studies that measured αB crystallin in mutant SOD1 transgenic mice (43, 115, 196). Our results further suggest that mutant SOD1 can activate αB crystallin and that some mutants are better substrates for αB crystallin than other mutants.

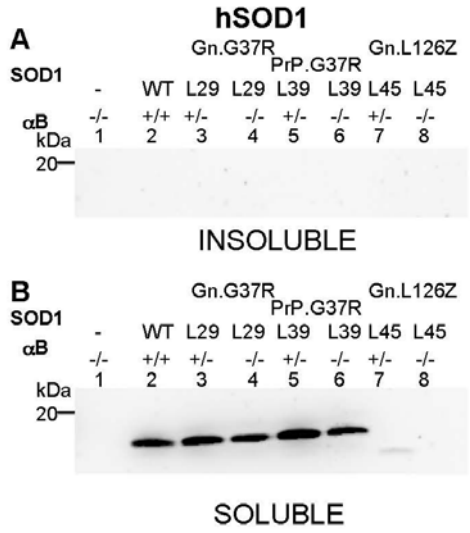

Figure 5-6. SOD1 aggregation is absent in muscle tissue. Muscle tissue from hindlimbs were isolate from mice and extracted in non-ionic detergent and run on 18% Tris-Glycine gels. Immunoblots were probed with hSOD1 antiserum. A) Detergent-insoluble (20 μg). B) Detergent-soluble (5 μg). The image shown is representative of 2 repetitions of the experiment.

To examine possible changes in the types of neural cells that accumulate misfolded SOD1 when αB crystallin levels were reduced (+/-) or eliminated (-/-), spinal cords from each variant were fixed, and frozen sections were stained using cell-type specific markers. In this study, we used an antiserum that recognizes a peptide from amino acids 24-36 that is unique to human SOD1 (113). To determine if this antibody exclusively recognizes misfolded SOD1 protein or if it is also able to recognize normally folded SOD1, we immunoprecipitated purified WT SOD1 protein (made by D. Winkler in the laboratory of Dr. P. John Hart, University of Texas Health Science Center at San Antonio) with the hSOD1 antibody (Fig. 5-11). We found that purified WT SOD1 protein could only be captured with the hSOD1 antibody when the protein was

denatured (Fig 5-11). Thus, it is likely that this antibody recognizes protein that is not in its native state; however, in fixed tissues, we do not know whether natively folded SOD1 could be immunoreactive. Thus, our study sought to determine whether the general pattern of SOD1 immunoreactivity differed between mice that express wild-type levels of αB crystallin and mice that express reduced or no αB crystallin. To identify cell types within these tissues, we used standard cell markers (GFAP and NeuN) to identify astrocytes and neurons, respectively.

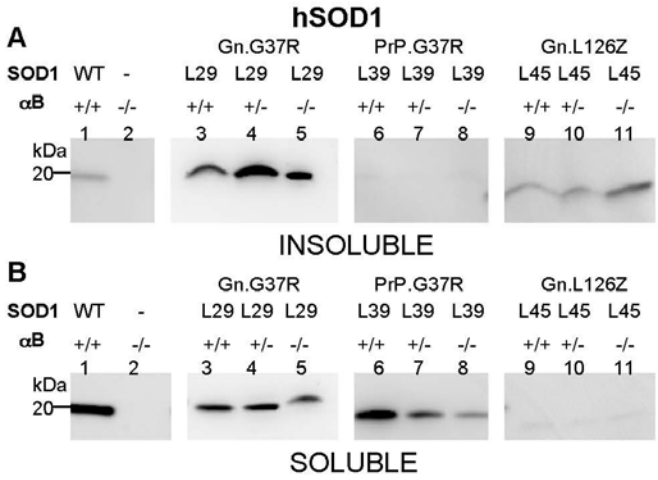

Figure 5-7. Reduction or elimination of αB crystallin in SOD1 transgenic mice does not alter aggregation in spinal cord tissue. Spinal cords were extracted in non-ionic detergent and run on 18% Tris-Glycine gels. Immunoblots were probed with hSOD1 antiserum. A) Detergent-insoluble (20 μg). B) Detergent-soluble (5 μg). The image shown is representative of 3 repetitions of the experiment.

In Gn.G37R (Fig. 5-12) and Gn.L126Z mice (Fig. 5-13), and in each αB crystallin variant (+/+, +/-, -/-), no novel appearance of SOD1 immunoreactivity in activated astrocytes was detected. Astrocytes appeared to surround SOD1 positive motor neurons (Figs. 5-12 and 5-13, panels A-C, G-I, M-O, S-U). In all variants of PrP.G37R mice, little GFAP staining was detected, which was consistent with the lack of overall pathology, including astrocytosis, in these mice (Fig. 5-14, panels A-C, G-I, M-O, S-U). To determine whether SOD1 accumulates in motor neurons, tissue from each SOD1 mutant with each αB crystallin variant (+/+, +/-, -/-) were co-stained for human SOD1 and NeuN, a neuronal marker. In Gn.G37R (Fig. 5-12, panels D-F,

J-L, P-R, V-X) and Gn.L126Z (Fig. 5-13, panels D-F, J-L, P-R, V-X) (in mice expressing all levels of αB crystallin), SOD1 predominantly co-localized with NeuN positive neurons. In asymptomatic PrP.G37R αB crystallin variants (Fig. 5-14, panels D-F, J-L, P-R, V-X), human SOD1 immunoreactivity co-localized with NeuN positive neurons. Thus, when αB crystallin is reduced (+/-) or eliminated (-/-), there are no obvious changes in the location of SOD1 immunoreactivity compared with SOD1 transgenic mice expressing wild-type levels of αB crystallin.

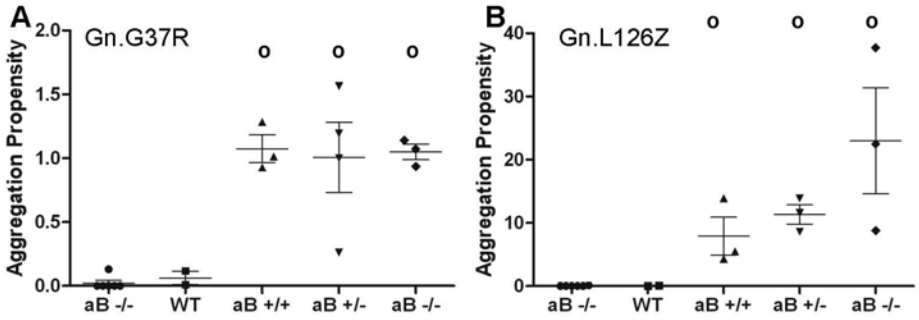

Figure 5-8. SOD1 aggregation propensity in mice expressing varying levels of αB crystallin. The ratio of detergent-insoluble to detergent-soluble SOD1 was measured in spinal cord tissue (see Fig. 5-7) and each measurement was graphed. °, significantly different from WT SOD1 ($p<0.05$). A) Gn.G37R. B) Gn.L126Z.

Previously, αB crystallin has been described to become induced in astrocytes once mice become symptomatic (115). Thus, we sought to examine the location of αB crystallin in all the variants of mice. Consistent with what we have previously shown, in symptomatic Gn.L126Z mice, αB crystallin was upregulated primarily in astrocytes, with some staining of oligodendrocytes (Fig. 5-15, panels G-H). However, in Gn.G37R mice, αB crystallin was primarily present in oligodendrocytes (Fig. 5-15, panels A-B). Similarly, in PrP.G37R mice, αB crystallin was only detected in oligodendrocytes (Fig. 5-15, panels D-E). Only background αB crystallin immuostaining was detected in SOD1 transgenic mice in which αB crystallin was eliminated (Fig. 5-15, panels C, F, I). Thus, induction of αB crystallin in astrocytes is not

universal to all the SOD1 mouse models, indicating that there must be a unique signal presented by the accumulating mutant L126Z SOD1.

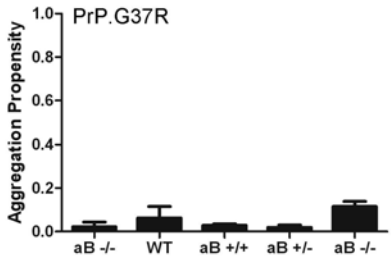

Figure 5-9. SOD1 aggregation propensity in PrP.G37R mice expressing varying levels of αB crystallin. The ratio of detergent-insoluble to detergent-soluble SOD1 was measured in spinal cord tissue (see Figures 4 and 5) and measured as SEM.

Discussion

In this study, we examined the role of αB crystallin as a potential modifier of mutant SOD1 misfolding. First, in cell culture, we found that αB crystallin selectively reduced mutant SOD1 aggregation, indicating that αB crystallin possesses the capacity to modulate mutant SOD1 misfolding. Using available mice with the targeted deletion of αB crystallin, we asked whether reducing or eliminating αB crystallin in mutant SOD1 transgenic mice would alter the disease course and, or, change parameters of mutant SOD1 aggregation. Elimination of αB crystallin in Gn.G37R and Gn.L126Z mice modestly shortened the interval (statistically validated) to which these mice reach human endpoints (obvious paralysis). Eliminating αB crystallin in mice that express G37R SOD1 at levels below the threshold for inducing disease was not sufficient to produce FALS-like symptoms. Muscle tissue, which does not accumulate aggregates in mutant SOD1 mice, contained no detectable aggregates in the absence of αB crystallin. Similarly, the absence of αB crystallin did not alter the amount of detergent-insoluble, sedimentable SOD1 that accumulated in the spinal cord. We did not observe an obvious change in the distribution of SOD1 immunoreactivity that accumulated in spinal cords

of mutant mice lacking αB crystallin. Together, this study illustrates that αB crystallin is not a major factor in modulating the formation of toxic forms of mutant SOD1 or in moderating mutant protein aggregation.

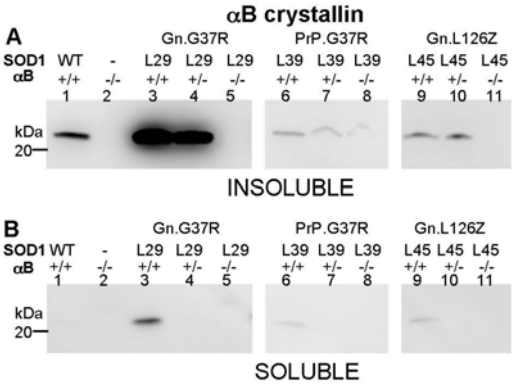

Figure 5-10. αB crystallin is upregulated in SOD1 transgenic mice. Spinal cords were extracted in non-ionic detergent and run on 18% Tris-Glycine gels. Immunoblots were probed with αB crystallin antiserum. A) Detergent-insoluble (20 μg). B) Detergent-soluble (5 μg). The image shown is representative of 3 repetitions of the experiment.

Myopathy Associated with ALS Disease Course

Muscle pathology has been described early in the disease course in mutant SOD1 transgenic mice (181). The αB crystallin KO mice we used develop a profound myopathy (192), which we anticipated could synergize with the activities of mutant SOD1 to hasten the onset of disease. Gn.G37R and Gn.L126Z αB crystallin KO mice developed symptoms slightly earlier than mutant mice expressing wild-type levels of αB crystallin without a corresponding change in overt phenotype and without a change in aggregate accumulation. This slight change in disease course may be due to an interaction between compromised muscle and neurotrophic disease induced by mutant SOD1. The absence of αB crystallin in SOD1 transgenic mice did not alter the accumulation of detergent-insoluble SOD1 aggregation in muscle, and it did not appear that the myopathic phenotypes were hastened by the expression of mutant SOD1. However, it is

possible that the absence of αB crystallin increases oxidative stress or other pathology that could hasten disease course. Dobrowolny and collegues recently showed that the specific expression of mutant SOD1 in muscle resulted in a myopathy without motor neuron disease (139). If the loss of αB crystallin interacted with mutant SOD1 to worsen the myopathic disease, the effect was not sufficiently robust to be noticeable.

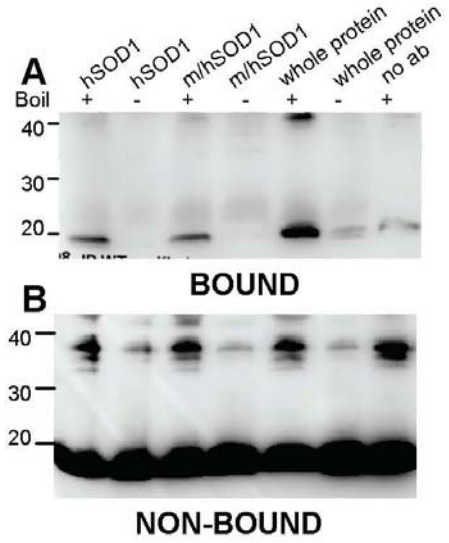

Figure 5-11. SOD1 antibodies recognize denatured forms for SOD1. WT purified protein was incubated with hSOD1, m/hSOD1, and whole protein SOD1 antiserum in detergent (0.25% SDS, 0.5% NP40, 0.5% DOC) and in the presence or absence of heat (95°C). Immunoblots were probed with whole protein SOD1 antiserum. A) Binding fraction (10 µl). B) Non-binding fraction (10 µl). The image shown is representative of 3 repetitions of the experiment.

The Role of Heat Shock Proteins in the ALS Disease Course

When activated, αB crystallin forms large heterogeneous multimers that range in size from 300 to 1000 kDa and can contain as many as 40 subunits (197). By binding to exposed hydrophobic surfaces on denatured or misfolded proteins, αB crystallin inhibits protein aggregation (183-188). Our finding in cell culture that αB crystallin reduced mutant SOD1 aggregation and that αB crystallin is upregulated into the detergent-insoluble fraction when co-transfected with mutant SOD1 suggests that αB crystallin binds to misfolded mutant SOD1 and

prevents aggregation. However, we do not have conclusive evidence that αB crystallin stably binds to mutant SOD1.

In ALS, motor neurons are less capable of inducing heat shock proteins (198). In mouse models of FALS, Hsp40, Hsp60. Hsp70, and Hsp90 remain unchanged throughout the disease course (196). Only the small heat shock proteins Hsp25 and αB crystallin are upregulated in symptomatic SOD1 transgenic mice (196). Previous studies investigating the effects of heat shock proteins on ALS have shown little, if any, effect on disease course and progression (199-201). However, these studies focus largely on Hsp27 and Hsp70, which are normally expressed in motor neurons; thus, overexpression of these proteins may not enhance the ability of the cell to combat accumulating mutant SOD1.

Our findings that mutant SOD1 aggregates in cells in which Hsp70 and Hsp40 are constitutively, highly expressed, suggests that Hsp70 and Hsp40 may be less capable of inhibiting SOD1 aggregation. However, it is also possible that Hsp70 and Hsp40 have little effect on SOD1 aggregation in cell culture due to the high levels of overexpression of the mutant protein in this model.

Disease Threshold in SOD1 Transgenic Mice

To determine whether αB crystallin is capable of altering disease course and pathology in SOD1 transgenic mice, an asymptomatic transgenic mouse, PrP.G37R, was studied. Heterozygous PrP.G37R mice do not develop ALS pathology and do not form SOD1 aggregates; however, homozygous PrP.G37R develop hindlimb paralysis and form SOD1 aggregates in the spinal cord (149). Thus, the acquisition of the ALS phenotype in our mouse model is based on threshold levels of mutant SOD1. Using heterozygous PrP.G37R mice, we asked if reducing or eliminating αB crystallin could lower the threshold of mutant SOD1 expression that is required

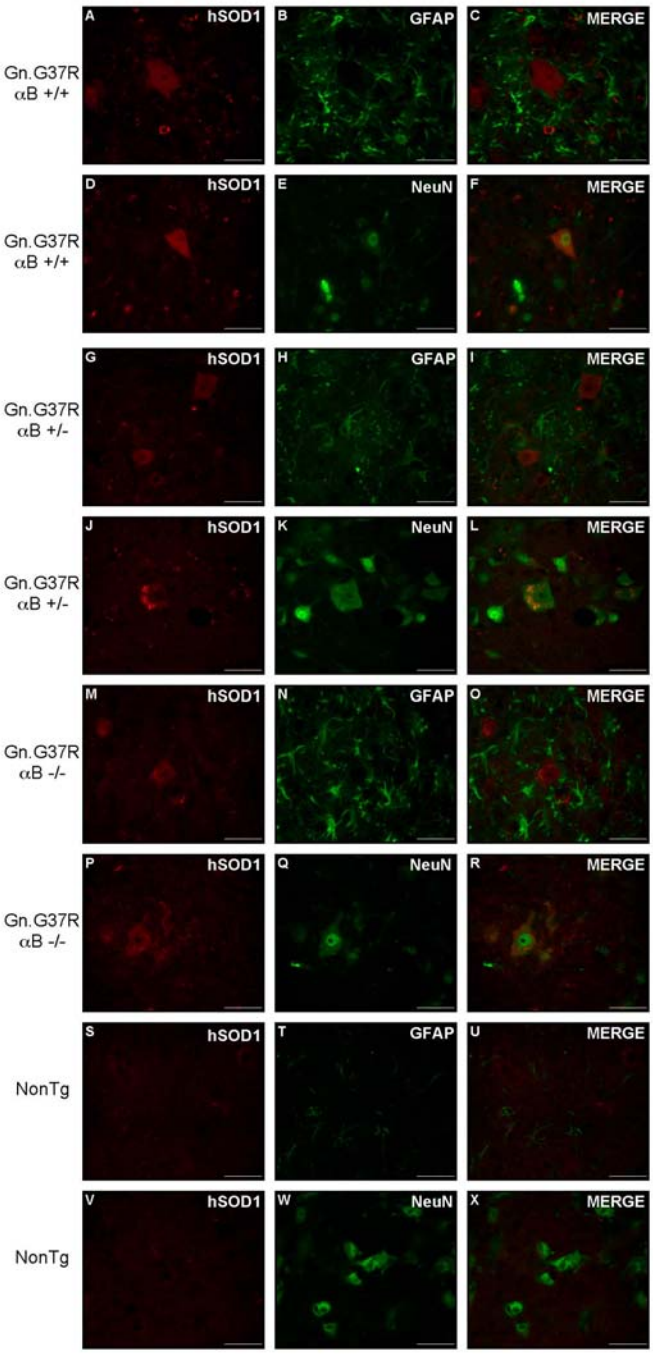

Figure 5-12. In Gn.G37R mice, αB crystallin does not alter localization of SOD1 accumulation. Mice were perfused with 4% paraformaldehyde and spinal cord tissue was immersed in sucrose prior to cryostat sectioning (14 microns). Sections were stained with hSOD1 antiserum (A, D, G, J, M, P, S, V) and GFAP (B, H, N, T) or NeuN (E, K, Q, W). Sections were stained with secondary fluorescent antibodies: anti-rabbit-AlexaFluor 568 (A, D, G, J, M, P, S, V) and anti-mouse-AlexaFluor 488 (B, E, H, K, N, Q, T, W). Ventral horn. 40x magnification. The image shown is representative of 4 repetitions of the experiment.

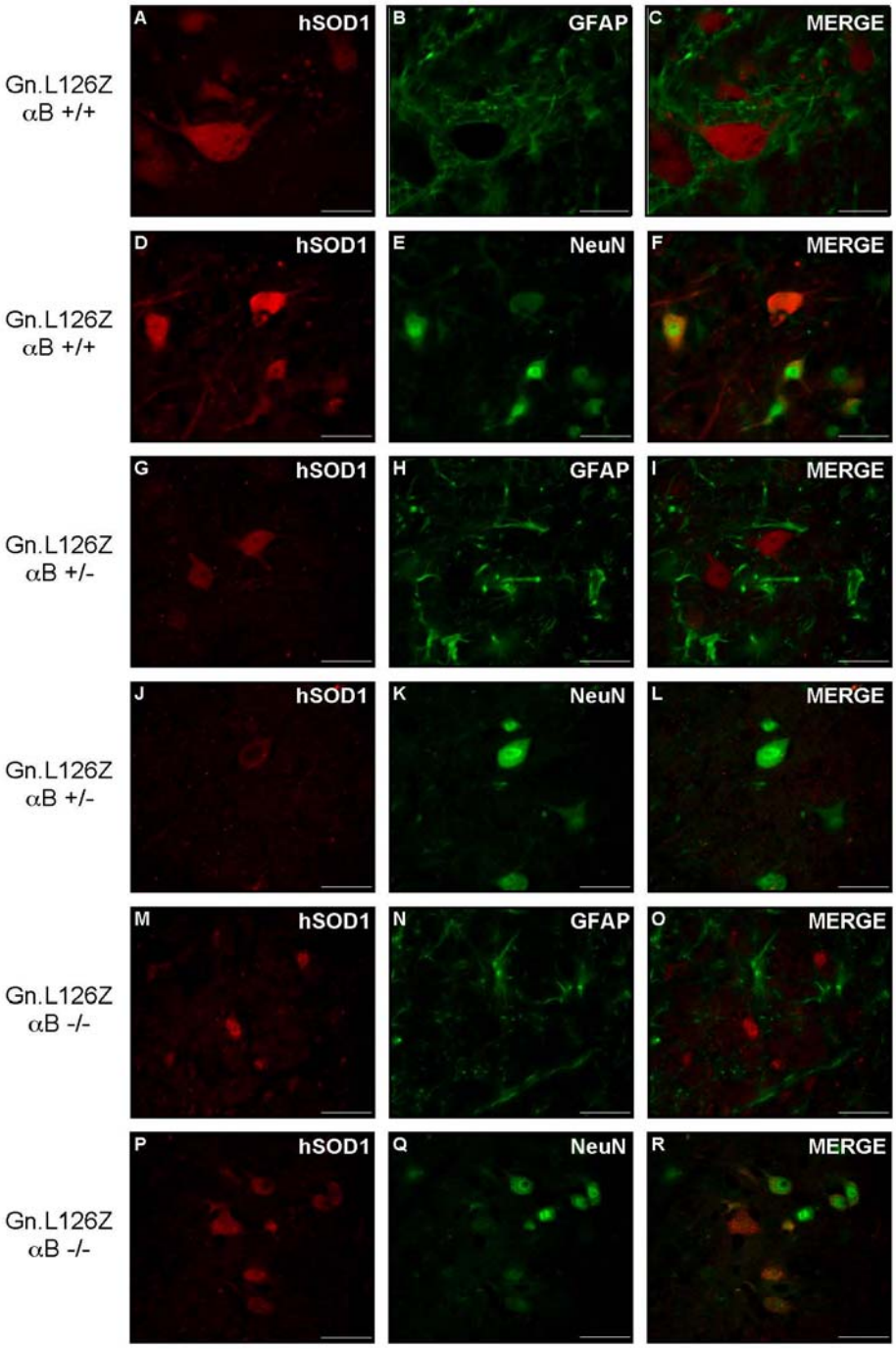

Figure 5-13. In Gn.L126Z mice, αB crystallin does not alter localization of SOD1 accumulation. Mice were perfused with 4% paraformaldehyde and spinal cord tissue was immersed in sucrose prior to cryostat sectioning (14 microns). Sections were stained with hSOD1 antiserum (A, D, G, J, M, P) and GFAP (B, H, N) or NeuN (E, K, Q). Sections were stained with secondary fluorescent antibodies: anti-rabbit-AlexaFluor 568 (A, D, G, J, M, P) and anti-mouse-AlexaFluor 488 (B, E, H, K, N, Q). Ventral horn. 40x magnification. The image shown is representative of 4 repetitions of the experiment.

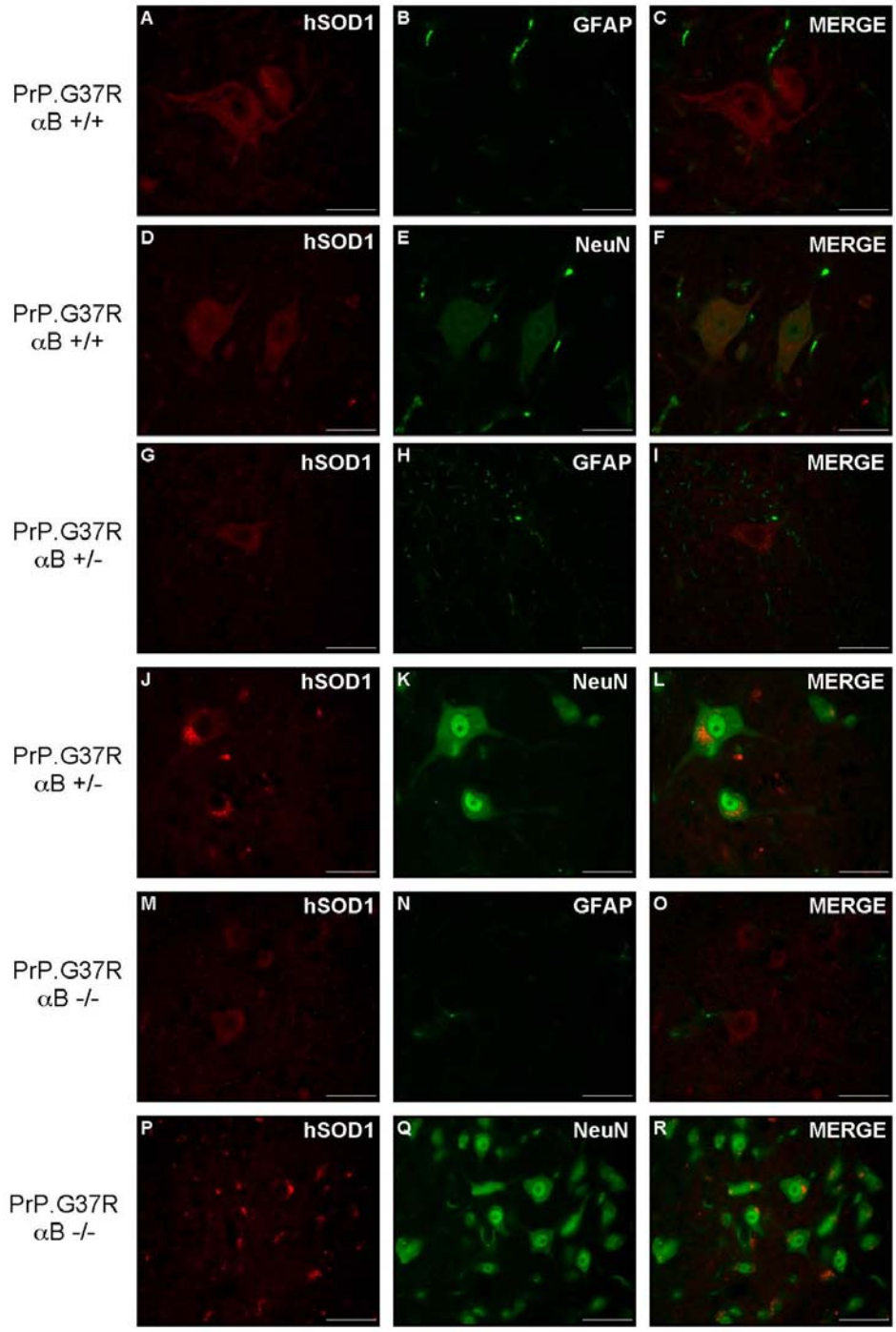

Figure 5-14. In PrP.G37R mice, αB crystallin does not alter localization of SOD1 accumulation. Mice were perfused with 4% paraformaldehyde and spinal cord tissue was immersed in sucrose prior to cryostat sectioning (14 microns). Sections were stained with hSOD1 antiserum (A, D, G, J, M, P) and GFAP (B, H, N) or NeuN (E, K, Q). Sections were stained with secondary fluorescent antibodies: anti-rabbit-AlexaFluor 568 (A, D, G, J, M, P) and anti-mouse-AlexaFluor 488 (B, E, H, K, N, Q). Ventral horn. 40x magnification. The image shown is representative of 4 repetitions of the experiment.

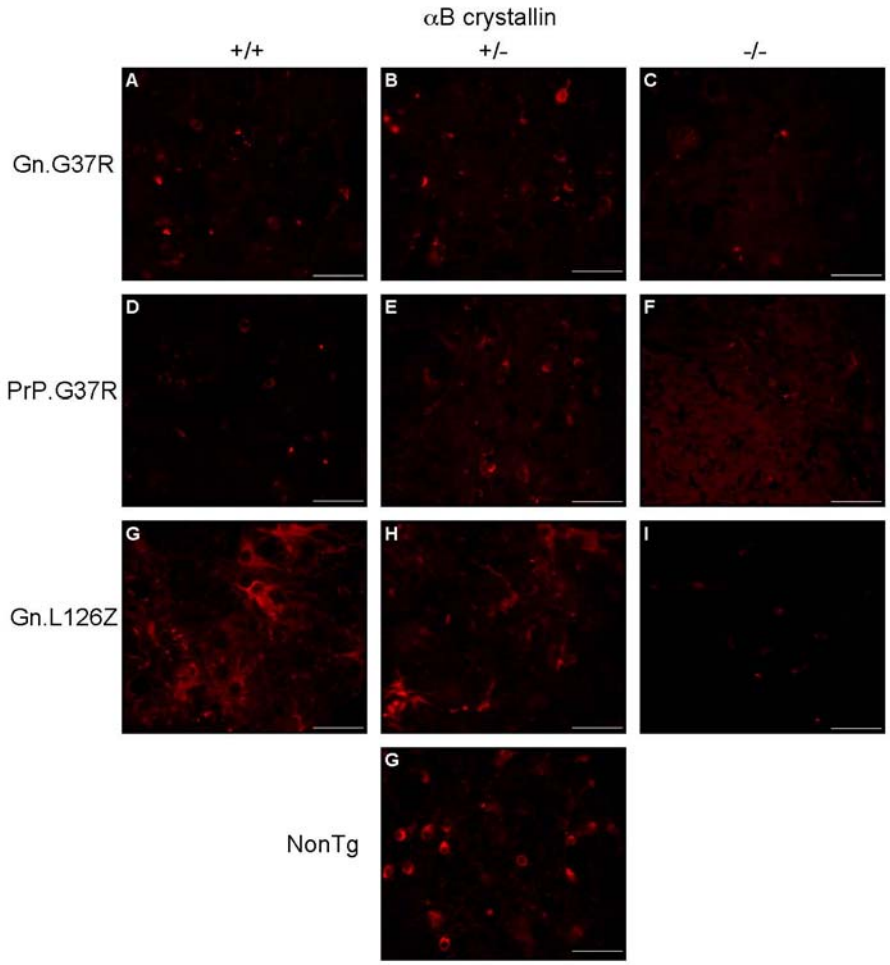

Figure 5-15. αB crystallin is upregulated in astrocytes of Gn.L126Z mice. Mice were perfused with 4% paraformaldehyde and spinal cord tissue was immersed in sucrose prior to cryostat sectioning (14 microns). Sections were stained with αB crystallin. Sections were stained with secondary fluorescent antibodies: anti-rabbit-AlexaFluor 568. Ventral horn. 40x magnification. The image shown is representative of 4 repetitions of the experiment.

to induce disease. Reduction or elimination of αB crystallin did not produce a phenotype or SOD1 aggregation in PrP.G37R mice (data not shown). These results suggest that the absence of αB crystallin does not produce enough of a burden to induce disease. However, we cannot disregard evidence in symptomatic SOD1 transgenic mice (Gn.G37R and Gn.L126Z), which developed the ALS phenotype at significantly earlier ages when αB crystallin was reduced or

eliminated. Collectively, these mice demonstrate that αB crystallin is likely only a modest modifier of disease phenotype.

Conclusions

In cell culture, small heat shock proteins are robust modifiers of SOD1 aggregation. However, heat shock proteins show modest effects on the ALS disease course *in vivo*. Thus, it is possible that the induction of one small heat shock protein alone is not robust enough to modify disease. It may be possible that heat shock proteins can work in concert to prevent protein misfolding and mutant SOD1 toxicity.

CHAPTER 6
CONCLUSIONS

SOD1-linked FALS is characterized by aggregation of the mutant SOD1 protein. To date, all FALS-linked SOD1 mutants studied in cell culture share a propensity to form aggregates, despite variable biophysical characteristics of individual SOD1 mutants. All SOD1 transgenic mice that overexpress FALS-linked SOD1 mutants develop hindlimb paralysis, motor neuron loss, and SOD1 aggregates in the brainstem and spinal cord. Wild-type (WT) SOD1 does not form SOD1 aggregates in cell culture, and WT SOD1 transgenic mice do not develop the ALS phenotype. Despite the apparent importance of SOD1 aggregates, the mechanisms of mutant SOD1 aggregate formation and how these structures contribute to disease pathogenesis is poorly understood. In this study, we hypothesized that SOD1 aggregates mediate ALS. We used cell culture and mouse models to study the factors that mediate SOD1 aggregate formation and to understand the role of SOD1 aggregates in the ALS disease course.

Composition of Mutant SOD1 Aggregates

In these studies, we provide evidence that inherent structural aspects of the SOD1 protein mediate aggregate formation. Previous work has suggested that SOD1 aggregates are predominantly stabilized by high-molecular-weight, disulfide cross-linked species (23, 141). Through the manipulation of the four cysteine residues in the SOD1 protein, we found that cysteine 6 and cysteine 111 are important for mediating SOD1 aggregate formation and that these residues mediate aggregation by a mechanism other than disulfide cross-linking (Chapter 2). However, we demonstrated that cysteine residues are not required for SOD1 aggregation to occur (Chapter 2).

We provide evidence that eliminating cysteine 111 in the context of a highly aggregating FALS mutant significantly reduces aggregate formation (Chapter 2). Some groups suggest that

cysteine 111 is vulnerable to oxidative modification or aberrant copper binding (152-155), but it is also possible that cysteine 111 works in concert with other residues in the SOD1 protein to promote misfolding. We provide evidence that aggregation is enhanced in FALS mutants via residues in β-strand 6 and β-strand 7, which includes cysteine 111 (Chapter 3). Because β-strands 6 and 7 contain structures that are vital for stability of the protein, including copper binding sites and portions of the dimer interface (38), and because we have yet to identify a single residue that is required for SOD1 aggregation, we propose that SOD1 mutations result in global misfolding of the protein, mediated by destabilization between β-strand 6 and β-strand 7.

To define the composition of SOD1 aggregates, we studied spinal cord tissues from symptomatic mutant SOD1 transgenic mice. We demonstrate that aggregates at disease endstage are predominantly composed of disulfide-reduced SOD1 protein (Chapter 4). It has been suggested that SOD1 must bind copper and zinc before the intramolecular disulfide bond can form between cysteine 57 and cysteine 146. Thus, immature forms of the protein (with respect to metal binding and disulfide bond formation) are more prone to aggregate. It is possible that the immature forms of the mutant protein are sufficiently degraded early in the disease; however, over time, these species accumulate and become preferentially incorporated into aggregates that are prominent at disease endstage (Fig. 6-1). Whether these immature forms of the protein also form soluble oligomers remains unknown. Despite evidence that disulfide cross-linked species are prominent at disease endstage (23, 141), this work demonstrates that disulfide cross-linking is not required for aggregate stabilization. Aggregates remain intact in the presence of high concentrations of reducing agents, which dissociate the disulfide cross-links (Chapter 4). Thus, we suggest that aberrant disulfide bonding occurs after the aggregates are stabilized by other bonding forces (Fig. 6-1). SOD1 aggregates may become stabilized by extensive β-strand

stacking, as many SOD1 transgenic mice have Thioflavin-S positive inclusions in affected tissues (104).

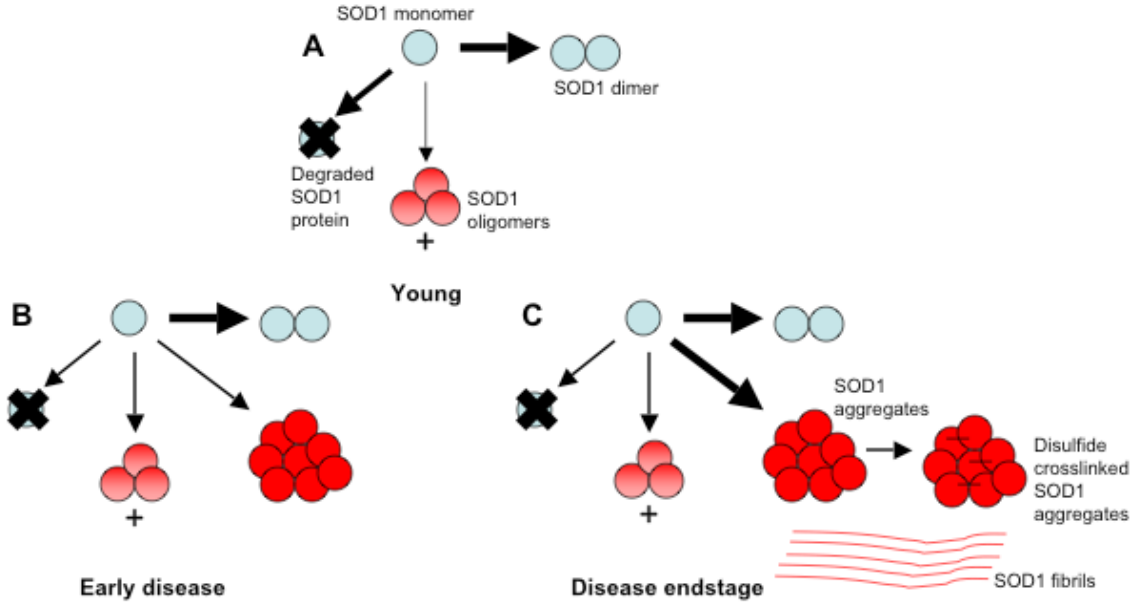

Figure 6-1. Mutant SOD1 folding pathways throughout the ALS disease course. Proposed folding pathways of mutant SOD1. When mice are asymptomatic (A), misfolded SOD1 protein is sufficiently degraded. It is possible that toxic, soluble oligomers are present and impart toxicity. As mice approach disease onset (B), detergent-insoluble aggregates are present. These aggregates become more extensively disulfide cross-linked as the mice approach disease endstage (C). Arrow thickness reflects relative abundance. +, proposed SOD1 oligomers that are larger than two monomers.

The Role of SOD1 Aggregates in ALS Disease Course

Understanding the role of SOD1 aggregation in disease course is crucial to our understanding of the disease mechanism. In mouse models of ALS, we found that aggregation occurs late in the disease (Chapter 4). Low levels of SOD1 aggregates were detected just prior to overt paralysis, suggesting that these species are important for acquisition of disease phenotype (paralysis) (Chapter 4). SOD1 aggregate progression was similar in mutant SOD1 transgenic mice that expressed mutants with a range of biophysical characteristics. Furthermore, we found that high-molecular-weight, disulfide cross-linked SOD1 species formed concurrently with detergent-insoluble aggregates at disease endstage, which provides further evidence that

disulfide cross-linking is a secondary structural feature of aggregates (Chapter 4).

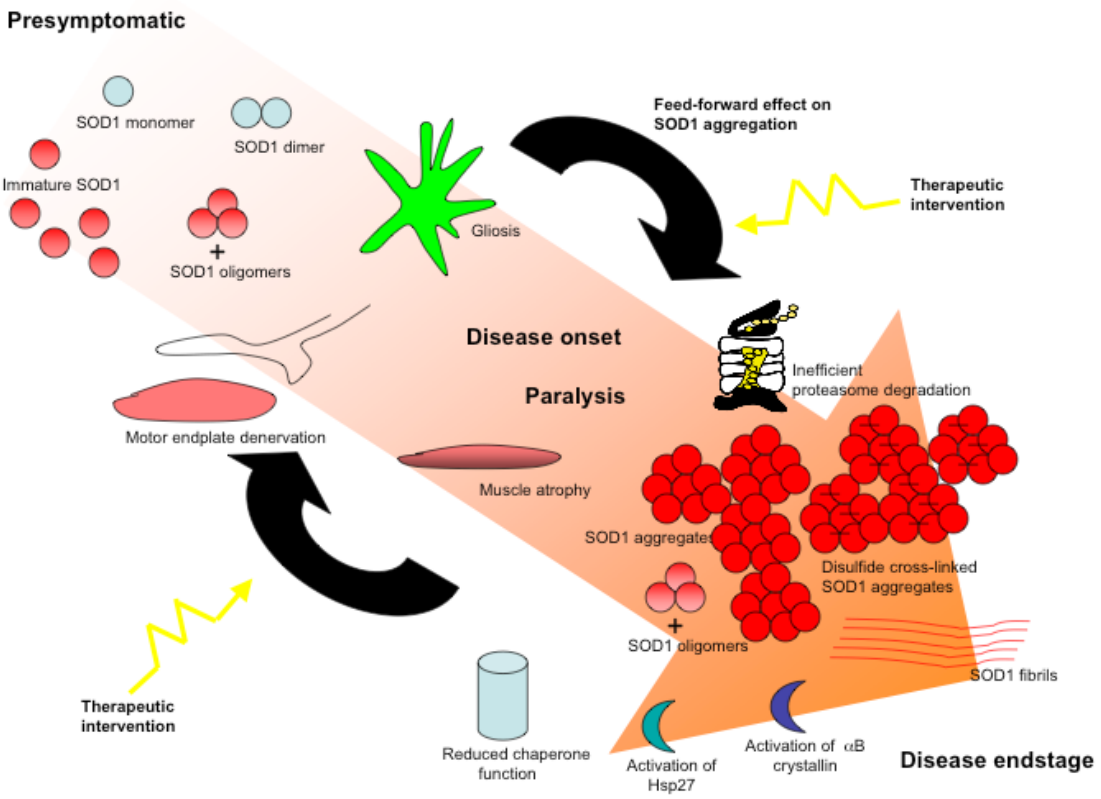

Figure 6-2. Disease progression in SOD1 transgenic mice. During presymptomatic stages of the disease, portions of SOD1 are normally folded (blue circles) with a small fraction of SOD1 protein that does not have the intramolecular disulfide bond (red circles). Pathology including gliosis and motor endplate denervation are prominent prior to disease endstage. After disease onset, SOD1 aggregates (detergent-insoluble SOD1) are prominent in addition to disulfide cross-linked SOD1 aggregates. Pathology including muscle atrophy, reduced chaperone function, activation of small heat shock proteins, and paralysis occur at disease endstage. Soluble SOD1 oligomers may be toxic at disease stages; however, currently, we do not have techniques to isolate these species. We propose that at disease onset, the formation of SOD1 aggregates triggers enhanced misfolding of immature SOD1 monomer, which becomes preferentially incorporated into the aggregate. This feed forward loop results in a rapid increase in aggregates and disease endstage.

Despite the robust presence of aggregates at disease endstage in SOD1 transgenic mice, we found that abnormal pathology occurs prior to the formation of detergent-insoluble SOD1 aggregates, including denervation of the motor endplate, gliosis, and motor neuron loss (Chapter 2). Together, our studies suggest that early toxic events occur in SOD1 transgenic mice that are

not directly associated with the presence of detergent-insoluble SOD1 aggregates (Fig. 6-2). Yet, it remains possible that other forms of mutant SOD1 are toxic early in the disease which are distinct from detergent-insoluble SOD1 aggregates or which are precursors to the species detectable at disease endstage (Figs. 6-1 and 6-2).

Modifiers of SOD1 Aggregation and FALS Pathogenesis

From our study in mouse models of ALS, SOD1 aggregation appears to coincide with disease endstage. Because all mice that develop hindlimb paralysis have detectable levels of mutant SOD1 aggregates in the brainstem and spinal cord, aggregation remains an important pathological feature of the disease. Several groups have described inhibition of aggregation in cell culture with the application of heat shock proteins (131); however, these effects have translated poorly *in vivo* (199-201). We chose an alternative approach: to study a small heat shock protein that is upregulated at disease endstage and not expressed in affected tissues. In cell culture, we found that the small heat shock protein αB crystallin was a strong modifier of mutant SOD1 aggregation (Chapter 5). However, *in vivo* evidence suggests that αB crystallin modifies disease only slightly, as we were unable to detect any change in the localization or the abundance of SOD1 aggregates in the absence of αB crystallin. This study demonstrates that αB crystallin is not a critical factor in disease. However, it does not rule out the possibility that overexpression of αB crystallin in motor neurons in SOD1 transgenic mice may have some suppressive effect on aggregate and disease course.

Insights into Therapeutics

Currently, therapies are largely ineffective in treating or slowing disease in ALS patients. This study provides insight into the disease course and possible new avenues to approach

treatment. Our findings suggest that SOD1 aggregation is associated with onset of disease (paralysis).

Our findings that SOD1 aggregation occurs late in the disease course and that pathologic events occur prior to SOD1 aggregation, suggest that therapeutic approaches targeted to disruption of detergent-insoluble SOD1 aggregates will likely have effects on the rate of disease progression. Because aggregates are detected so late in disease, it is possible that toxic soluble forms of the mutant protein cause early pathologic abnormalities and aggregates form as a consequence of oligomer-induced toxicity. It is possible that these forms that must be targeted early in the disease prior to extensive muscle denervation and motor neuron loss.

The identification of two regions of the human mutant SOD1 protein that enhance aggregation in cell culture may provide new avenues for drug targets. If small compounds are identified that can stabilize the interactions between β-strands 6 and 7, perhaps the protein can stably fold or the rate of aggregation can be slowed. This avenue is attractive because it is not specific to individual SOD1 mutants. This approach is dependent on some form of misfolded SOD1 protein imparting toxicity. Because our results suggest that SOD1 aggregation occurs at the onset of paralysis and rapidly increases at disease endstage, drugs that stabilize the mutant SOD1 protein and slow the rate of aggregation may slow the progression of paralysis.

Additionally, our findings that αB crystallin has only slight effects on disease course when absent in SOD1 transgenic mice taken with previous studies that demonstrate negligible effects on disease course when Hsp70, Hsp25, or Hsf1 are overexpressed (199-201), provides evidence that modulating a single heat shock protein or a single pathway is insufficient to alter disease course. Thus, SOD1 aggregation and ALS pathogenesis is likely a breakdown of multiple systems and will require therapies that have many targets.

Future Directions

Protein misfolding and aggregation are hallmark pathologic features in many neurodegenerative diseases. Conclusive evidence is lacking regarding which forms of the misfolded proteins are toxic and the mechanism of this toxicity. In ALS, SOD1 aggregation is still poorly understood, and new techniques must be pursued to identify alternative forms of misfolded SOD1. Attempts have been made to isolate SOD1 oligomers by exploiting hydrophobic residues that are enhanced in the misfolded protein (168). These methods, however, can only identify a subset of mutants, and because we are searching for a common mechanism of toxicity, new techniques for isolating oligomeric forms of the protein will be important.

To better study SOD1 aggregation and SOD1 toxicity, we are looking into new model systems to screen SOD1 mutants. While SOD1 transgenic mice are excellent models of FALS disease course, developing and characterizing these models is time consuming and costly. Because all mutant SOD1 transgenic mice develop motor neuron loss, SOD1 aggregates in the brainstem and spinal cord, and hindlimb paralysis, developing a new mutant SOD1 transgenic mouse requires a mutant or paradigm that could provide new insights into the disease. Using the most interesting cysteine mutations, we are currently establishing *C. elegans* that express SOD1 mutants under the control of muscle and neuronal promoters in collaboration with the laboratory of Dr. Richard Morimoto (202). Using this worm model, we will screen these mutants for effects on SOD1 aggregation and toxicity (measured by change in motility). This model is appealing because it allows for more rapid screening of a large variety of mutants. However, there are also several caveats: the model utilizes YFP fused to SOD1, which likely alters folding patterns of the protein and the mutant SOD1 worms that have been characterized develop

aggregates with low toxicity (202). Nevertheless, new model systems may provide insight into fundamental questions of SOD1 misfolding and toxicity.

Until a SOD1 mutant is identified that causes the disease without the formation of SOD1 aggregates in the affected tissues, we cannot be sure that aggregates are not participating in important toxic events in the ALS disease course. To further examine the contribution of aggregates to disease, we can create transgenic SOD1 mice that conditionally overexpress mutant SOD1 protein. Using a tTA system, expression of the mutant SOD1 transgene can be turned off using doxycycline at time points throughout the disease course. This system will require high expression levels of the mutant protein (as dose effects determine the acquisition of disease phentoype in this model (133, 149)) and extensive characterization of the disease course when the transgene remains active is critical to ensure that any changes in disease progression are real effects. This conditional model could address several unanswered questions in the field: 1) at what rate do aggregate form *in vivo*; 2) does the rate of aggregation depend on the stage of disease; 3) do aggregates precursors contribute to toxicity; and 4) are SOD1 aggregates responsible for disease phenotype.

Conclusions

These studies provide new insights into how SOD1 aggregates form and how these structures evolve in ALS disease course. While much remains unknown as to which structures are toxic, our findings suggest that SOD1 aggregates are composed of globally misfolded, immature protein. Based on these studies, it appears that SOD1 aggregation is associated with a single phase of the disease: disease duration after onset. Together, these findings will allow for new avenues in therapeutic design and research into disease mechanisms.

LIST OF REFERENCES

1. Mulder DW, Kurland LT, Offord KP, *et al.* (1986) Familial adult motor neuron disease: amyotrophic lateral sclerosis. *Neurology* 36:511-517.

2. Bendotti C & Carri MT (2004) Lessons from models of SOD1-linked familial ALS. *Trends Mol Med* 10:393-400.

3. Bensimon G, Lacomblez L, & Meininger V (1994) A controlled trial of riluzole in amyotrophic lateral sclerosis. ALS/Riluzole Study Group. *N Engl J Med* 330:585-591.

4. Rosen DR, Siddique T, Patterson D, *et al.* (1993) Mutations in Cu/Zn superoxide dismutase gene are associated with familial amyotrophic lateral sclerosis. *Nature* 362:59-62.

5. Hand CK, Khoris J, Salachas F, *et al.* (2002) A novel locus for familial amyotrophic lateral sclerosis, on chromosome 18q. *Am J Hum Genet* 70:251-256.

6. Vance C, Rogelj B, Hortobagyi T, *et al.* (2009) Mutations in FUS, an RNA processing protein, cause familial amyotrophic lateral sclerosis type 6. *Science* 323:1208-1211.

7. Abalkhail H, Mitchell J, Habgood J, *et al.* (2003) A new familial amyotrophic lateral sclerosis locus on chromosome 16q12.1-16q12.2. *Am J Hum Genet* 73:383-389.

8. Sapp PC, Hosler BA, McKenna-Yasek D, *et al.* (2003) Identification of two novel loci for dominantly inherited familial amyotrophic lateral sclerosis. *Am J Hum Genet* 73:397-403.

9. Sreedharan J, Blair IP, Tripathi VB, *et al.* (2008) TDP-43 mutations in familial and sporadic amyotrophic lateral sclerosis. *Science* 319:1668-1672.

10. Hosler BA, Siddique T, Sapp PC, *et al.* (2000) Linkage of familial amyotrophic lateral sclerosis with frontotemporal dementia to chromosome 9q21-q22. *Jama* 284:1664-1669.

11. Hutton M, Lendon CL, Rizzu P, *et al.* (1998) Association of missense and 5'-splice-site mutations in tau with the inherited dementia FTDP-17. *Nature* 393:702-705.

12. Hirokawa N (1994) Microtubule organization and dynamics dependent on microtubule-associated proteins. *Curr Opin Cell Biol* 6:74-81.

13. Puls I, Jonnakuty C, LaMonte BH, *et al.* (2003) Mutant dynactin in motor neuron disease. *Nat Genet* 33:455-456.

14. Waterman-Storer CM, Karki S, & Holzbaur EL (1995) The p150Glued component of the dynactin complex binds to both microtubules and the actin-related protein centractin (Arp-1). *Proc Natl Acad Sci U S A* 92:1634-1638.

15. Nishimura AL, Mitne-Neto M, Silva HC, *et al.* (2004) A mutation in the vesicle-trafficking protein VAPB causes late-onset spinal muscular atrophy and amyotrophic lateral sclerosis. *Am J Hum Genet* 75:822-831.

16. Nishimura AL, Mitne-Neto M, Silva HC, *et al.* (2004) A novel locus for late onset amyotrophic lateral sclerosis/motor neurone disease variant at 20q13. *J Med Genet* 41:315-320.

17. Foster LJ, Weir ML, Lim DY, *et al.* (2000) A functional role for VAP-33 in insulin-stimulated GLUT4 traffic. *Traffic* 1:512-521.

18. Chance PF, Rabin BA, Ryan SG, *et al.* (1998) Linkage of the gene for an autosomal dominant form of juvenile amyotrophic lateral sclerosis to chromosome 9q34. *Am J Hum Genet* 62:633-640.

19. Chen YZ, Bennett CL, Huynh HM, *et al.* (2004) DNA/RNA helicase gene mutations in a form of juvenile amyotrophic lateral sclerosis (ALS4). *Am J Hum Genet* 74:1128-1135.

20. Kunita R, Otomo A, Mizumura H, *et al.* (2004) Homo-oligomerization of ALS2 through its unique carboxyl-terminal regions is essential for the ALS2-associated Rab5 guanine nucleotide exchange activity and its regulatory function on endosome trafficking. *J Biol Chem* 279:38626-38635.

21. Otomo A, Hadano S, Okada T, *et al.* (2003) ALS2, a novel guanine nucleotide exchange factor for the small GTPase Rab5, is implicated in endosomal dynamics. *Hum Mol Genet* 12:1671-1687.

22. Hentati A, Ouahchi K, Pericak-Vance MA, *et al.* (1998) Linkage of a commoner form of recessive amyotrophic lateral sclerosis to chromosome 15q15-q22 markers. *Neurogenetics* 2:55-60.

23. Wang J, Xu G, & Borchelt DR (2006) Mapping superoxide dismutase 1 domains of non-native interaction: roles of intra- and intermolecular disulfide bonding in aggregation. *J Neurochem* 96:1277-1288.

24. Borchelt DR, Lee MK, Slunt HS, *et al.* (1994) Superoxide dismutase 1 with mutations linked to familial amyotrophic lateral sclerosis possesses significant activity. *Proc Natl Acad Sci U S A* 91:8292-8296.

25. Potter SZ & Valentine JS (2003) The perplexing role of copper-zinc superoxide dismutase in amyotrophic lateral sclerosis (Lou Gehrig's disease). *J Biol Inorg Chem* 8:373-380.

26. Valentine JS & Hart PJ (2003) Misfolded CuZnSOD and amyotrophic lateral sclerosis. *Proc Natl Acad Sci U S A* 100:3617-3622.

27. Hayward LJ, Rodriguez JA, Kim JW, *et al.* (2002) Decreased metallation and activity in subsets of mutant superoxide dismutases associated with familial amyotrophic lateral sclerosis. *J Biol Chem* 277:15923-15931.

28. Nishida CR, Gralla EB, & Valentine JS (1994) Characterization of three yeast copper-zinc superoxide dismutase mutants analogous to those coded for in familial amyotrophic lateral sclerosis. *Proc Natl Acad Sci U S A* 91:9906-9910.

29. Ratovitski T, Corson LB, Strain J, *et al.* (1999) Variation in the biochemical/biophysical properties of mutant superoxide dismutase 1 enzymes and the rate of disease progression in familial amyotrophic lateral sclerosis kindreds. *Hum Mol Genet* 8:1451-1460.

30. Wiedau-Pazos M, Goto JJ, Rabizadeh S, *et al.* (1996) Altered reactivity of superoxide dismutase in familial amyotrophic lateral sclerosis. *Science* 271:515-518.

31. Tiwari A & Hayward LJ (2003) Familial amyotrophic lateral sclerosis mutants of copper/zinc superoxide dismutase are susceptible to disulfide reduction. *J Biol Chem* 278:5984-5992.

32. Reaume AG, Elliott JL, Hoffman EK, *et al.* (1996) Motor neurons in Cu/Zn superoxide dismutase-deficient mice develop normally but exhibit enhanced cell death after axonal injury. *Nat Genet* 13:43-47.

33. Beckman G, Lundgren E, & Tarnvik A (1973) Superoxide dismutase isozymes in different human tissues, their genetic control and intracellular localization. *Hum Hered* 23:338-345.

34. Crapo JD, Oury T, Rabouille C, *et al.* (1992) Copper,zinc superoxide dismutase is primarily a cytosolic protein in human cells. *Proc Natl Acad Sci U S A* 89:10405-10409.

35. Keller GA, Warner TG, Steimer KS, *et al.* (1991) Cu,Zn superoxide dismutase is a peroxisomal enzyme in human fibroblasts and hepatoma cells. *Proc Natl Acad Sci U S A* 88:7381-7385.

36. Jaarsma D, Rognoni F, van Duijn W, *et al.* (2001) CuZn superoxide dismutase (SOD1) accumulates in vacuolated mitochondria in transgenic mice expressing amyotrophic lateral sclerosis-linked SOD1 mutations. *Acta Neuropathol (Berl)* 102:293-305.

37. Potter SZ, Zhu H, Shaw BF, *et al.* (2007) Binding of a single zinc ion to one subunit of copper-zinc superoxide dismutase apoprotein substantially influences the structure and stability of the entire homodimeric protein. *J Am Chem Soc* 129:4575-4583.

38. Parge HE, Hallewell RA, & Tainer JA (1992) Atomic structures of wild-type and thermostable mutant recombinant human Cu,Zn superoxide dismutase. *Proc Natl Acad Sci U S A* 89:6109-6113.

39. Lyons TJ, Gralla EB, & Valentine JS (1999) Biological chemistry of copper-zinc superoxide dismutase and its link to amyotrophic lateral sclerosis. *Met Ions Biol Syst* 36:125-177.

40. Nakanishi T, Kishikawa M, Miyazaki A, *et al.* (1998) Simple and defined method to detect the SOD-1 mutants from patients with familial amyotrophic lateral sclerosis by mass spectrometry. *J Neurosci Methods* 81:41-44.

41. Nakano R, Sato S, Inuzuka T, *et al.* (1994) A novel mutation in Cu/Zn superoxide dismutase gene in Japanese familial amyotrophic lateral sclerosis. *Biochem Biophys Res Commun* 200:695-703.

42. Rosen DR, Bowling AC, Patterson D, *et al.* (1994) A frequent ala 4 to val superoxide dismutase-1 mutation is associated with a rapidly progressive familial amyotrophic lateral sclerosis. *Hum Mol Genet* 3:981-987.

43. Wang J, Slunt H, Gonzales V, *et al.* (2003) Copper-binding-site-null SOD1 causes ALS in transgenic mice: aggregates of non-native SOD1 delineate a common feature. *Hum Mol Genet* 12:2753-2764.

44. Rodriguez JA, Valentine JS, Eggers DK, *et al.* (2002) Familial amyotrophic lateral sclerosis-associated mutations decrease the thermal stability of distinctly metallated species of human copper/zinc superoxide dismutase. *J Biol Chem* 277:15932-15937.

45. Morita M, Aoki M, Abe K, *et al.* (1996) A novel two-base mutation in the Cu/Zn superoxide dismutase gene associated with familial amyotrophic lateral sclerosis in Japan. *Neurosci Lett* 205:79-82.

46. Karch CM & Borchelt DR (2008) A limited role for disulfide cross-linking in the aggregation of mutant SOD1 linked to familial amyotrophic lateral sclerosis. *J Biol Chem* 283:13528-13537.

47. Kohno S, Takahashi Y, Miyajima H, *et al.* (1999) A novel mutation (Cys6Gly) in the Cu/Zn superoxide dismutase gene associated with rapidly progressive familial amyotrophic lateral sclerosis. *Neurosci Lett* 276:135-137.

48. Hirano M, Fujii J, Nagai Y, *et al.* (1994) A new variant Cu/Zn superoxide dismutase (Val7-->Glu) deduced from lymphocyte mRNA sequences from Japanese patients with familial amyotrophic lateral sclerosis. *Biochem Biophys Res Commun* 204:572-577.

49. Valentine JS, Doucette PA, & Zittin Potter S (2005) Copper-zinc superoxide dismutase and amyotrophic lateral sclerosis. *Annu Rev Biochem* 74:563-593.

50. Siddique T & Deng HX (1996) Genetics of amyotrophic lateral sclerosis. *Hum Mol Genet* 5 Spec No:1465-1470.

51. Andersen PM, Sims KB, Xin WW, *et al.* (2003) Sixteen novel mutations in the Cu/Zn superoxide dismutase gene in amyotrophic lateral sclerosis: a decade of discoveries, defects and disputes. *Amyotroph Lateral Scler Other Motor Neuron Disord* 4:62-73.

52. Kim NH, Kim HJ, Kim M, *et al.* (2003) A novel SOD1 gene mutation in a Korean family with amyotrophic lateral sclerosis. *J Neurol Sci* 206:65-69.

53. Penco S, Schenone A, Bordo D, *et al.* (1999) A SOD1 gene mutation in a patient with slowly progressing familial ALS. *Neurology* 53:404-406.

54. Andersen PM, Nilsson P, Keranen ML, *et al.* (1997) Phenotypic heterogeneity in motor neuron disease patients with CuZn-superoxide dismutase mutations in Scandinavia. *Brain* 120 (Pt 10):1723-1737.

55. Deng HX, Tainer JA, Mitsumoto H, *et al.* (1995) Two novel SOD1 mutations in patients with familial amyotrophic lateral sclerosis. *Hum Mol Genet* 4:1113-1116.

56. Kawamata J, Shimohama S, Takano S, *et al.* (1997) Novel G16S (GGC-AGC) mutation in the SOD-1 gene in a patient with apparently sporadic young-onset amyotrophic lateral sclerosis. *Hum Mutat* 9:356-358.

57. Jones CT, Swingler RJ, & Brock DJ (1994) Identification of a novel SOD1 mutation in an apparently sporadic amyotrophic lateral sclerosis patient and the detection of Ile113Thr in three others. *Hum Mol Genet* 3:649-650.

58. Shi SG, Li LS, Chen KN, *et al.* (2004) [Identification of the mutation of SOD1 gene in a familial amyotrophic lateral sclerosis]. *Zhonghua Yi Xue Yi Chuan Xue Za Zhi* 21:149-152.

59. Boukaftane Y, Khoris J, Moulard B, *et al.* (1998) Identification of six novel SOD1 gene mutations in familial amyotrophic lateral sclerosis. *Can J Neurol Sci* 25:192-196.

60. Gellera C, Castellotti B, Riggio MC, *et al.* (2001) Superoxide dismutase gene mutations in Italian patients with familial and sporadic amyotrophic lateral sclerosis: identification of three novel missense mutations. *Neuromuscul Disord* 11:404-410.

61. Aoki M, Ogasawara M, Matsubara Y, *et al.* (1993) Mild ALS in Japan associated with novel SOD mutation. *Nat Genet* 5:323-324.

62. Enayat ZE, Orrell RW, Claus A, *et al.* (1995) Two novel mutations in the gene for copper zinc superoxide dismutase in UK families with amyotrophic lateral sclerosis. *Hum Mol Genet* 4:1239-1240.

63. Garcia-Redondo A, Bustos F, Juan YSB, *et al.* (2002) Molecular analysis of the superoxide dismutase 1 gene in Spanish patients with sporadic or familial amyotrophic lateral sclerosis. *Muscle Nerve* 26:274-278.

64. Shaw CE, Enayat ZE, Chioza BA, *et al.* (1998) Mutations in all five exons of SOD-1 may cause ALS. *Ann Neurol* 43:390-394.

65. Stewart HG, Mackenzie IR, Eisen A, *et al.* (2006) Clinicopathological phenotype of ALS with a novel G72C SOD1 gene mutation mimicking a myopathy. *Muscle Nerve* 33:701-706.

66. Segovia-Silvestre T, Andreu AL, Vives-Bauza C, *et al.* (2002) A novel exon 3 mutation (D76V) in the SOD1 gene associated with slowly progressive ALS. *Amyotroph Lateral Scler Other Motor Neuron Disord* 3:69-74.

67. Alexander MD, Traynor BJ, Miller N, *et al.* (2002) "True" sporadic ALS associated with a novel SOD-1 mutation. *Ann Neurol* 52:680-683.

68. Andersen PM (2006) Amyotrophic lateral sclerosis associated with mutations in the CuZn superoxide dismutase gene. *Curr Neurol Neurosci Rep* 6:37-46.

69. Beck M, Sendtner M, & Toyka KV (2007) Novel SOD1 N86K mutation is associated with a severe phenotype in familial ALS. *Muscle Nerve* 36:111-114.

70. Hayward C, Brock DJ, Minns RA, *et al.* (1998) Homozygosity for Asn86Ser mutation in the CuZn-superoxide dismutase gene produces a severe clinical phenotype in a juvenile onset case of familial amyotrophic lateral sclerosis. *J Med Genet* 35:174.

71. Rezania K, Yan J, Dellefave L, *et al.* (2003) A rare Cu/Zn superoxide dismutase mutation causing familial amyotrophic lateral sclerosis with variable age of onset, incomplete penetrance and a sensory neuropathy. *Amyotroph Lateral Scler Other Motor Neuron Disord* 4:162-166.

72. Andersen PM, Nilsson P, Ala-Hurula V, *et al.* (1995) Amyotrophic lateral sclerosis associated with homozygosity for an Asp90Ala mutation in CuZn-superoxide dismutase. *Nat Genet* 10:61-66.

73. Chou CM, Huang CJ, Shih CM, *et al.* (2005) Identification of three mutations in the Cu,Zn-superoxide dismutase (Cu,Zn-SOD) gene with familial amyotrophic lateral sclerosis: transduction of human Cu,Zn-SOD into PC12 cells by HIV-1 TAT protein basic domain. *Ann N Y Acad Sci* 1042:303-313.

74. Esteban J, Rosen DR, Bowling AC, *et al.* (1994) Identification of two novel mutations and a new polymorphism in the gene for Cu/Zn superoxide dismutase in patients with amyotrophic lateral sclerosis. *Hum Mol Genet* 3:997-998.

75. Elshafey A, Lanyon WG, & Connor JM (1994) Identification of a new missense point mutation in exon 4 of the Cu/Zn superoxide dismutase (SOD-1) gene in a family with amyotrophic lateral sclerosis. *Hum Mol Genet* 3:363-364.

76. Hosler BA, Nicholson GA, Sapp PC, *et al.* (1996) Three novel mutations and two variants in the gene for Cu/Zn superoxide dismutase in familial amyotrophic lateral sclerosis. *Neuromuscul Disord* 6:361-366.

77. Hand CK, Mayeux-Portas V, Khoris J, *et al.* (2001) Compound heterozygous D90A and D96N SOD1 mutations in a recessive amyotrophic lateral sclerosis family. *Ann Neurol* 49:267-271.

78. Yulug IG, Katsanis N, de Belleroche J, *et al.* (1995) An improved protocol for the analysis of SOD1 gene mutations, and a new mutation in exon 4. *Hum Mol Genet* 4:1101-1104.

79. Sato T, Yamamoto Y, Nakanishi T, *et al.* (2004) Identification of two novel mutations in the Cu/Zn superoxide dismutase gene with familial amyotrophic lateral sclerosis: mass spectrometric and genomic analyses. *J Neurol Sci* 218:79-83.

80. Jones CT, Shaw PJ, Chari G, *et al.* (1994) Identification of a novel exon 4 SOD1 mutation in a sporadic amyotrophic lateral sclerosis patient. *Mol Cell Probes* 8:329-330.

81. Tan CF, Piao YS, Hayashi S, *et al.* (2004) Familial amyotrophic lateral sclerosis with bulbar onset and a novel Asp101Tyr Cu/Zn superoxide dismutase gene mutation. *Acta Neuropathol* 108:332-336.

82. Ikeda M, Abe K, Aoki M, *et al.* (1995) Variable clinical symptoms in familial amyotrophic lateral sclerosis with a novel point mutation in the Cu/Zn superoxide dismutase gene. *Neurology* 45:2038-2042.

83. Orrell RW, Habgood JJ, Gardiner I, *et al.* (1997) Clinical and functional investigation of 10 missense mutations and a novel frameshift insertion mutation of the gene for copper-zinc superoxide dismutase in UK families with amyotrophic lateral sclerosis. *Neurology* 48:746-751.

84. Shibata N, Kawaguchi M, Uchida K, *et al.* (2007) Protein-bound crotonaldehyde accumulates in the spinal cord of superoxide dismutase-1 mutation-associated familial amyotrophic lateral sclerosis and its transgenic mouse model. *Neuropathology* 27:49-61.

85. Kostrzewa M, Burck-Lehmann U, & Muller U (1994) Autosomal dominant amyotrophic lateral sclerosis: a novel mutation in the Cu/Zn superoxide dismutase-1 gene. *Hum Mol Genet* 3:2261-2262.

86. Jackson M, Al-Chalabi A, Enayat ZE, *et al.* (1997) Copper/zinc superoxide dismutase 1 and sporadic amyotrophic lateral sclerosis: analysis of 155 cases and identification of a novel insertion mutation. *Ann Neurol* 42:803-807.

87. Pramatarova A, Goto J, Nanba E, *et al.* (1994) A two basepair deletion in the SOD 1 gene causes familial amyotrophic lateral sclerosis. *Hum Mol Genet* 3:2061-2062.

88. Takehisa Y, Ujike H, Ishizu H, *et al.* (2001) Familial amyotrophic lateral sclerosis with a novel Leu126Ser mutation in the copper/zinc superoxide dismutase gene showing mild clinical features and lewy body-like hyaline inclusions. *Arch Neurol* 58:736-740.

89. Pramatarova A, Figlewicz DA, Krizus A, *et al.* (1995) Identification of new mutations in the Cu/Zn superoxide dismutase gene of patients with familial amyotrophic lateral sclerosis. *Am J Hum Genet* 56:592-596.

90. Watanabe M, Aoki M, Abe K, *et al.* (1997) A novel missense point mutation (S134N) of the Cu/Zn superoxide dismutase gene in a patient with familial motor neuron disease. *Hum Mutat* 9:69-71.

91. Nogales-Gadea G, Garcia-Arumi E, Andreu AL, *et al.* (2004) A novel exon 5 mutation (N139H) in the SOD1 gene in a Spanish family associated with incomplete penetrance. *J Neurol Sci* 219:1-6.

92. Naini A, Musumeci O, Hayes L, *et al.* (2002) Identification of a novel mutation in Cu/Zn superoxide dismutase gene associated with familial amyotrophic lateral sclerosis. *J Neurol Sci* 198:17-19.

93. Deng HX, Hentati A, Tainer JA, *et al.* (1993) Amyotrophic lateral sclerosis and structural defects in Cu,Zn superoxide dismutase. *Science* 261:1047-1051.

94. Sapp PC, Rosen DR, Hosler BA, *et al.* (1995) Identification of three novel mutations in the gene for Cu/Zn superoxide dismutase in patients with familial amyotrophic lateral sclerosis. *Neuromuscul Disord* 5:353-357.

95. Kostrzewa M, Damian MS, & Muller U (1996) Superoxide dismutase 1: identification of a novel mutation in a case of familial amyotrophic lateral sclerosis. *Hum Genet* 98:48-50.

96. Valentine JS (2002) Do oxidatively modified proteins cause ALS? *Free Radic Biol Med* 33:1314-1320.

97. Yim HS, Kang JH, Chock PB, *et al.* (1997) A familial amyotrophic lateral sclerosis-associated A4V Cu, Zn-superoxide dismutase mutant has a lower Km for hydrogen peroxide. Correlation between clinical severity and the Km value. *J Biol Chem* 272:8861-8863.

98. Yim MB, Chock PB, & Stadtman ER (1990) Copper, zinc superoxide dismutase catalyzes hydroxyl radical production from hydrogen peroxide. *Proc Natl Acad Sci U S A* 87:5006-5010.

99. Beckman JS, Carson M, Smith CD, *et al.* (1993) ALS, SOD and peroxynitrite. *Nature* 364:584.

100. Crow JP, Ye YZ, Strong M, *et al.* (1997) Superoxide dismutase catalyzes nitration of tyrosines by peroxynitrite in the rod and head domains of neurofilament-L. *J Neurochem* 69:1945-1953.

101. Estevez AG, Crow JP, Sampson JB, *et al.* (1999) Induction of nitric oxide-dependent apoptosis in motor neurons by zinc-deficient superoxide dismutase. *Science* 286:2498-2500.

102. Goto JJ, Zhu H, Sanchez RJ, *et al.* (2000) Loss of in vitro metal ion binding specificity in mutant copper-zinc superoxide dismutases associated with familial amyotrophic lateral sclerosis. *J Biol Chem* 275:1007-1014.

103. Strange RW, Antonyuk S, Hough MA, *et al.* (2003) The structure of holo and metal-deficient wild-type human Cu, Zn superoxide dismutase and its relevance to familial amyotrophic lateral sclerosis. *J Mol Biol* 328:877-891.

104. Wang J, Xu G, Gonzales V, *et al.* (2002) Fibrillar inclusions and motor neuron degeneration in transgenic mice expressing superoxide dismutase 1 with a disrupted copper-binding site. *Neurobiol Dis* 10:128-138.

105. Cleveland DW & Rothstein JD (2001) From Charcot to Lou Gehrig: deciphering selective motor neuron death in ALS. *Nat Rev Neurosci* 2:806-819.

106. Khare SD, Caplow M, & Dokholyan NV (2004) The rate and equilibrium constants for a multistep reaction sequence for the aggregation of superoxide dismutase in amyotrophic lateral sclerosis. *Proc Natl Acad Sci U S A* 101:15094-15099.

107. Khare SD, Wilcox KC, Gong P, *et al.* (2005) Sequence and structural determinants of Cu, Zn superoxide dismutase aggregation. *Proteins* 61:617-632.

108. DiDonato M, Craig L, Huff ME, *et al.* (2003) ALS mutants of human superoxide dismutase form fibrous aggregates via framework destabilization. *J Mol Biol* 332:601-615.

109. Stathopulos PB, Rumfeldt JA, Karbassi F, *et al.* (2006) Calorimetric analysis of thermodynamic stability and aggregation for apo and holo amyotrophic lateral sclerosis-associated Gly-93 mutants of superoxide dismutase. *J Biol Chem* 281:6184-6193.

110. Leinweber B, Barofsky E, Barofsky DF, *et al.* (2004) Aggregation of ALS mutant superoxide dismutase expressed in Escherichia coli. *Free Radic Biol Med* 36:911-918.

111. Durham HD, Roy J, Dong L, *et al.* (1997) Aggregation of mutant Cu/Zn superoxide dismutase proteins in a culture model of ALS. *J Neuropathol Exp Neurol* 56:523-530.

112. Matsumoto S, Kusaka H, Ito H, *et al.* (1996) Golgi apparatus and intraneuronal inclusions of anterior horn cells in amyotrophic lateral sclerosis: an immunohistochemical study. *Acta Neuropathol (Berl)* 91:603-607.

113. Bruijn LI, Becher MW, Lee MK, *et al.* (1997) ALS-linked SOD1 mutant G85R mediates damage to astrocytes and promotes rapidly progressive disease with SOD1-containing inclusions. *Neuron* 18:327-338.

114. Wang J, Xu G, & Borchelt DR (2002) High molecular weight complexes of mutant superoxide dismutase 1: age-dependent and tissue-specific accumulation. *Neurobiol Dis* 9:139-148.

115. Wang J, Xu G, Li H*, et al.* (2005) Somatodendritic accumulation of misfolded SOD1-L126Z in motor neurons mediates degeneration: alphaB-crystallin modulates aggregation. *Hum Mol Genet* 14:2335-2347.

116. Okado-Matsumoto A & Fridovich I (2002) Amyotrophic lateral sclerosis: a proposed mechanism. *Proc Natl Acad Sci U S A* 99:9010-9014.

117. Johnston JA, Dalton MJ, Gurney ME*, et al.* (2000) Formation of high molecular weight complexes of mutant Cu, Zn-superoxide dismutase in a mouse model for familial amyotrophic lateral sclerosis. *Proc Natl Acad Sci U S A* 97:12571-12576.

118. Boillee S, Vande Velde C, & Cleveland DW (2006) ALS: a disease of motor neurons and their nonneuronal neighbors. *Neuron* 52:39-59.

119. Gurney ME, Pu H, Chiu AY*, et al.* (1994) Motor neuron degeneration in mice that express a human Cu,Zn superoxide dismutase mutation. *Science* 264:1772-1775.

120. Wong PC & Borchelt DR (1995) Motor neuron disease caused by mutations in superoxide dismutase 1. *Curr Opin Neurol* 8:294-301.

121. Ripps ME, Huntley GW, Hof PR*, et al.* (1995) Transgenic mice expressing an altered murine superoxide dismutase gene provide an animal model of amyotrophic lateral sclerosis. *Proc Natl Acad Sci U S A* 92:689-693.

122. Jonsson PA, Graffmo KS, Brannstrom T*, et al.* (2006) Motor neuron disease in mice expressing the wild type-like D90A mutant superoxide dismutase-1. *J Neuropathol Exp Neurol* 65:1126-1136.

123. Jonsson PA, Ernhill K, Andersen PM*, et al.* (2004) Minute quantities of misfolded mutant superoxide dismutase-1 cause amyotrophic lateral sclerosis. *Brain* 127:73-88.

124. Gurney ME (1997) Transgenic animal models of familial amyotrophic lateral sclerosis. *J Neurol* 244 Suppl 2:S15-20.

125. Watanabe M, Dykes-Hoberg M, Culotta VC*, et al.* (2001) Histological evidence of protein aggregation in mutant SOD1 transgenic mice and in amyotrophic lateral sclerosis neural tissues. *Neurobiol Dis* 8:933-941.

126. Bruijn LI, Houseweart MK, Kato S*, et al.* (1998) Aggregation and motor neuron toxicity of an ALS-linked SOD1 mutant independent from wild-type SOD1. *Science* 281:1851-1854.

127. Cheroni C, Peviani M, Cascio P, *et al.* (2005) Accumulation of human SOD1 and ubiquitinated deposits in the spinal cord of SOD1G93A mice during motor neuron disease progression correlates with a decrease of proteasome. *Neurobiol Dis* 18:509-522.

128. Basso M, Massignan T, Samengo G, *et al.* (2006) Insoluble mutant SOD1 is partly oligoubiquitinated in amyotrophic lateral sclerosis mice. *J Biol Chem* 281:33325-33335.

129. Seilhean D, Takahashi J, El Hachimi KH, *et al.* (2004) Amyotrophic lateral sclerosis with neuronal intranuclear protein inclusions. *Acta Neuropathol (Berl)* 108:81-87.

130. Stieber A, Gonatas JO, & Gonatas NK (2000) Aggregates of mutant protein appear progressively in dendrites, in periaxonal processes of oligodendrocytes, and in neuronal and astrocytic perikarya of mice expressing the SOD1(G93A) mutation of familial amyotrophic lateral sclerosis. *J Neurol Sci* 177:114-123.

131. Shinder GA, Lacourse MC, Minotti S, *et al.* (2001) Mutant Cu/Zn-superoxide dismutase proteins have altered solubility and interact with heat shock/stress proteins in models of amyotrophic lateral sclerosis. *J Biol Chem* 276:12791-12796.

132. Watanabe Y, Yasui K, Nakano T, *et al.* (2005) Mouse motor neuron disease caused by truncated SOD1 with or without C-terminal modification. *Brain Res Mol Brain Res* 135:12-20.

133. Jaarsma D, Teuling E, Haasdijk ED, *et al.* (2008) Neuron-specific expression of mutant superoxide dismutase is sufficient to induce amyotrophic lateral sclerosis in transgenic mice. *J Neurosci* 28:2075-2088.

134. Deng HX, Shi Y, Furukawa Y, *et al.* (2006) Conversion to the amyotrophic lateral sclerosis phenotype is associated with intermolecular linked insoluble aggregates of SOD1 in mitochondria. *Proc Natl Acad Sci U S A* 103:7142-7147.

135. Boillee S, Yamanaka K, Lobsiger CS, *et al.* (2006) Onset and progression in inherited ALS determined by motor neurons and microglia. *Science* 312:1389-1392.

136. Miller TM, Smith RA, & Cleveland DW (2006) Amyotrophic lateral sclerosis and gene therapy. *Nat Clin Pract Neurol* 2:462-463.

137. Lobsiger CS, Boillee S, & Cleveland DW (2007) Inaugural Article: Toxicity from different SOD1 mutants dysregulates the complement system and the neuronal regenerative response in ALS motor neurons. *Proc Natl Acad Sci U S A* 104:7319-7326.

138. Clement AM, Nguyen MD, Roberts EA, *et al.* (2003) Wild-type nonneuronal cells extend survival of SOD1 mutant motor neurons in ALS mice. *Science* 302:113-117.

139. Dobrowolny G, Aucello M, Rizzuto E, *et al.* (2008) Skeletal muscle is a primary target of SOD1G93A-mediated toxicity. *Cell Metab* 8:425-436.

140. Prudencio M, Durazo A, Whitelegge JP, *et al.* (2009) Modulation of mutant superoxide dismutase 1 aggregation by co-expression of wild-type enzyme. *J Neurochem* 108:1009-1018.

141. Furukawa Y, Fu R, Deng HX, *et al.* (2006) Disulfide cross-linked protein represents a significant fraction of ALS-associated Cu, Zn-superoxide dismutase aggregates in spinal cords of model mice. *Proc Natl Acad Sci U S A* 103:7148-7153.

142. Jonsson PA, Graffmo KS, Andersen PM, *et al.* (2006) Disulphide-reduced superoxide dismutase-1 in CNS of transgenic amyotrophic lateral sclerosis models. *Brain* 129:451-464.

143. Banci L, Bertini I, Durazo A, *et al.* (2007) Metal-free superoxide dismutase forms soluble oligomers under physiological conditions: A possible general mechanism for familial ALS. *Proc Natl Acad Sci U S A* 104:11263-11267.

144. Cozzolino M, Amori I, Pesaresi MG, *et al.* (2008) Cysteine 111 Affects Aggregation and Cytotoxicity of Mutant Cu,Zn-superoxide Dismutase Associated with Familial Amyotrophic Lateral Sclerosis. *J Biol Chem* 283:866-874.

145. Niwa J, Yamada S, Ishigaki S, *et al.* (2007) Disulfide bond mediates aggregation, toxicity, and ubiquitylation of familial amyotrophic lateral sclerosis-linked mutant SOD1. *J Biol Chem* 282:28087-28095.

146. Mizushima S & Nagata S (1990) pEF-BOS, a powerful mammalian expression vector. *Nucleic Acids Res* 18:5322.

147. Wong PC, Pardo CA, Borchelt DR, *et al.* (1995) An adverse property of a familial ALS-linked SOD1 mutation causes motor neuron disease characterized by vacuolar degeneration of mitochondria. *Neuron* 14:1105-1116.

148. Laemmli UK (1970) Cleavage of structural proteins during the assembly of the head of bacteriophage T4. *Nature* 227:680-685.

149. Wang J, Xu G, Slunt HH, *et al.* (2005) Coincident thresholds of mutant protein for paralytic disease and protein aggregation caused by restrictively expressed superoxide dismutase cDNA. *Neurobiol Dis* 20:943-952.

150. Murphy RM (2002) Peptide aggregation in neurodegenerative disease. *Annu Rev Biomed Eng* 4:155-174.

151. Shaw BF, Lelie HL, Durazo A, *et al.* (2008) Detergent insoluble aggregates associated with amyotrophic lateral sclerosis in transgenic mice contain primarily full-length, unmodified superoxide dismutase-1. *J Biol Chem*.

152. Watanabe S, Nagano S, Duce J, *et al.* (2007) Increased affinity for copper mediated by cysteine 111 in forms of mutant superoxide dismutase 1 linked to amyotrophic lateral sclerosis. *Free Radic Biol Med* 42:1534-1542.

153. Schinina ME, Carlini P, Polticelli F, *et al.* (1996) Amino acid sequence of chicken Cu, Zn-containing superoxide dismutase and identification of glutathionyl adducts at exposed cysteine residues. *Eur J Biochem* 237:433-439.

154. Ogawa Y, Kosaka H, Nakanishi T, *et al.* (1997) Stability of mutant superoxide dismutase-1 associated with familial amyotrophic lateral sclerosis determines the manner of copper release and induction of thioredoxin in erythrocytes. *Biochem Biophys Res Commun* 241:251-257.

155. Fujiwara N, Nakano M, Kato S, *et al.* (2007) Oxidative modification to cysteine sulfonic acid of Cys111 in human copper-zinc superoxide dismutase. *J Biol Chem* 282:35933-35944.

156. Krishnan U, Son M, Rajendran B, *et al.* (2006) Novel mutations that enhance or repress the aggregation potential of SOD1. *Mol Cell Biochem* 287:201-211.

157. Son M, Puttaparthi K, Kawamata H, *et al.* (2007) Overexpression of CCS in G93A-SOD1 mice leads to accelerated neurological deficits with severe mitochondrial pathology. *Proc Natl Acad Sci U S A* 104:6072-6077.

158. Stromer T & Serpell LC (2005) Structure and morphology of the Alzheimer's amyloid fibril. *Microsc Res Tech* 67:210-217.

159. Guo JT, Wetzel R, & Xu Y (2004) Molecular modeling of the core of Abeta amyloid fibrils. *Proteins* 57:357-364.

160. Morimoto A, Irie K, Murakami K, *et al.* (2002) Aggregation and neurotoxicity of mutant amyloid beta (A beta) peptides with proline replacement: importance of turn formation at positions 22 and 23. *Biochem Biophys Res Commun* 295:306-311.

161. Sawaya MR, Sambashivan S, Nelson R, *et al.* (2007) Atomic structures of amyloid cross-beta spines reveal varied steric zippers. *Nature* 447:453-457.

162. Thakur AK & Wetzel R (2002) Mutational analysis of the structural organization of polyglutamine aggregates. *Proc Natl Acad Sci U S A* 99:17014-17019.

163. Elam JS, Taylor AB, Strange R, *et al.* (2003) Amyloid-like filaments and water-filled nanotubes formed by SOD1 mutant proteins linked to familial ALS. *Nat Struct Biol* 10:461-467.

164. Shaw BF, Durazo A, Nersissian AM, *et al.* (2006) Local unfolding in a destabilized, pathogenic variant of superoxide dismutase 1 observed with H/D exchange and mass spectrometry. *J Biol Chem* 281:18167-18176.

165. Khare SD, Ding F, & Dokholyan NV (2003) Folding of Cu, Zn superoxide dismutase and familial amyotrophic lateral sclerosis. *J Mol Biol* 334:515-525.

166. Sasaki S, Nagai M, Aoki M, *et al.* (2007) Motor neuron disease in transgenic mice with an H46R mutant SOD1 gene. *J Neuropathol Exp Neurol* 66:517-524.

167. Fujita Y & Okamoto K (2005) Golgi apparatus of the motor neurons in patients with amyotrophic lateral sclerosis and in mice models of amyotrophic lateral sclerosis. *Neuropathology* 25:388-394.

168. Zetterstrom P, Stewart HG, Bergemalm D, *et al.* (2007) Soluble misfolded subfractions of mutant superoxide dismutase-1s are enriched in spinal cords throughout life in murine ALS models. *Proc Natl Acad Sci U S A* 104:14157-14162.

169. Furukawa Y, Kaneko K, Yamanaka K, *et al.* (2008) Complete loss of post-translational modifications triggers fibrillar aggregation of SOD1 in the familial form of amyotrophic lateral sclerosis. *J Biol Chem* 283:24167-24176.

170. Furukawa Y, Torres AS, & O'Halloran TV (2004) Oxygen-induced maturation of SOD1: a key role for disulfide formation by the copper chaperone CCS. *Embo J* 23:2872-2881.

171. Wang J, Caruano-Yzermans A, Rodriguez A, *et al.* (2007) Disease-associated mutations at copper ligand histidine residues of superoxide dismutase 1 diminish the binding of copper and compromise dimer stability. *J Biol Chem* 282:345-352.

172. Lindberg MJ, Normark J, Holmgren A, *et al.* (2004) Folding of human superoxide dismutase: disulfide reduction prevents dimerization and produces marginally stable monomers. *Proc Natl Acad Sci U S A* 101:15893-15898.

173. Hart PJ (2006) Pathogenic superoxide dismutase structure, folding, aggregation and turnover. *Curr Opin Chem Biol* 10:131-138.

174. Yim MB, Kang JH, Yim HS, *et al.* (1996) A gain-of-function of an amyotrophic lateral sclerosis-associated Cu,Zn-superoxide dismutase mutant: An enhancement of free radical formation due to a decrease in Km for hydrogen peroxide. *Proc Natl Acad Sci U S A* 93:5709-5714.

175. Stathopulos PB, Rumfeldt JA, Scholz GA, *et al.* (2003) Cu/Zn superoxide dismutase mutants associated with amyotrophic lateral sclerosis show enhanced formation of aggregates in vitro. *Proc Natl Acad Sci U S A* 100:7021-7026.

176. Fischer LR, Culver DG, Tennant P, *et al.* (2004) Amyotrophic lateral sclerosis is a distal axonopathy: evidence in mice and man. *Exp Neurol* 185:232-240.

177. Kennel PF, Finiels F, Revah F, *et al.* (1996) Neuromuscular function impairment is not caused by motor neurone loss in FALS mice: an electromyographic study. *Neuroreport* 7:1427-1431.

178. Hegedus J, Putman CT, & Gordon T (2007) Time course of preferential motor unit loss in the SOD1 G93A mouse model of amyotrophic lateral sclerosis. *Neurobiol Dis* 28:154-164.

179. Borchelt DR, Wong PC, Becher MW, *et al.* (1998) Axonal transport of mutant superoxide dismutase 1 and focal axonal abnormalities in the proximal axons of transgenic mice. *Neurobiol Dis* 5:27-35.

180. Turner BJ & Talbot K (2008) Transgenics, toxicity and therapeutics in rodent models of mutant SOD1-mediated familial ALS. *Prog Neurobiol* 85:94-134.

181. Kasperaviciute D, Weale ME, Shianna KV, *et al.* (2007) Large-scale pathways-based association study in amyotrophic lateral sclerosis. *Brain*.

182. Kabashi E & Durham HD (2006) Failure of protein quality control in amyotrophic lateral sclerosis. *Biochim Biophys Acta* 1762:1038-1050.

183. Devlin GL, Carver JA, & Bottomley SP (2003) The selective inhibition of serpin aggregation by the molecular chaperone, alpha-crystallin, indicates a nucleation-dependent specificity. *J Biol Chem* 278:48644-48650.

184. Sathish HA, Stein RA, Yang G, *et al.* (2003) Mechanism of chaperone function in small heat-shock proteins. Fluorescence studies of the conformations of T4 lysozyme bound to alphaB-crystallin. *J Biol Chem* 278:44214-44221.

185. Tanksale A, Ghatge M, & Deshpande V (2002) Alpha-crystallin binds to the aggregation-prone molten-globule state of alkaline protease: implications for preventing irreversible thermal denaturation. *Protein Sci* 11:1720-1728.

186. Kumar MS, Kapoor M, Sinha S, *et al.* (2005) Insights into hydrophobicity and the chaperone-like function of alphaA- and alphaB-crystallins: an isothermal titration calorimetric study. *J Biol Chem* 280:21726-21730.

187. Horwitz J (2003) Alpha-crystallin. *Exp Eye Res* 76:145-153.

188. Narberhaus F (2002) Alpha-crystallin-type heat shock proteins: socializing minichaperones in the context of a multichaperone network. *Microbiol Mol Biol Rev* 66:64-93; table of contents.

189. Kumar LV & Rao CM (2000) Domain swapping in human alpha A and alpha B crystallins affects oligomerization and enhances chaperone-like activity. *J Biol Chem* 275:22009-22013.

190. Dubin RA, Wawrousek EF, & Piatigorsky J (1989) Expression of the murine alpha B-crystallin gene is not restricted to the lens. *Mol Cell Biol* 9:1083-1091.

191. Iwaki T, Kume-Iwaki A, & Goldman JE (1990) Cellular distribution of alpha B-crystallin in non-lenticular tissues. *J Histochem Cytochem* 38:31-39.

192. Brady JP, Garland DL, Green DE, *et al.* (2001) AlphaB-crystallin in lens development and muscle integrity: a gene knockout approach. *Invest Ophthalmol Vis Sci* 42:2924-2934.

193. Suzuki A, Sugiyama Y, Hayashi Y, *et al.* (1998) MKBP, a novel member of the small heat shock protein family, binds and activates the myotonic dystrophy protein kinase. *J Cell Biol* 140:1113-1124.

194. Shama KM, Suzuki A, Harada K, *et al.* (1999) Transient up-regulation of myotonic dystrophy protein kinase-binding protein, MKBP, and HSP27 in the neonatal myocardium. *Cell Struct Funct* 24:1-4.

195. Jakob U, Gaestel M, Engel K, *et al.* (1993) Small heat shock proteins are molecular chaperones. *J Biol Chem* 268:1517-1520.

196. Wang J, Martin E, Gonzales V, *et al.* (2007) Differential regulation of small heat shock proteins in transgenic mouse models of neurodegenerative diseases. *Neurobiol Aging*.

197. Sun Y & MacRae TH (2005) Characterization of novel sequence motifs within N- and C-terminal extensions of p26, a small heat shock protein from Artemia franciscana. *Febs J* 272:5230-5243.

198. Batulan Z, Shinder GA, Minotti S, *et al.* (2003) High threshold for induction of the stress response in motor neurons is associated with failure to activate HSF1. *J Neurosci* 23:5789-5798.

199. Liu J, Shinobu LA, Ward CM, *et al.* (2005) Elevation of the Hsp70 chaperone does not effect toxicity in mouse models of familial amyotrophic lateral sclerosis. *J Neurochem* 93:875-882.

200. Krishnan J, Vannuvel K, Andries M, *et al.* (2008) Over-expression of Hsp27 does not influence disease in the mutant SOD1(G93A) mouse model of amyotrophic lateral sclerosis. *J Neurochem* 106:2170-2183.

201. Sharp PS, Akbar MT, Bouri S, *et al.* (2008) Protective effects of heat shock protein 27 in a model of ALS occur in the early stages of disease progression. *Neurobiol Dis* 30:42-55.

202. Gidalevitz T, Krupinski T, Garcia S, *et al.* (2009) Destabilizing Protein Polymorphisms in the Genetic Background Direct Phenotypic Expression of Mutant SOD1 Toxicity. *PLoS Genet* 5:e1000399.

BIOGRAPHICAL SKETCH

Celeste Karch was born in South Field, Michigan, in 1983. After graduating from Northville High School in 2001, she attended Kalamazoo College for her undergraduate studies. She graduated with a Bachelor of Arts degree in biology in 2005. She began her graduate studies in the Interdisciplinary Program for Biomedical Research at the University of Florida in 2005. She joined the laboratory of Dr. David Borchelt in 2006.